Design of a Magnetorheological Fluid for an MR Prosthetic Knee Actuator with an Optimal Geometry

Ketill Heiðar Guðmundsson

FACULTY OF INDUSTRIAL ENGINEERING, MECHANICAL ENGINEERING AND COMPUTER SCIENCE
UNIVERSITY OF ICELAND
2011

Design of a Magnetorheological Fluid for an MR Prosthetic Knee Actuator with an Optimal Geometry

Ketill Heiðar Guðmundsson

A thesis submitted to the Faculty of Industrial Engineering, Mechanical Engineering and Computer Science, University of Iceland for the degree *Philosophiae Doctor* in Mechanical Engineering

Thesis Supervisor
Dr. Fjóla Jónsdóttir

Doctoral committee
Dr. Fjóla Jónsdóttir (chairman)
School of Engineering and Natural Sciences, University of Iceland.

Dr. Halldór Pálsson
School of Engineering and Natural Sciences, University of Iceland.

Dr. Hilmar Bragi Janusson
Ossur Inc., Iceland.

Dr. Oliver Gutfleisch
Leibniz Institute for Solid State and Materials Research Dresden, Germany.

Opponents

Professor Antonio José Faria Bombard
Department of Physics and Chemistry, Federal University at Itajubá, Brazil.

Professor Faramarz Gordaninejad
Department of Mechanical Engineering, University of Nevada, Reno.

Design of a Magnetorheological Fluid for an MR Prosthetic Knee Actuator with an Optimal Geometry
A thesis submitted to the School of Engineering and Natural Sciences, University of Iceland for the degree *Philosophiae Doctor* in Mechanical Engineering

Faculty of Industrial Engineering, Mechanical Engineering and Computer Science
School of Engineering and Natural Sciences
University of Iceland
VR II, Hjarðarhaga 2-6
107 Reykjavík
Iceland

ISBN 978-9979-9935-5-1

Prentun: Háskólaprent
Reykjavík, May 2011

Ágrip (in Icelandic)

Kveikjan að rannsókninni er rafsegulvökva gervihnjáliður sem þarfnast betrumbóta. Gervihnjáliðurinn er aðlögunarhæfur, í rauntíma, með hjálp rafsegulvökva. Vandamál hafa komið upp þegar gervihnjáliðurinn er notaður í krefjandi aðstæðum, eins og fjallgöngu sem dæmi. Markmið verkefnisins er tvíþætt: að auka bremsuvægi hnjáliðarins undir áhrifum segulsviðs og samtímis að minnka bremsuvægi hnjáliðarins þegar segulsviðs nýtur ekki við. Til að ná markmiðunum tveimur er notuð samþættuð aðferð vökvahönnunar og rafsegulvökvavirkjarahönnunar. Rafsegulvökvi er hannaður, sérsniðinn fyrir notkun í gervihnjálið. Samhliða vökvahönnuninni, er rafsegulvökva snúningsbremsa hönnuð fyrir gervihné.

Við rafsegulvökvahönnunina er notuð aðferð tilrauna. Tuttugu og tvær vænlegar rafsegulvökvablöndur eru metnar í mælitækjum, til notkunar í gervihnjáliðnum. Vökvar þessir eru blandaðir og þeim gefin einkunn samkvæmt hönnunar markmiðum gervihnjáliðarins. Vænlegar rafsegulvökvablöndur eru meðal annars; eintoppa rafsegulvökvar með breytilegri agnastærð og agnamagni, tvítoppa rafsegulvökvar með blöndu af tveimur gerðum af ögnum í míkrómetra skala, og tvítoppa rafsegulvökvar með ögnum í nanómetra skala. Mælikvarði á gæði vökva er skilgreindur sem hlutfallið milli skerspennu í vökvanum, þegar hann er undir áhrifum segulsviðs, á móti seigju vökvans, þegar segulsviðs nýtur ekki við. Sá vökvi sem hefur hæsta hlutfallið mun leiða til víðs sviðs bremsuvægis í gervihnjáliðnum.

Við hönnun rafsegulvökvavirkjarans eru notaðar aðferðir líkanagerðar og bestunar. Líkön eru smíðuð fyrir bremsuvægi gervihnjáliðarins, með og án segulsviðs, þar sem segulsviðslíkanið byggir á smábútagreiningu. Hönnunarmarkmið gervihnjáliðarins eru: hátt bremsuvægi undir áhrifum segulsviðs, lágt bremsuvægi þegar segulsviðs nýtur ekki við og litla þyngd. Málamiðlanir milli hönnunarmarkmiða eru rannsakaðar með fjöl-markmiða bestun. Greiningin leiðir í ljós betrumbætur á hönnun sem hefur verið nýtt í framleiðslu á nýrri og bættri útgáfu af rafsegulvökva gervihnjáliðnum.

Abstract

The motivation for this study is a magnetorheological (MR) prosthetic knee joint. The MR prosthetic knee is adaptive in real-time via an MR fluid. Problems have been experienced when the prosthetic device is used in demanding situations, like hill-climbing for example. The goal of this project is twofold; to increase the on-state torque output of the prosthetic device and, at the same time, to decrease the off-state torque. To achieve the two goals, a combined MR fluid design approach and an MR actuator design approach is adopted. An MR fluid is designed that is tailored for this specific application. Parallel to the fluid design, an MR rotary brake actuator is designed for the prosthetic knee.

The MR fluid design is approached by experimentally evaluating twenty-two potential MR fluid compositions for the proposed device. These fluids are mixed and rated against the design objectives of the prosthetic device. Potential MR fluid compositions include; unimodal MR fluids, with a varying particle size and a variable solid loading, bimodal MR fluids with two grades of micron-sized particles, and bimodal MR fluids with nanoparticles. A fluid figure of merit is defined that is the ratio between the on-state shear yield stress and the off-state viscosity. The fluid with the highest ratio will result in the widest torque range for prosthetic device.

The MR actuator design is approached by building torque models of the device and optimizing the models. An off-state and an on-state model are developed where the on-state model is based on a magnetic finite element analysis. Design objectives for the device are: high on-state braking torque, low the off-state rotational stiffness and low weight. Trade-offs between the design objectives are explored with a multi-objective optimization technique. The analysis suggests design improvements that have been realized in a newly built and an enhanced version of the MR prosthetic knee.

Preface

This dissertation has been prepared in partial fulfillment of the requirements for a Ph.D. degree in Mechanical Engineering at the University of Iceland. The research was carried out at the Department of Industrial Engineering, Mechanical Engineering and Computer Science at the University of Iceland, in the testing laboratories of Ossur Inc. in Iceland and at the Leibniz Institute of Solid State and Materials Research Dresden, in Germany.

The work was funded by the University of Iceland Doctoral research fund and RANNIS grant no. 090035021. The work was supported by Ossur Inc.

To my family

Acknowledgements

First of all I would like to thank my advisor, Dr. Fjóla Jónsdóttir, for a fruitful cooperation. She was actively involved in the project and took part in many of the experiments. Thank you, Fjóla. Then I would like to thank my doctoral committee, Dr. Halldór Pálssson, Dr. Hilmar Bragi Janusson and Dr. Oliver Gutfleisch for their support.

I would like to thank our collaborators at Ossur Inc., Freygarður Þorsteinsson, Björn Sighvatsson, Binh, Andrew Bache and Sigurður Ólafsson for the help in mixing the fluids and with other practical aspects of the project. Also, I would like to thank professor Ingvar Helgi Árnason, at the University of Iceland, for helping us mixing the nano fluids.

At the Leibniz Institute for Solid State and Materials Research Dresden, I would like to thank Dr. Dietrich Hinz for teaching us how to use the rheometer. Also, I would like to thank Dr. Julia Lyubina, Dr. Nils Scheerbaum and Juliane Thielsch, at the institute, for their help.

Last but not least, I would like to thank my lovely wife, Kristín Konráðsdóttir, for her support and encouragement. Without her support this would not have been completed. I would like to thank our children, Konráð Björn, Rakel Karen and Sylvía Rut for being there. Then I would like to thank my family and Kristín’s family for their interest in the project.

Contents

Figures

6.6	The on-state shear yield stress as function of the off-state viscosity, for the unimodal fluids each representing a particular iron powder. The yield stress is measured at a magnetic flux density of 0.55 T and the off-state viscosity is measured at a shear-rate of 200 s^{-1}.
6.7	On-state measurements for a unimodal MR fluid having a solid concentration of 0.28 and the HS carbonyl iron powder. The Bingham model is fitted to the flow curves.
6.8a	The shear yield stress of the unimodal MR fluid, samples 21-25, as a function of the magnetic flux density.
6.8b	The shear yield stress of the unimodal MR fluids, samples 21-25, as a function of the solid concentration.
6.9	The off-state viscosity as a function of the shear rate for the unimodal MR fluids.
6.10	Flow curves for bimodal MR fluids and their corresponding unimodal MR fluids. Measurements are performed at a magnetic flux density of 0.55 T.
6.11	The field-induced shear yield stress, as a function of the magnetic flux density, for bimodal MR fluids and their corresponding unimodal fluids.
6.12	The off-state viscosity, as a function of shear-rates, for bimodal MR fluids and their corresponding unimodal fluids.
6.13	The shear yield stress as a function of the off-state viscosity, for the bimodal fluids and their corresponding unimodal fluids. The yield stress is measured at a magnetic flux density of 0.55 T and the off-state viscosity is measured at a shear-rate of 200 s^{-1}.
6.14	Flow curves for a unimodal fluid with a solid concentration of 60% by mass and two bimodal fluids with nano-sized particle concentration of 5% and a micron-sized particle concentration of 55% by mass. Measurements were conducted at a magnetic flux density of 0.55 T.
6.15	Shear-yield stress of MR fluid compositions with 25 nm and 100-250 nm particles at various concentrations, compared to the shear-yield stress of the corresponding unimodal fluid. The total solid concentration is 0.28 in all cases.
6.16	The shear yield stress as a function of the magnetic flux density for MR fluid compositions, containing 55% micron-sized particles and 5% nano-sized particles, and the corresponding unimodal MR fluid.
6.17	The post-yield viscosity as a function of the magnetic flux density for MR fluid compositions containing 55% micron-sized particles and 5% nano-sized particles and the corresponding unimodal MR fluid.
6.18	The off-state viscosity as a function of the shear rate for a unimodal fluid and bimodal fluid samples with a total solid concentration of 60%.
6.19	Shear yield-stress as a function of off-state viscosity for the bimodal nanoparticle fluid compositions.
7.1	The magnetization hysteresis loop of a perfluorinated polyether (PFPE) based MR fluid sample with a solid loading of 0.28, by volume, and an average particle diameter of approximately 2 μm. Particles have an iron content of 97%. Measurements are performed at a temperature of 20°C.
7.2	The B-H relation for a perfluorinated polyether (PFPE) based MR fluid with a solid concentration of 0.28, by volume, and an average particle diameter of 2

	μm. Particles have an iron content of 97%. A B-H model for established MR fluids is also shown and a fine tune of that model for a FPEE based MR fluid composition.
7.3	The shear-yield stress of perfluorinated polyether (PFPE) based MR fluid samples with a solid loading ranging from 0.25 to 0.35, by volume, and an average particle diameter of 2 μm. An empirically fitted model, based on Carlson (2005), is also shown for each particle loading. Measurements are performed at a temperature of 20°C.
7.4	The shear-yield stress of perfluorinated polyether (PFPE) based MR fluids with a solid loading ranging from 0.25 to 0.35, by volume, and an average particle diameter of 2 microns. An empirically fitted model, based on Ginder et al. (1994; 1996), is also shown. Measurements are performed at a temperature of 20°C.

Tables

Abbreviations

CIP	Carbonyl iron powder
FE	Finite element
MFD	Magnetic flux density
MR	Magnetorheological
PFPE	Perfluorinated polyether

1 Introduction

Regaining biomechanical function, comfort and quality of every-day life is a prime consideration when designing prosthetic devices for amputees. The magnetorheological (MR) prosthetic knee, which is the subject of this study, is an example of such a device. The study presents a comprehensive and a combined MR device design and MR fluid design approach, aiming to advance the MR prosthetic knee.

1.1 Background

MR fluids are a class of smart materials whose rheological properties can be controlled with a magnetic field. Conventional MR fluids consist of a base fluid, immersed with ferromagnetic micron-sized particles. With the application of a magnetic field, the iron particles are drawn together in electromagnetic chains. Hence, the stronger the magnetic flux in the fluid, the stronger the particle chains. MR fluids have many industrial applications. They are, for example, increasingly being considered in a variety of devices, such as, dampers, valves, brakes and clutches (Carlson et al., 2001; Kavlicoglu et al., 2002; Li et al., 2003; Wereley et al., 2008). Examples of MR prosthetic devices are a variable stiffness knee joint (Herr et al., 2003; Ossur Inc., 2011) and a variable stiffness, below knee, leg (Carlson et al., 2001; Biedermann, 2002). An example of an MR orthotic device is a variable stiffness brace (Zite et al., 2006).

An MR prosthetic knee, manufactured by the company Ossur Inc. (Ossur Inc., 2011), is called the Rheo knee. It was originally developed by a group of scientists at the Massachusetts Institute of Technology and patented under US patent specification 6,764,520 (Deffenbaugh et al., 2001). The knee is a synergy of artificial intelligence, advanced sensors and MR actuator technology and is described in detail in Chapter Two. The knee uses a magnetic field to vary the viscosity of the MR fluid, and thereby its flexion resistance. Unlike existing hydraulic systems, the resistance offered by the MR fluid is activated only when the individual needs it, and it is activated instantly. Hence, the stiffness of the knee can vary in real time as the amputee walks. This results in a natural and effortless motion. The knee is equipped with an MR rotary brake that utilized the MR fluid in direct-shear mode. The brake consists of a magnetic coil which is fed with electrical current to generate a controlled magnetic field in the fluid. The core and the core sides are made of a cobalt-iron alloy, named Vacoflux (Vacuumschmelze, 2011). This alloy has the highest magnetic saturation of all known soft magnetic materials. The outer and the inner houses are made of aluminum and titanium, respectively, which are non-magnetic materials. The steel blades are arranged tightly, side by side in the chamber to enlarge the area that is affected by the shear force. The blades are connected alternately to

the outer house (stator) and to the inner house (rotor). The stator is connected to the amputee's residual limb while the rotor is connected to the amputee's lower part of the leg (below the knee), producing the relative motion between the stator and the rotor. The gap between the blades, where the fluid resides is small compared to the thickness of the blades. As the knee rotates into flexion or extension, the thin rotary blades shear the particle chains to create resistance. The result is a varied fluid shear force within the knee, restoring more natural pelvic position during pre-swing and reducing fatigue levels. The research presented here aims to advance this device allowing amputees to tackle more demanding situations, like hill-climbing for example. The aim is to improve the quality of life for above-knee amputees using the MR prosthetic knee.

MR fluids have three common modes of usage, that is, flow mode, squeeze mode and shear mode. Flow mode and squeeze mode are used, for example, in dampers and shock absorbers. The shear mode is used in the field of brakes and clutches which this project is concerned with. In shear mode, the fluid is contained between two plates that move relative to one another. When considering the use of a MR fluid in a particular application, there are three main concerns associated with the fluids: namely, the strength of the fluid (i.e., the achievable yield stress), the stability of the fluid, and the durability of the fluid (Carlson, 2002). All three areas, mentioned above, are important in the design of prosthetic devices. The field-induced braking torque of a prosthetic knee is affected directly by the shear-yield stress of the MR fluid and the stability of the knee is affected by the sedimentation stability of the MR fluid. In addition to the three common concerns mentioned above, a very important factor in the design of prosthetic and orthotic devices, is the zero-field or off-state viscosity of the fluid. The off-state viscosity controls the ability of the device to move freely in the absence of magnetic field. This is of utmost importance for the user of a prosthetic knee cause it results in a more natural and effortless motion. Although, all areas mentioned above, are important, to limit the scope of this project, the focus will be on the strength and the off-state viscosity of MR fluids and to the on-state and off-state torque of an MR rotary brake device.

A number of research groups have investigated how to enhance the strength of MR fluids; see for example (Tang et al., 2000; Martys, 2005). Perhaps the most widely employed technique for increasing the yield stress in MR fluids is increasing the volume fraction of iron powder. The problem is that these methods also increase the field-independent plastic viscosity (Heyes et al., 2004). In the field of suspension rheology, it is well known that the particle size distribution has considerable effects on the viscosity of the suspension (Barnes et al., 1989). A suspension with a broad particle size distribution will have a lower viscosity than a suspension with a narrow particle size distribution. The mechanism by which the viscosity is reduced is related to the particle packing characteristics. In recent years, a number of magnetic fluid formulations have used bimodal distributions to increase the iron concentration while simultaneously reducing the viscosity of the fluid; see, for example (Thurm et al., 2003; Golden et al. 2005). It has been reported that adding nano particles to a MR fluid sample increases the field-induced yield stress of the fluid (Chaudhuri et al., 2005; Wereley et al., 2006). This holds true, up to a certain point. A decrease in yield stress is observed when nano particle concentration is increased to 7.5% by weight which indicates an optimum in yield stress when a nano particle concentration of 5% by weight is used (Chaudhuri et al., 2005). This result is based on particles sizes of 10 microns and 30-40 nm particles. Our application requires smaller micron sized particles since the prosthetic knee actuator can not be loaded with particles

bigger than 7-9 microns in size. The project will aim to find the optimum particle combination for the proposed application.

As said before, the goals of the projects are approached from a device point of a view and from a MR fluid point of view. This is done by focusing simultaneously on the device and the fluid. The geometrical design of an MR rotary brake is investigated. A model is build describing the on-state and the off-state torque of the device. An optimization is performed on the structure, aiming to increase the on-state torque and to lower the off-state torque, at the same time. Summarizing, the project is concerned with developing an MR fluid and an MR rotary brake for a particular application in a prosthetic knee. Results will show that, what at first might seem as two contradictory goals, increasing the on-state torque and lowering the off-state torque, can both be achieved with an appropriate MR fluid composition and an optimal MR rotary brake for the proposed application.

1.2 Motivation and goals

Motivated by the use of MR technology in prosthetic devices and to improve an existing design of an MR prosthetic knee, the goals of this study are twofold:

- To develop an MR fluid composition for the prosthetic knee actuator.
- To develop an MR rotary brake for the prosthetic knee joint.

An MR fluid composition is sought with a suitable balance between the field-induced shear yield stress and the off-state viscosity, tailored for the requirements of the proposed application. An MR rotary brake design is sought to deliver the desired torque range in the knee joint.

The research is an MR fluid design endeavor and an MR actuator design endeavor. The aim is to develop an MR fluid for the proposed application and to optimize an MR actuator to maximize to torque output range of the prosthetic device. The MR fluid design is approached by indentifying constraints, implicated by the proposed application, regarding solid loading, particle size and the base fluid. These constrain influence the choice of potential MR fluid compositions. The resulting MR fluids are experimentally evaluated and rated against the proposed application.

Motivated by reducing the cost of testing and of experiments in the development of the prosthetic device, on-state and off-state torque models are built that describe the torque output of the device. The model is validated against actual torque measurements of a working device and has been shown to be accurate. The models predictions will reduce the cost in advancing the MR prosthetic knee and accelerate developments.

1.3 Contribution

The contribution of the research is fivefold:

1. The research presents a device model of an MR rotary brake actuator. Models of direct-shear mode devices have been built by other authors (Kavlicoglu et al., 2006; Wereley et al., 2008). The model presented here is comprehensive and quantitative

(Gudmundsson et al., 2010). Based on MR fluid characteristics, magnetic finite element analysis (FEA) and the geometry of the actuator, the model predicts the torque output of the device. The model has been validated, with actual torque measurements of the device, and is shown to accurately describe the torque output of a direct-shear mode, multi-plate, MR rotary brake (Gudmundsson et al., 2010).

2. A multi-objective optimization procedure for an MR rotary brake is presented. Optimization of MR structures has been investigated by numerous authors (Nguyen et al., 2007; Yang et al., 2008). The research presented here realizes that trade-offs between design objectives exist (Gudmundsson et al., 2010). Three design objectives are considered: high on-state torque, low off-state torque and low weight. The optimization procedure explores the coupling between these three design objectives. The procedure is believed to be a contribution to the MR device design community.

3. The effect of nanoparticles on the on-state and the off-state characteristics of MR fluids have been experimentally investigated. Nanoparticles in MR fluids have received the attention of numerous researches during the last decade (Chaudhuri et al., 2001; Wereley et al., 2006). This research implies that nanoparticles can be used to moderately increase the on-state shear yield stress (Wereley et al., 2006). For the proposed device, nanoparticles were believed to be attractive due to the small micron-sized gap in the actuator. A comprehensive experimental investigation on the effect of two grades of nanoparticles is presented (Jonsdottir et al., 2010). The research shows a moderate increase in the on-state shear-yield stress. This was expected at the outset and has been reported by other authors (Wereley et al., 2006). However, the research shows a considerable increase in off-state viscosity, even with a small concentration of nanoparticles (Jonsdottir et al., 2010). The large negative effect on the off-state viscosity was not expected. For the proposed application in an MR prosthetic knee, where sedimentation is not a problem, nanoparticles are shown not be desirable option. This is believed to provide additional information to the MR fluid research community, especially for researchers developing MR fluids where off-state viscosity is of importance.

4. The effect of particle size on the characteristics of MR fluids is experimentally investigated. This has been researched to a large extent, both theoretically (Lemaire et al., 1995) and experimentally (Genc et al., 2002). The literature does not, however, provide the numerical data needed to make predictions for the goals of this project. The research presented here provides the quantitative data, needed to suggest a carbonyl iron powder for the proposed application (Gudmundsson et al., 2011). This is believed to provide valuable information to MR fluid designers and MR device designers.

5. A preliminary experimental investigation into the effect of mixing two grades of micron-sized particles is presented. This has been investigated by other authors, theoretically by Kittipoomwong et al. (2005) and experimentally by Foister (1997) and by Bombard et al. (2005), for example. The results of this study show that the off-state viscosity of MR fluids can be decreased by mixing two grades of micron-sized particles (Gudmundsson et al., 2011) which is in agreement with previous studies. At the same time, the on-state shear yield stress can be maintained when

mixing two grades of micron-sized particles (Gudmundsson et al., 2011) but an increase in on-state shear yield stress was not observed. MR fluids using a mixture of two grades of micron-sized particles are shown to be an attractive option for the proposed application.

1.4 Overview of the thesis

The thesis starts by introducing the application that motivates the study in Chapter Two. This is an adaptive MR prosthetic knee with a variable torque output. The output is controlled with a microprocessor that actively controls the magnetic field in the MR fluid based on sensors in the knee. The design of an MR rotary brake is described that utilizes the MR fluid in direct-shear mode.

Chapter Three describes an on-state and an off-state torque model for an MR rotary brake. The models are based on on-state and off-state characteristics of the employed MR fluid and the geometrical design of the device. The models are validated with torque measurements from a reference design of the device.

In Chapter Four, the models of Chapter Three are used to optimize the device for torque output. The device design is investigated as a single objective maximization problem and as a multi-objective maximization / minimization problem. The multi-objective approach explores the trade-offs between the on-state and the off-state torque of the device.

Chapter Five describes the MR fluid design procedure adopted for the prosthetic knee. The chapter lists the ingredients of the MR fluids and the constraints the effect the chose of ingredients. Twenty-two resulting MR fluid compositions are presented that will be evaluated for a potential application in a prosthetic knee.

Chapter Six first describes an experimental setup that is used to evaluate the MR fluids. The chapter then presents on-state and off-state rheological measurements for the twenty-two potential MR fluids. The MR fluids are ranked, for the proposed application, according to a figure of merit. The figure of merit is the ratio between the on-state shear yield stress and the off-state viscosity. Prominent MR fluids are selected for the prosthetic knee.

Chapter Seven describes MR fluid shear-yield stress models. The chapter starts be introducing a preliminary simple dipole model. The model is calibrated with magnetic characteristics of a particular carbonyl powder, resulting in correct order of magnitude predictions of shear-yield stress.

Finally conclusions and suggestions about further work are presented.

2 Magnetorheological (MR) Prosthetic Knee

This chapter introduces the application that motivates this research. This is an MR prosthetic knee equipped with an MR rotary brake actuator. The MR fluid in the actuator is sheared by densely pack steel blades in the fluid chamber, utilizing the fluid in direct shear-mode.

2.1 Background

Magnetorheological (MR) fluids are currently used in a variety of applications due to their property of varying viscosity under the influence of a magnetic field (Jolly et al., 1999; Carlson, 2005; Wereley, 2008). A sector in which MR fluids have been successfully introduced is prosthetic devices (Carlson et al., 2001). For example, MR fluids are used in prosthetic dampers (Biederman, 2002) and in prosthetic rotary disk brakes, utilizing the fluid in direct shear mode (Herr and Wilkenfeld, 2003; Deffenbaugh et al., 2004). An MR prosthetic knee is an example of a direct shear mode device (Jonsdottir et al., 2009; Gudmundsson et al., 2010) and this device is the motivation for the research. In this device, the field-induced characteristics and the off-state characteristics of the MR fluid are of equal importance. The field-induced shear yield stress determines how rigid the knee joint is, under the influence of a magnetic field, and the off-state viscosity determines how flexible it is, in the absence of a magnetic field.

Besides MR damping, the most common variable torque brakes that have been employed in prosthetic knees in the past are: dry friction brakes, where one material surface rubs against another surface with variable force, and viscous torque brakes, which use hydraulic fluid, squeezed through a variable sized orifice or flow restriction plate. Each of these technologies, as conventionally practiced in the field of prosthetics, can pose certain disadvantages. For example, the frictional pads tend to wear and thereby change the frictional characteristics of the brake and the torque response. Viscous torque brakes are susceptible to leakage of hydraulic fluid due to excessive pressure build up. The MR prosthetic knee can overcome most of the limitations of above technologies (Ossur, 2006; Deffenbaugh et al., 2001). The chapter will now describe the MR prosthetic knee.

2.2 MR rotary brake

The reference design of the prosthetic knee, manufactured by Ossur Inc., shown in Figure 2.1 can only support light weighted patients. The goal of this work is to investigate ways to increase the maximum obtainable torque of knee, for it to be able to support heavier patients without decreasing the flexibility of the knee joint. Heavier patients require a higher maximum braking torque when walking down a staircase, but still require a low off-state stiffness for comfortable movement in free motion.

Figure 2.1. An MR prosthetic knee joint and a carbon fiber prosthetic foot (Ossur Inc., 2011).

The problem is approached by deriving a device model that describes the on-state and off-state torque of the knee. Selected design parameters in this model are varied, to determine which changes can be made to the reference design in order to maximize the braking torque and the knee's operational range. Since the torque transmissibility of the MR devices, shown in Figure 2.2, greatly depends on the rheological properties of the MR fluid, it is important to fully understand its behavior for different conditions.

Figure 2.2. An adaptive MR prosthetic knee joint (Ossur Inc., 2011).

The power source in the actuator is a 3 cell Lithium-Ion battery, each cell having a voltage of 3.7 V when it is fully charged, which results in a total voltage of 11.1 V. The total voltage drops to approximately 9 V for near empty batteries. The voltage to the coil is controlled with a high speed MOSFET transistor. The actuator is equipped with current feed-back loop to ensure that the required current in the coil is obtained. This is necessary since a non-linear relationship has been observed between the current in the coil and the applied voltage. This gives a maximum power output of approximately 17 W and allows for over 24 hours usage of the prosthetic knee without a recharge. At the knee's rotational axis is an MR rotary brake actuator (Herr and Wilkenfeld, 2003; Deffenbaugh et al., 2004), shown if Figure 2.3.

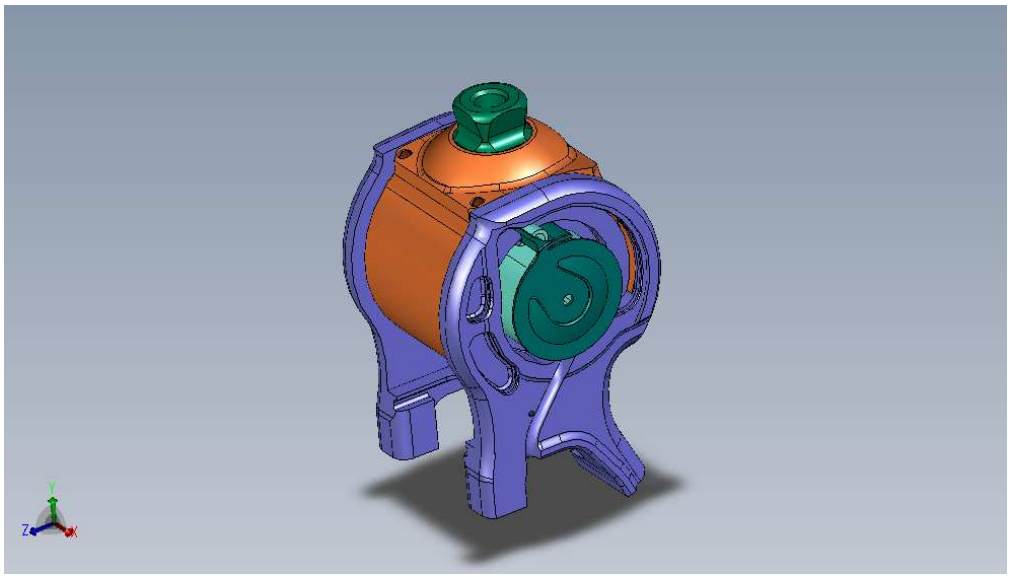

Figure 2.3. The MR rotary brake actuator (Ossur Inc., 2011).

This is a rotary disk type of an actuator, utilizing the MR fluid in direct-shear mode. The fluid is sheared by densely packed rotating blades with a micron-sized gap,

approximately 20 μm (Jonsdottir et al., 2009). The small gap between blades constrains the particle size and the solid loading in the MR fluid. The MR rotary brake in the knee joint is micro-processor controlled based on sensors in the leg. This allows for a user-adaptive control during gait (Herr et al., 2003). The brake consists mainly of a magnetic circuit, a fluid chamber and housing. An amputee, weighting 90 kg, requires a braking moment of approximately 40-45 Nm, when walking down stairs. This is what the current reference design of the knee joint can support. The motivation for this study is to increase the usability of the knee for heavier patients and for more demanding applications, like hill climbing. The aim is to increase the field-induced braking torque while at the same time consider how this will affect the off-state rotary speed of the knee joint and its weight. Figure 2.4 shows the inner parts of the device.

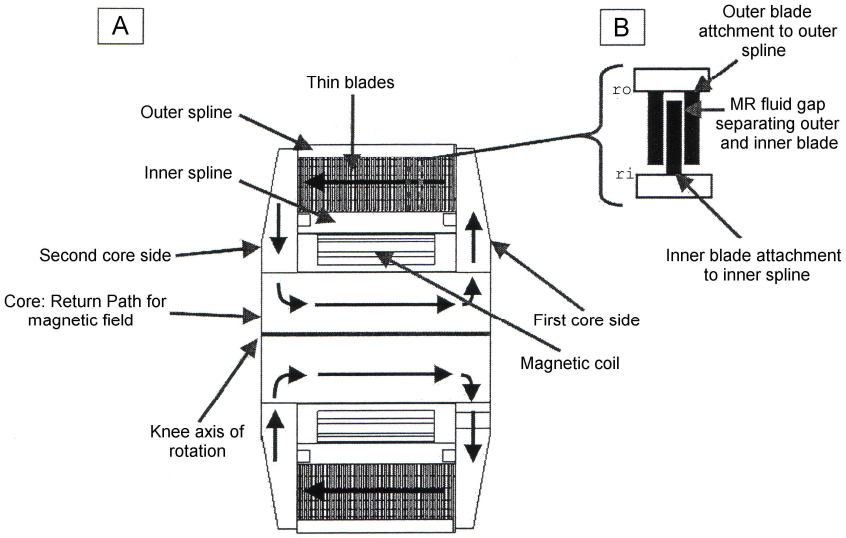

Figure 2.4. The configuration of the MR rotary brake actuator (Deffenbaugh et al., 2001).

The actuator consists of a magnetic coil which is fed with electrical current to generate a controlled magnetic field in the brake. The arrows inside the actuator, in Figure 2.4, show the direction of the magnetic flux. The core and the core sides are made of a cobalt-iron alloy, named Vacoflux (Vacuumshmelze, 2011). This alloy has a high magnetic saturation value. The outer and the inner houses are made of aluminum, nickel and titanium. The steel blades are arranged tightly, side by side in the chamber to enlarge the area that is affected by the shear force. The blades are connected alternately to the outer house (stator) and to the inner house (rotor). The MR fluid separates the stator from the rotor. The inner parts belong to the rotor while the outer house along with half of the blades belong to the stator. The stator is connected to the amputee's residual limb while the rotor is connected to the amputee's lower part of the leg (below the knee), producing the relative motion between the stator and the rotor. The gap between the blades, where the fluid resides, is small compared to the width of the blades. Without a magnetic field, the fluid flows freely between the blades. When a magnetic field is applied, carbonyl iron spheres in the MR fluid are drawn together, forming chains that extend from one blade to an adjacent one. As the knee rotates into flexion or extension, the thin rotary blades shear the particle chains to create resistance. The result is a varied fluid shear force within the knee, restoring more natural pelvic position during pre-swing and reducing fatigue levels.

This particular device introduces constraints on the particle size and the solid loading of the MR fluid in the device due to a small micro-sized gap between the rotating blades in

the actuator, shown in Figure 2.4. These constraints are considered in a MR fluid design procedure aiming to develop an optimal fluid for the proposed application.

3 An Actuator Model

An actuator analysis will now commence, analyzing and developing an MR rotary brake for the prosthetic knee. Mathematical models are developed that describe the on-state and the off-state rotary torque of the MR prosthetic knee joint and its weight. The applicability of the prosthetic knee joint to heavy amputees is decided by the field-induced torque of the MR rotary brake. The finite element method is used to evaluate the magnetic flux density in the MR fluid. The rotational speed is decided the off-state torque and the weight affects the usability of the knee joint. Low weight of the brake facilitates for heavy components like batteries to be installed in the prosthetic knee. The device and the models will now be described.

3.1 Background

The subject of this study is an MR rotary brake device to be used in a prosthetic knee joint. An axisymmetric view of the configuration of the magnetic circuit and the fluid chamber in the brake is shown in Figure 3.1, where r_i and r_o are the inner and outer radii of the fluid chamber, respectively.

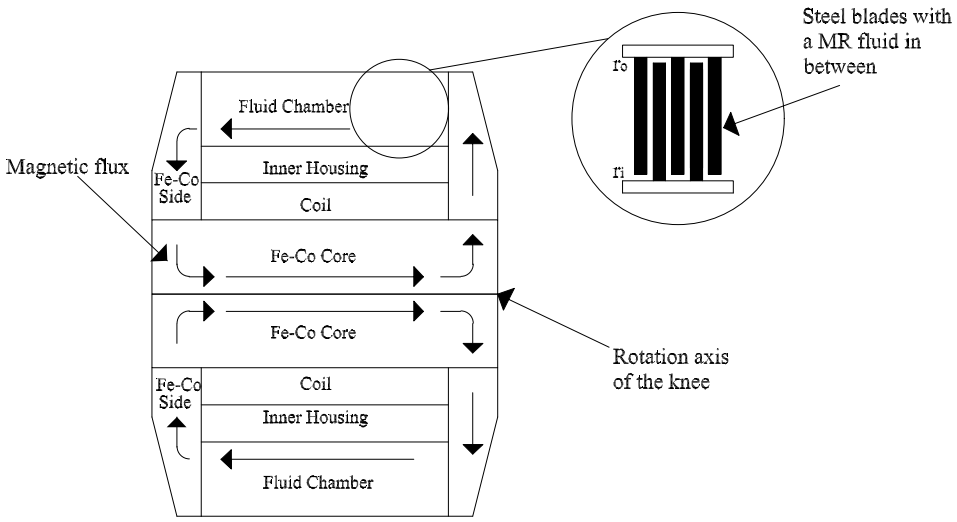

Figure 3.1. A schematic view of the layout of the magnetic circuit and the fluid chamber. The schematic is based on the original design of Herr et al. (2003) and Deffenbaugh et al. (2004).

The figure describes the original design of the brake from Herr et al. (2003) and Deffenbaugh et al. (2004). The magnetic circuit in the brake consists of a coil wound around a cobalt-iron alloy core. The magnetic field is directed towards the fluid via cobalt-iron alloy sides that are connected to the ends of the fluid chamber. The cobalt-iron alloy is chosen because of its high magnetic saturation value of 2.2 T (Jonsdottir et al., 2009). The gap between the blades, where the fluid resides, is micron-sized and small compared to the thickness of the blades. As the knee rotates into flexion or extension, the rotary blades shear the particle chains to create resistance. The result is a varied fluid shear force within the knee, restoring more natural pelvic position during pre-swing and reducing fatigue levels.

3.2 On-state torque model

The geometry of the brake determines the on-state torque output of the brake along with two MR fluid parameters; the shear-yield stress and the post-yield viscosity. The linear Bingham model (Philips, 1969) is used to represent the shear yield stress in the fluid. The MR fluid in the actuator, the size of the area that interacts with the fluid, and the magnetic flux density in the fluid, are factors that affect the field-induced braking torque. The braking torque is estimated by integrating the shear-stress, in the fluid, over half of the total area of blades. Only half of the area is used since only half of the blades are sheared by the MR fluid. The other half is stationary since they are connected to the stator of the actuator.

The yield part of the braking torque can be derived as follows and is shear-rate independent:

$$T_{yield} = \int_{r_i}^{r_o} n_{blades} \cdot r \cdot \tau_y(B) \cdot dA = 2\pi \int_{r_i}^{r_o} n_{blades} \cdot \tau_y(B) \cdot r^2 dr \tag{3.1}$$

where $\tau_y(B)$ is the field-induced shear yield stress in the fluid, r_i and r_o are the inner and outer radii of the fluid chamber, respectively. The yield part of the on-state torque is therefore:

$$T_{yield} = \frac{2\pi \cdot \tau_y(B) \cdot n_{blades}}{3}(r_o^3 - r_i^3) \tag{3.2}$$

The post-yield viscosity part of the braking torque can be derived as follows. The shear stress is given by:

$$\tau = \mu_{p-y} \cdot \frac{du}{dy} \tag{3.3}$$

where $\mu_{p\text{-}y}$ is the post-yield viscosity of the MR fluid. The velocity profile is denoted by u and is a function of the angular velocity, ω, and the radius, r, measured from the axis of rotation; that is:

$$u = \omega \cdot r \tag{3.4}$$

A linear velocity profile between the blades is assumed and therefore:

$$\tau = \mu_{p-y} \cdot \frac{\omega \cdot r}{d} \tag{3.5}$$

where d is the distance between the rotating blades in the fluid chamber. The braking force is:

$$dF = \tau \cdot dA = \mu_{p-y} \cdot \frac{\omega \cdot r}{d} \cdot 2\pi \cdot r dr \cdot n_{blades} \tag{3.6}$$

where n_{blades} is the number of blade gaps in the fluid chamber. The on-state post-yield part of the torque is therefore:

$$dT_{p-y} = r \cdot dF = \frac{2\pi \cdot \mu_{p-y} \cdot \omega \cdot n_{blades}}{d} \cdot r^3 dr \tag{3.7}$$

$$T_{vis} = \int_{r_i}^{r_o} dT_{p-y} = \frac{\pi \cdot \mu_{p-y} \cdot \omega \cdot n_{blades}}{2d} (r_o^4 - r_i^4) \tag{3.8}$$

Equation (3.8) describes the on-state torque contributed from the post-yield viscosity of the MR fluid. This part of the on-state torque depends on the shear-rate. Combining equations (3.2) and (3.8) gives the on state braking torque in the knee:

$$T_{on} = \frac{2}{3} \cdot \pi \cdot \tau(B) \cdot n_{blades} \cdot (r_o^3 - r_i^3) + \frac{1}{2} \cdot \frac{\pi \cdot \mu_{p-y} \cdot \omega \cdot n_{blades}}{d} (r_o^4 - r_i^4) \tag{3.9}$$

The field-induced shear stress in the MR fluid interacts with steel blades in the fluid chamber, producing the braking torque of the knee. Friction in oil seals and bearings is not included in Equation (3.9) since it is small compared to the field-induced shear stress in the MR fluid. A magnetic finite element analysis is employed to evaluate the magnetic flux density in the fluid and on-state characteristics of a reference MR fluid is used to quantify the analysis.

3.2.1 On-state characteristics of a reference MR fluid

The on-state braking torque model is based on shear-yield stress measurements for a PFPE-based MR fluid that is currently employed in the brake. The fluid was characterized with an Anton-Paar Physica MCR 100 rheometer (Anton Paar, 2011), using parallel plate geometry at a temperature of 20°C. Plates with a diameter of 20 mm were used with a gap size of 1 mm. The MR fluid shear yield stress curve is represented by:

$$\tau_y(B) = 29000 - 29000 \cdot \cos(\pi \cdot B) \tag{3.10}$$

where τ_y is the yield stress and B is the average MFD in the fluid. Figure 3.2 shows the shear yield stress curve for the reference MR fluid.

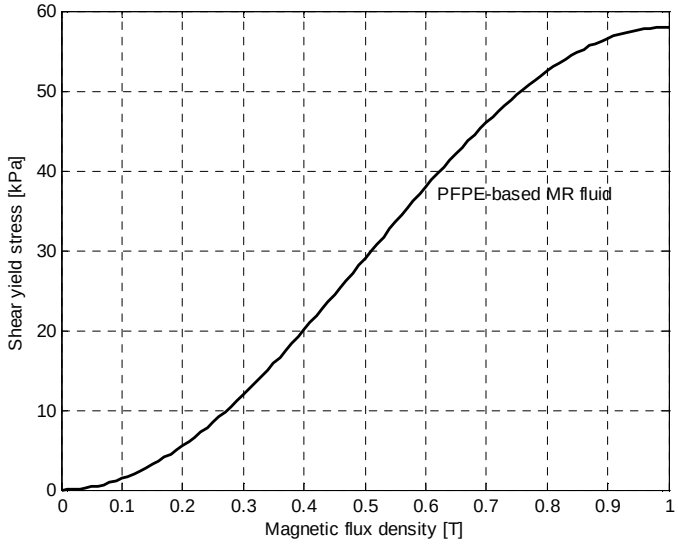

Figure 3.2. The shear-yield stress versus magnetic flux density for the reference MR fluid.

The shear yield-stress curve is in agreement with measured characteristis of MR fluid with a solid loading of 0.28 by volume and with the HS iron powder, shown in Chapter Six.

The post-yield viscosity of the reference MR fluid has been measured to be $\mu_{P\text{-}Y}$ = 4 Pa·s at a magnetic flux density of 0.55 T. It is obtained by fitting the linear Bingham model to a measured flow curve at 0.55 T. This value of the magnetic flux density is representative for flux values in the actuator. The angular speed is assumed to be 8.2 rpm which is representative for the working angular speed of the knee and it equals the speed in a test rig used to measure the torque of the brake. This defines the on-state MR fluid characteristics for the device model.

3.2.2 Magnetic finite element model

At the outset of this research, an existing two-dimensional finite element model of the magnetic circuit existed (Thorarinsson, Jonsdottir and Palsson, 2006a; Thorarinsson, Jonsdottir and Palsson, 2006b). The model is significantly refined in this work, in order to determine the magnetic fields in various components of the knee. The magnetic field in the MR fluid relates directly to the braking power of the knee via the shear yield stress curve of the MR fluid. The finite element analysis evaluates the magnetic flux density in the fluid and the yield stress curve gives the shear stress in the fluid. A coil current of 1.5 A is used which is the maximum obtainable with the current configuration of batteries in the knee.

The magnetic circuit consists of a Co-Fe alloy core and sides, and a braking fluid chamber, with an MR fluid contained between steel blades. The housing is made of titanium. Figure 3.3 shows the material configuration of the FE model.

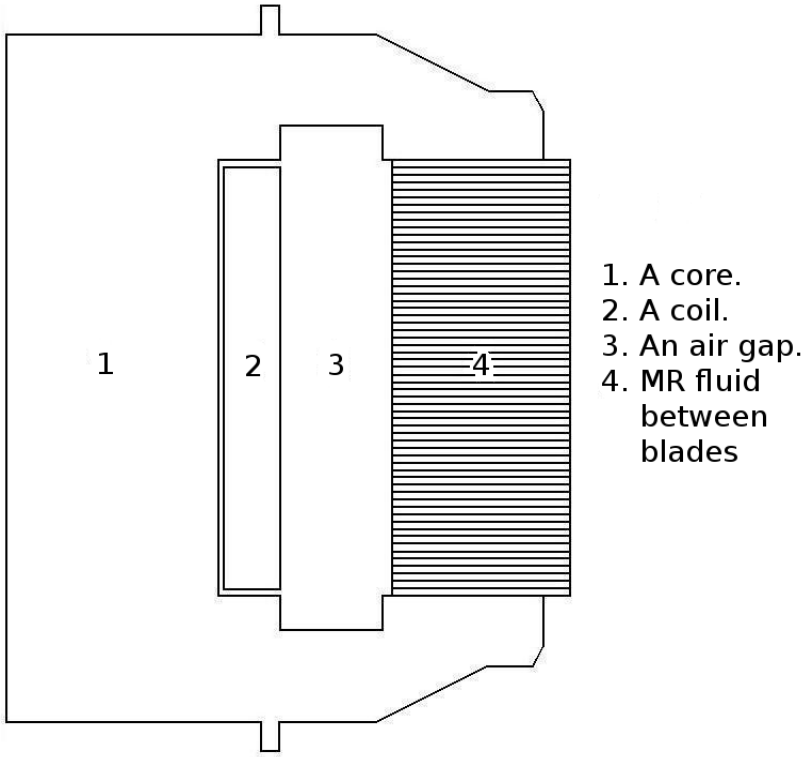

Figure 3.3: Schematic of a finite element model of the MR actuator.

Material 1 in Figure 3.3 is the magnetic Co-Fe core that magnifies the magnetic field, generated by the coil. Material 2 is the coil that generates the magnetic field. Material 3 in Figure 3.3 is an internal titanium housing that is modeled as air, since titanium is a non-magnetic material. Material 4 is the fluid chamber of the knee. The model includes the configuration details of the blades in the fluid chamber. At last, a large atmospheric area is modeled around the knee, simulating the surroundings of the knee.

A non-linear magnetic finite element (FE) analysis is used to estimate the MFD in the fluid. The commercial FE software Ansys (Ansys, 2011) is used in the analysis. The knee is approximately axi-symmetric and the model is therefore chosen as a 2D axi-symmetric model. The PLANE53 elements were used to model the magnetic flux density originating in a coil wound around the core. This element is a 8node 2D plane element, solely with electromagnetic degrees of freedom. The magnetic field is directed with a magnetic circuit through the MR fluid and back into the core. The magnetic circuit and its surroundings are all modeled with the PLANE53 elements where each material receives different magnetic permeability properties. An average MFD value in the fluid is calculated to determine a single value for the shear-yield stress in the MR fluid. Figure 3.3 shows an example of the FE analysis a reference design of the brake.

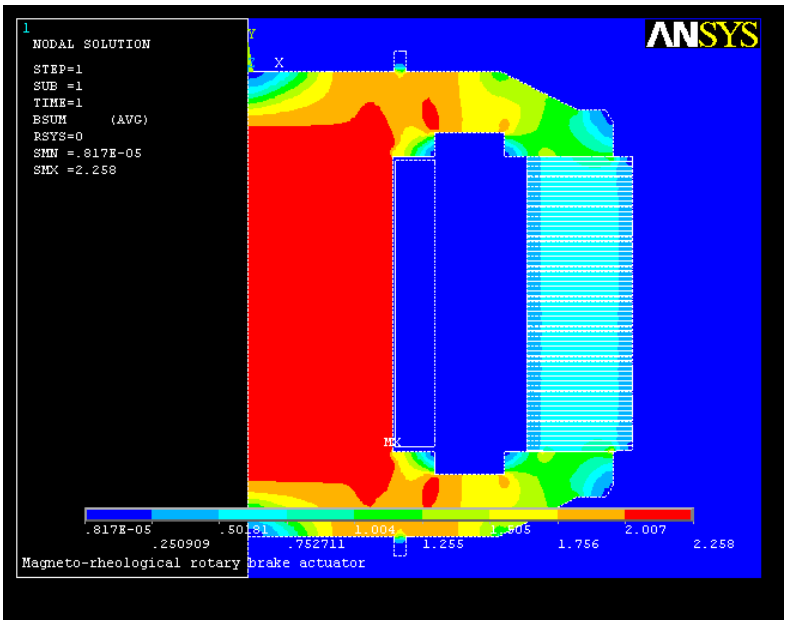

Figure 3.3 . A magnetic finite element analysis for a reference design of the brake.

The figure shows a saturated cobalt-iron core with a MFD of 2.2 T. The MFD in the fluid is approximately 0.6 T. The FE analysis shows that the variability of the MFD inside the fluid chamber is low.

Material properties (Jonsdottir et al., 2009) in the FE model are in the form of non-linear B-H curves which is the magnetic permeability of the materials, resulting in a non-linear FE analysis. Figure 3.4 shows the B-H curve for the Co-Fe alloy (Vacuumschmelze, 2007). Note that it has a magnetic saturation value of about 2.35 T.

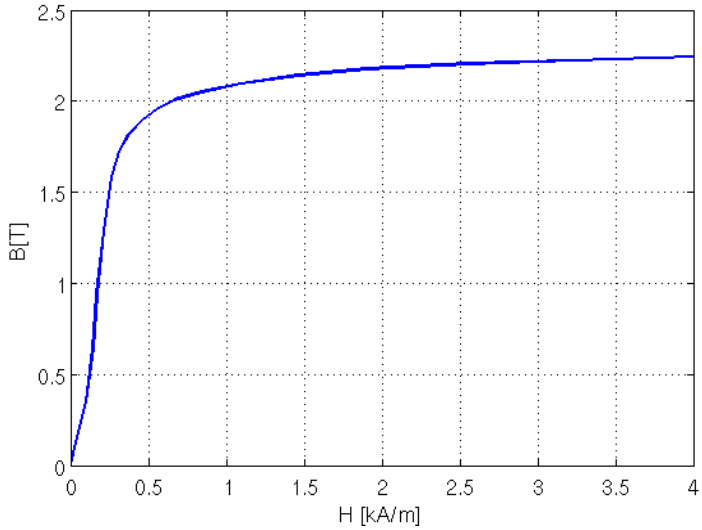

Figure 3.4. B-H curve for Cobalt-Iron alloy (Vacuumschmelze, 2011).

Figure 3.5 shows the B-H curve for the reference MR fluid (Jonsdottir et al., 2009).

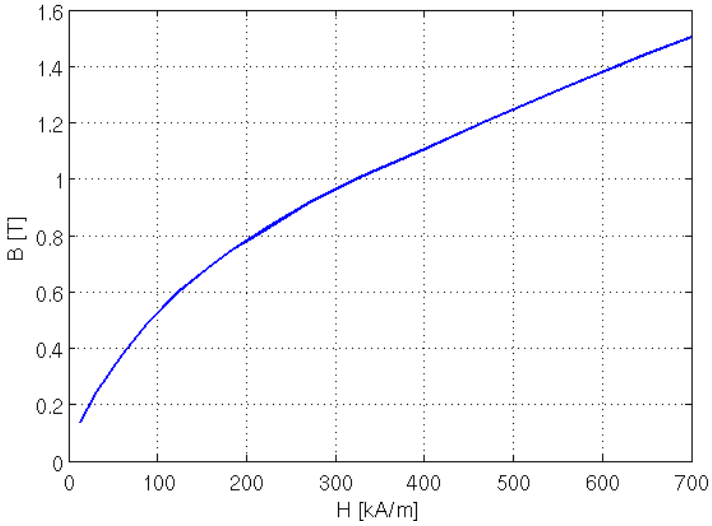

Figure 3.5: B-H curve for the reference MR fluid (Jonsdottir et al., 2009).

It can be seen that the MR fluid has a more linear magnetic property when the applied magnetic field is small, compared to the Co-Fe alloy. As the magnetic field increases, a gradual magnetic saturation is observed and consequently, the MR fluid yield stress saturates.

Figure 3.6 shows the B-H curve for the steel blades (Jonsdottir et al. 2009).

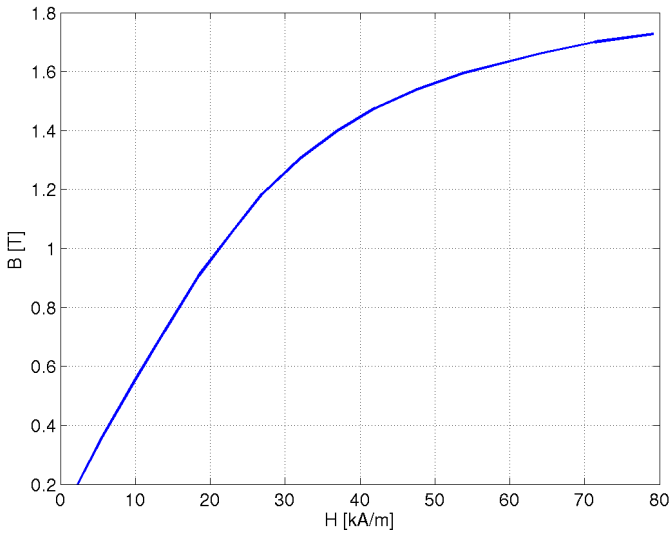

Figure 3.6. B-H curve for the steel blades in the fluid chamber.

The steel blade B-H curve has a lower saturation value than the Co-Fe alloy and reaches the saturation at a much higher excitation. The Co-Fe alloy is therefore a much better magnetic magnifier compared to standard steel.

The magnetic properties of the atmosphere are constant and approximately the same as of the vacuum. A constant μ = 1.257 x 10^{-6} H/m relates B and H and describes the magnetic behavior of the atmosphere.

The magnetic flux density in the fluid is a function of the geometry of the magnetic circuit, making the braking torque a function of additional parameters. Figure 3.7 shows the design parameters and the geometry of the brake.

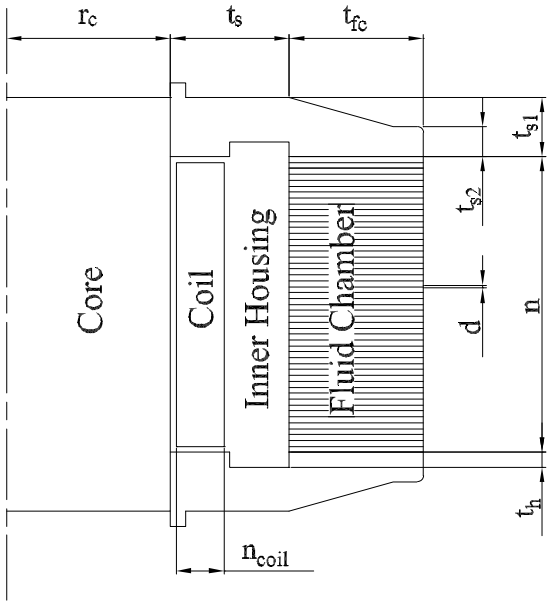

Figure 3.7. Geometry of the MR rotary brake and its design parameters.

It is an axisymmetric view where the axis of symmetry is at the center of the core. Table 3.1 shows a list of the design parameters. It includes a short description of each parameter.

Table 3.1. A list of design parameters.

Parameter	**Description**
r_c	Radius of the core
n_{coil}	Number of windings in the coil
t_{s1}	Initial thickness of the sides (at the core)
t_{s2}	Final thickness of the side (at the fluid chamber)
t_s	Start of side thickness reduction (distance from the core)
t_{fc}	Thickness of the fluid chamber
d	Distance between blades in the fluid chamber
n	Number of blades in the fluid chamber
t_h	Thickness of inner housing seat (side cut out)

The inner radius of the fluid chamber, r_i, is determined by the radius of the core, the size of the coil and the size of the inner house, as:

$$r_i = r_c + \alpha_{coil} \cdot n_{coil} + d_{ih} \tag{3.11}$$

where the thickness of coil per winding is denoted by α_{coil}, the size of the inner housing by d_{ih}. The inner radius is therefore not a design parameter. The thickness of the fluid chamber, t_{fc}, is used rather than the outer radius of the fluid chamber, r_o, where $r_o = r_i + t_{fc}$. The current amplitude in the coil is not a design parameter but is held to a constant value of 1.5 A. This is the maximum the voltage generator can generate, given the length of the coil

wire in the current design of the brake. This defines the device design parameters of the study, $\boldsymbol{x} = (r_c, n_{coil}, t_{s1}, t_{s2}, t_s, t_{fc}, d, n, t_h)$.

3.3 Off-state torque model

The geometry of the brake determines the off-state torque output of the brake along with one MR fluid parameter; the off-state viscosity. An off-state viscosity measurement of the reference MR fluid is used to quantify the model. The main factors affecting the off-state stiffness are: the inner and outer radii of the blades, the number of blades, the gap between the blades, the friction in bearings and oils seals, and the off-state viscosity of the MR fluid.

The off-state viscosity of the reference MR fluid is shown in Figure 3.8

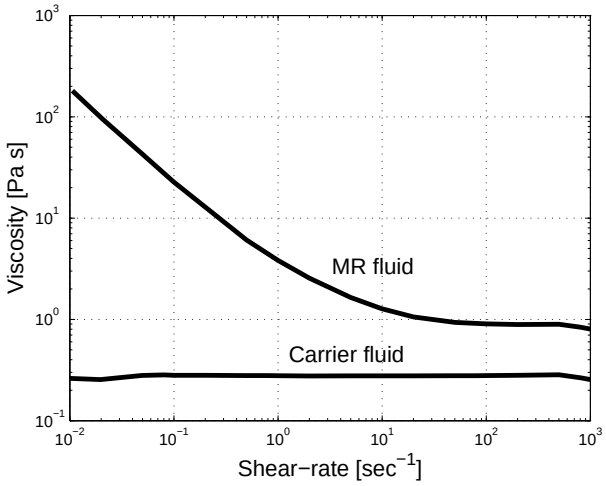

Figure 3.8. The off-state viscosity of the reference MR fluid.

It was measured using a StressTech rheometer using a coaxial cylinder geometry, with an inner and outer diameters of 25 mm and 27 mm, respectively, at a temperature of 20°C.

The off-state device model assumes a constant off-state viscosity of μ_{MR} = 0.9 Pa s. This is a reasonable assumption since a constant viscosity at high shear-rates is observed in Figure 3.8.

The off-state rotary stiffness of the brake is described by (Gudmundsson et al., 2010):

$$T_{off} = \frac{1}{2}\frac{\pi \cdot \mu_{off} \cdot \omega \cdot n}{d}(r_o^{\,4} - r_i^4) + T_b + T_o \tag{3.12}$$

where the off-state viscosity of the MR fluid is denoted by μ_{off}. The inner radius of the fluid chamber, r_i, is determined by the size of the core, the coil and the inner housing. The torque due to friction in bearings, T_b, has been measured to be 0.8 Nm at an angular speed of 8.2 rpm, and the friction in oil seals, T_o, has been measured to be 0.8 Nm, at the same angular speed.

3.3.1 Working shear-rate

A rough estimate of the shear-rate, assuming geometry values from a typical design of the knee (Gudmundsson et al., 2010) including a rotating speed of 5 rpm and a micron-sized gap of 20 μm, gives a shear-rate of approximately 500 s^{-1}, shown in Equation (3.13).

$$\dot{\gamma} = \frac{\omega \cdot r}{d} = \frac{5/60 \cdot 2\pi \cdot (r_o - r_i)/2}{d} \cong 500 s^{-1} \tag{3.13}$$

where angular speed is denoted by ω. Despite the low angular speed, the working shear-rate in the prosthetic knee is high due to the small micron-sized gap in the fluid chamber resulting in high shear-rates in the MR fluid. This defines the shear-rate dependent off-state viscosity that is used in the off-state torque model.

3.4 Weight model

The weight of the MR rotary brake is decisive in the total weight of the prosthetic knee joint and the below-knee prosthetic leg. The selected design parameters all relate to the magnetic circuit and the configuration of the fluid chamber. The total weight of the magnetic circuit, coil and the fluid chamber is:

$$M = V_{CoFe} \cdot \rho_{CoFe} + V_{Cu} \cdot \rho_{Cu} + V_{MR} \cdot \rho_{MR} + V_{Fe} \cdot \rho_{Fe} \tag{3.14}$$

where V is the volume of a material and ρ is the density of a material. The materials are: cobalt-iron alloy for the magnetic circuit, copper for the coil, PFPE oil and carbonyl iron powder for the MR fluid, and steel for the blades in the fluid chamber.

3.5 Model validation

To validate the proposed models, a test rig was used to measure the torque of the actuator, as a function of the current in the coil and the rotational speed. The test rig can be set to produce three different rotary speeds and the electric current can be adjusted to any value between 0.0 A and 1.5 A. Table 3.2 shows the results of the measurements, made on a reference design of the rotary actuator (Thorarinsson, 2006).

Table 3.2. Torque measurements made on a reference design of the actuator (Thorarinsson, 2006).

Coil current [A]	**Braking torque at a rotary speed of 1.4 rpm [Nm]**	**Braking torque at a rotary speed of 4.2 rpm [Nm]**	**Braking torque at a rotary speed of 8.2 rpm [Nm]**
0 (off-state)	1.0	1,2	2.4
0.2	6.4	7.8	8.9
0.4	13.1	15.2	17.4
0.7	23.6	26.5	29.1
0.9	29.7	32.6	35.3
1.0	32.8	35.4	37.6
1.1	35.3	37.4	39.7
1.3	37.9	39.9	42.3
1.5	39.7	41.7	43.8

A rotary speed of 8.2 rpm is believed to most closely represent the actuator in use. Table 5.2 shows the torque, in the absence of a magnetic field, to be 2.4 Nm at rotary speed of 8.2 rpm. The rotary speed in the models in this study is set to 8.2 rpm in all cases. Table 3.3 shows a comparison between the models predictions and the measured torque values at this rotary speed.

Table 3.3. A comparison between measured torque and modeled torque at a rotary speed of 8.2 rpm.

Coil current [A]	**Measured torque [Nm]**	**Predicted torque [Nm]**	**Model error [%]**
0 (off-state)	2.4	2.3	4
0.2	8.9	7.3	18
0.4	17.4	14.4	17
0.7	29.1	26.4	9
0.9	35.3	34.2	3
1.0	37.6	37.1	1
1.1	39.7	39.0	2
1.3	42.3	40.6	4
1.5	43.8	41.7	5

The table shows the device model to be in accordance with measured torque values in the prosthetic knee actuator. Based on the presented models, a design optimization will be performed.

4 Actuator Optimization

The geometrical design of an MR rotary brake is addressed in this chapter. This includes the design of the magnetic circuit and the geometry of the fluid chamber. The design is formulated as an optimization problem, aiming to maximize the braking torque. Subsequently, a multi-objective optimization problem is defined that considers three design objectives: the field-induced braking torque, the off-state rotary stiffness and the weight of the brake. Trade-offs between the three design objectives are investigated which provides a basis for informed design decisions regarding the qualities of the prosthetic knee.

4.1 Background

Optimization of MR structures has been investigated by various authors (Nguyen et al., 2007; Yang et al., 2008; Jonsdottir et al., 2009). This involves optimizing for, among other properties, the output response (Jonsdottir et al., 2009), the power consumption (Yang et al., 2008; Nguyen et al., 2008) and the volume of the structure (Nguyen et al., 2007) by varying the geometry of the device or the MR fluid composition (Yang et al., 2008). Structures utilizing the fluid in valve-mode (Nguyen et al., 2007 and 2008) have been optimized more thoroughly than structures utilizing the fluid in shear-mode. The focus of this study is on the optimization of a shear-mode MR rotary structure. The study demonstrates how multi-objective design optimization techniques can aid in the development of an MR rotary brake.

The prime consideration in existing studies has been on the field-induced responses, leaving the off-state response to a lesser attention. A parametric study has already been performed on the geometrical design of the MR rotary brake in question (Jonsdottir et al., 2009). This involved maximizing the braking torque of the knee but did not consider the off-state minimum rotary stiffness or the weight of the actuator. The previous study provides valuable insight into the influence of varying a single parameter in the model on the magnitude of the field-induced braking torque of the knee. The current study takes a wider perspective, looking at three design objectives and varying simultaneously all parameters. It maximizes the field-induced braking torque of the knee. This is important since it allows the knee to be able to support heavier users and to work in more demanding situations, such as hill climbing, for example. It minimizes the rotary stiffness of the knee in the absence of a magnetic field. This is important as it allows faster movements of the knee, when desired. Finally, the weight of the actuator is minimized for user comfort and to facilitate for the installment of heavy components, like batteries. It is realized that the design goals can not be addressed separately and to some extent, the design goals are contradictory.

4.2 Optimization problem definition

The actuator design problem is laid out as an optimization problem. Three objective functions are developed to represent the three design objectives. The optimization problem is a mixed integer-continuous problem with non-linear objective functions and non-linear constraints. First, the design problem is explored as a single objective problem. The single objective approach aims to maximize the field-induced strength, implementing the off-state rotary stiffness as a constraint. The constraint is set to a value that results in an acceptable rotary speed in the absence of a magnetic field, although a higher speed is desirable. This leads to a design problem, formulated as a multi-objective optimization problem. The three design objective functions represent the on-state braking torque, the off-state rotary stiffness and the weight of the brake. This approach gives interesting information on the interaction between three design objectives and valuable information about the design of the actuator.

4.2.1 On-state objective function

It is important to maximize the on-state braking torque of the actuator to facilitate the prosthetic knee for a wider usage. Objective function f_1 describes the field-induced braking torque and is based on Equation (3.9), and is given as:

$$f_1(\boldsymbol{x}) = n \cdot \tau_y(B) \cdot 2/3 \cdot \pi \cdot ((r_i + t_{fc})^3 - (r_i)^3) + \frac{1}{2} \cdot \frac{\pi \cdot \mu_{p-y} \cdot \omega \cdot n}{d} ((r_i + t_{fc})^4 - (r_i)^4) \quad (4.1)$$

To evaluate the objective function, a magnetic FE analysis is employed to estimate the magnetic flux density in the fluid. An average value for the magnetic flux density in the fluid is calculated giving a single shear yield stress value, $\tau_y(B)$, in the fluid for a given design parameter set. This completes the formulation of the first objective function.

4.2.2 Off-state objective function

It is important for the prosthetic knee joint to be able to rotate freely in the absence of a magnetic field as it is important for it to provide a rigid support under the influence of a magnetic field. Objective function f_2 describes the off-state rotary torque of the brake and is based on Equation (3.12), and is given as:

$$f_2(\boldsymbol{x}) = \frac{1}{2} \cdot \frac{\pi \cdot \mu_{off} \cdot \omega \cdot n}{d} \cdot ((r_i + t_{fc})^4 - (r_i)^4) + T_b + T_o \quad (4.2)$$

The parameters of objective function f_2 are the same as in objective function f_1 but fewer since the off-state rotary stiffness is unaffected by the strength of the magnetic field.

4.2.3 Weight objective function

Describing the material volumes as function of the design parameters gives objective function f_3 as:

$$\begin{aligned} f_3(\boldsymbol{x}) = {} & \rho_{CoFe}(\pi r_c^2(2t_{s1}+L_{coil})+\pi((r_c+t_s)^2-r_c^2)\cdot 2t_{s1} \\ & +\pi((r_i+t_{fc})^2-(r_c+t_s)^2)(t_{s1}-t_{s2}))+ \\ & \rho_{Cu}(n_{coil}\cdot 2\pi r_c\cdot\pi(d_{coil}/2)^2)+\rho_{MR}(n_{blades}\cdot d\cdot\pi((r_i+t_{fc})^2-r_i^2))+ \\ & \rho_{Fe}((L_{coil}-n_{blades}\cdot d)\cdot\pi((r_i+t_{fc})^2-r_i^2)) \end{aligned} \tag{4.3}$$

where L_{coil} and d_{coil} are constants representing the length and the diameter of the coil wire, respectively. This concludes the definition of the three design objectives.

4.2.4 Optimization problem

The design is approached in two ways. In a simpler approach, the rotary stiffness in the absence of magnetic field is represented as constraint in the optimization. A maximum of 2.4 Nm is allowed at a rotary speed of 8.2 rpm. The off-state torque value is the maximum tolerable off-state rotary stiffness and represents an acceptable rotary speed in the absence of a magnetic field. This value is the off-state rotary torque in a reference design of the actuator and whose value is shown in Table 3.3. Higher rotary speeds, in the absence of a magnetic field, are, however, desirable. This leads to the second approach, where the off-state rotary stiffness is represented as an additional objective function, treating the design problem as a multi-objective optimization problem. A third objective is also considered, the weight of the brake. The multi-objective approach shows the trade-offs between the on-state and off-state behavior and gives valuable information on design of the prosthetic knee.

To represent a limitation in the power capabilities of the batteries, a constraint is included in the optimization that limits the total length of the coil wire, to that of the reference design of the brake. This limits the total power consumption in the optimization and does, therefore, not reduce the capabilities of the batteries.
The optimization problem is defined as follows:

Approach 1:

max $f_1(\mathbf{x})$

subject to:

$f_2(\mathbf{x}) < 2.4$ Nm	This value is set has a constraint in optimization and limits off-state torque to that of the reference design of the brake.
$2\pi\cdot r_c\cdot n_{coil} < \pi\cdot 19.05\cdot 352$mm	The constraint is the maximum length of the coil wire based on that of the reference design.

Approach 2:

max $f_1(\mathbf{x})$ and min $f_2(\mathbf{x})$ and min $f_3(\mathbf{x})$.

subject to:

$$2\pi \cdot r_c \cdot n_{coil} < \pi \cdot 19.05 \cdot 352\text{mm}$$

The coil constraint in both approaches is due to a limitation in the power source of the actuator. The power source is 11.1 V and it can generate a maximum power of 17 W. The analysis assumes an unchanged power source. The optimization therefore implements a constraint on the total length of the coil wire or the wire resistance to that of the reference design of the actuator. This limits the analysis to the current power capabilities of the actuator.

4.2.5 Optimization algorithms

In approach 1, the single objective optimization, an evolution strategy algorithm (1+1)-ES (Coello et al., 2007) is used to maximize the field-induced braking torque. In approach 2, the multi-objective optimization, a particle swarm optimization (PSO) procedure (Coello et al., 2007) is used to map the trade-offs between the three design objectives. The PSO algorithm has been shown to have a fast rate of convergence (Coello et al., 2007) which is important for the current problem, since the evaluation of field-induced braking torque is computationally expensive. Also, evolutionary algorithms do not require any assumptions about the optimization problem, like differentiability of the objective functions for example. The PSO algorithm has been shown to perform well on a problem where continuity, differentiability or unimodality of the objective function is unknown (Ye et al., 2007). There is no single optimal solution for a multi-objective optimization problem. The solution space is, therefore, explored by inspecting a three dimensional trade-off surface for the three design objectives. This surface is called the pareto-front (Coello et al., 2007) and shows a set of solutions that exhibit what is best to be expected in the design of the brake with regards to the three design objectives.

4.3 Maximum on-state braking torque

Given a rational optimization process, the results of the single objective optimization procedure will now be investigated. Table 4.1 shows the optimal values of the design parameters compared to that of the reference design.

Table 4.1. Design parameter values for a maximum field-induced braking torque.

Parameter	**Optimized design**	**Reference design**
r_c	10.7 mm	9.5 mm
n_{coil}	310	350
t_{s1}	5.5 mm	4.2 mm
t_{s2}	3.5 mm	3.2 mm
t_s	14.0 mm	12.0 mm
t_{fc}	6.5 mm	5.0 mm
d	35 μm	20 μm
n	71	63
t_h	0.60 mm	0.80 mm

A maximum of 61 Nm modeled field-induced braking torque is achieved in the optimized design compared to a torque of 40-45 Nm in original design. The optimized design gives an off-state rotary stiffness of 2.4 Nm which equals the constraint representing the maximum tolerable off-state rotary stiffness. The mean magnetic flux density in the fluid is 0.57 T. The MR fluid is not saturated at this value as its shear yield stress curve in Figure 3.2 shows. Gains can, therefore, be expected in the braking torque by increasing the magnetic flux density in the MR fluid. The coil wire length constraint, however, restricts the size of the cobalt-iron core as a bigger core results in a longer wire for given number of windings. This result in a loss of current amplitude in the coil using the voltage generator currently employed in the brake. A core size of r_c = 10.7 mm is obtained, given the presented constraints, which represents the optimal design. This is a considerable larger core compared to that of the reference design, with a value of 9.5 mm.

Comparing the optimized design to the reference design of the MR rotary brake, Table 4.1 shows the parameter values for the current design of the brake compared to that of the optimized design. A measured braking torque for the current design of the prosthetic knee, at a rotary speed of 8.2 rpm, is 43 Nm, at maximum current amplitude of 1.5 A. The most prominent changes, implied by the optimization, are a bigger cobalt-iron core, fewer coil windings to facilitate for a bigger core, increased number of blades, larger blades, and a larger gap between blades. A bigger core increases the magnetic flux density in the MR fluid as the FE analysis has shown the core to be saturated at current amplitude of 1.5 A in the coil. A bigger core also increases the magnetic flux density in the fluid although the number of windings in the coil is decreased to maintain a constant wire length. Increasing the number of blades and their size has a strong effect on both the field-induced braking torque and the off-state rotary stiffness. The negative effect on the off-state behavior can however be countered with a larger gap between the blades. This holds the off-state rotary stiffness below a tolerable value of 2.4 Nm while an increased gap has a lesser effect on the magnetic flux density in the fluid. This results in a higher field-induced braking torque without increasing the off-state rotary stiffness.

This simple design approach has suggested interesting changes in the design of the MR rotary brake and will help in future development of the knee. This approach does, however, tend to over-size the magnetic circuit as it ignores the weight of the brake. It, also, does not consider opportunities to decrease the off-state rotary stiffness. A multi-objective design optimization technique is applied to the design problem to obtain more detailed information on the design of the brake.

4.4 Minimum off-state rotary stiffness and weight

Interestingly for the designer, a multi-objective optimization procedure produces a whole set of solutions that all are optimal with respect to the three design objectives. That is, no design is strictly better than another with respect to all three design objectives. Figure 4.1a and b show all optimal solutions in three dimensional space where the x-axis is the off-state rotary stiffness, y-axis is the weight and the z-axis is the field-induced braking torque. The figures are obtained using a cubic interpolation on all designs found to be on the trade-off surface.

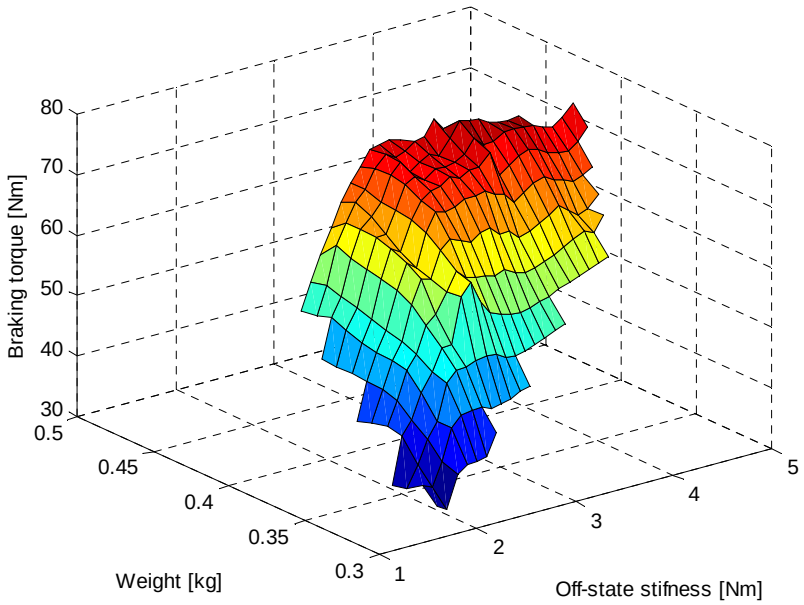

Figure 4.1a. The pareto-optimal solution set, representing a trade-off surface in three dimensional objective space.

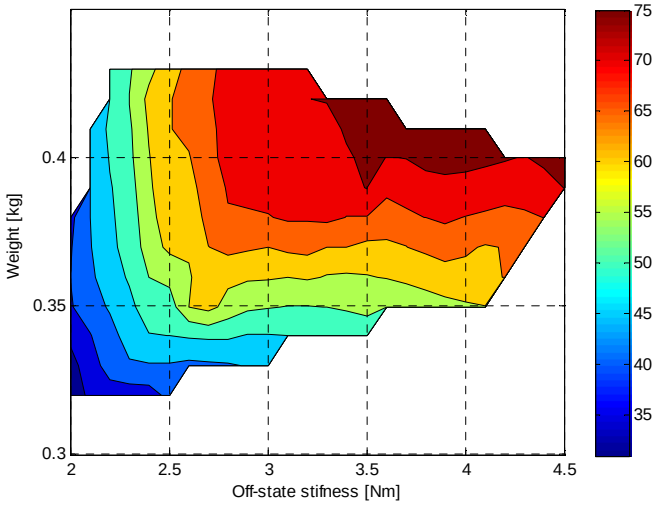

Figure 4.1b. The pareto-optimal solution set as contour plot, representing the trade-offs between the three design objectives.

The figures can give rise to various interpretations. It shows that low weight and low off-state rotary stiffness are not contradictory objectives. Designs exist with a low weight and a low off-state stiffness. The figures also show that a higher on-state braking torque results in higher weight and higher off-state stiffness. Clearly, a solution with a high field-induced braking torque is also high on weight and off-state rotary stiffness. A steep increase in field-induced braking torque is observed in Figure 4.1a at low values of the off-state rotary stiffness, ranging from 2.0 Nm to 3.5 Nm. For a higher value of off-state stiffness, the braking torque does not increase, implying a maximum in on-state behavior at an off-state stiffness of approximately 3.5 Nm. For the designer, this introduces trade-off decisions between design objectives. For example, if an off-state stiffness of 2.4 Nm is allowed, this results in a braking torque of approximately 60 Nm. Another approach would be to decide the weight of the brake and use the data to determine what braking torque is to be expected as a function of the off-state rotary stiffness. The set of optimal solutions is, therefore, a good basis for informed design decision in the development of the MR rotary brake.

The field-induced braking torque and the off-state rotary stiffness are design objectives that deserve more attention, in this particular application, rather than the weight. This is because the weight of the magnetic circuit and the fluid chamber is a small percentage of the total weight of the prosthetic leg. The weight of the prosthetic leg is approximately 5 kg and is comparable to that of a healthy leg of an average person. Figure 4.1 shows the weight of the magnetic circuit and the fluid chamber to be between 0.3 kg and 0.5 kg. Despite this fact, it is important to include the weight objective, since it prevents the optimization procedure to oversize the magnetic circuit and introduce unnecessary costs, weight or volume. Volume constrained designs, of MR structures have, been studied in more details by other researchers (Nguyen et al., 2007).

To visualize the trade-offs between these two objectives, an optimal curve is investigated in a two dimensional space ignoring the third design objective. This is done by selecting the optimal solutions without considering the value of the weight. Figure 4.2 shows a trade-off curve for the field-induced braking torque and the off-state rotary stiffness.

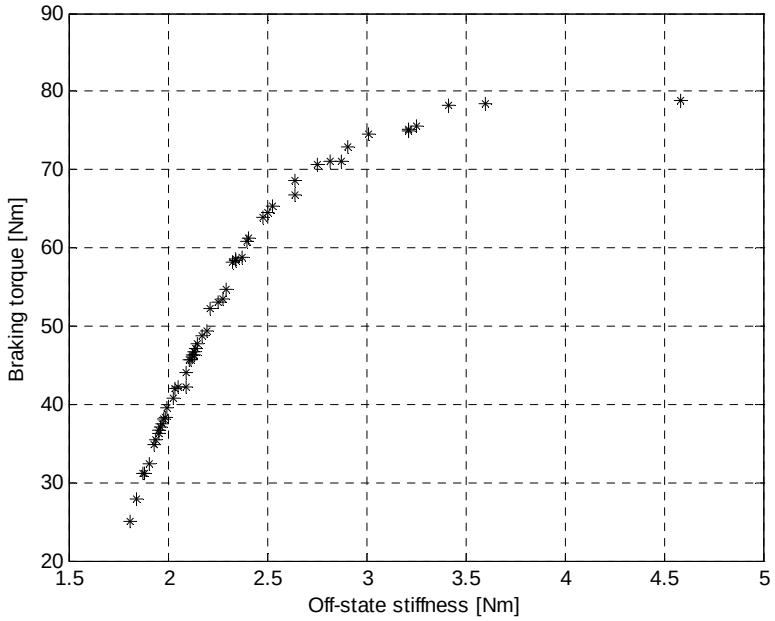

Figure 4.2 A pareto-optimal solution set, representing a trade-off curve in two dimensional objective space.

The figure shows how the off-state low limit moves as the on-state high limit increases. At an off-state low limit of 2.4 Nm the on-state high limit is approximately 60 Nm, which is in agreement with results obtained with the single-objective optimization. Surprisingly, there is an approximate linear relationship between the optimal braking torque and the optimal off-state rotary stiffness at low values of the off-state stiffness. The slope of the curve at an off-state stiffness of 2.4 Nm is approximately 20 Nm/Nm. This means that for every 1 Nm increase in field-induced braking torque, a 0.05 Nm increase in off-state rotary stiffness is expected. This is a design rule of thumb and is what is to be expected based on hundreds of simulated design cases.

Figure 4.2 also shows that optimal curve flattens out at high values of the off-state rotary stiffness. Gains in braking torque can be expected by allowing the off-state rotary stiffness to increase up to a value of 3.5 Nm. Negligible gains can be expected when exceeding this value.

The optimal values for the design parameters will now be investigated, which are behind the optimal designs in Figure 4.2. The multi-objective approach has produced a whole set of solutions that are said to be pareto-optimal, meaning that no solution exists that has, both, a higher field-induced torque and a lower off-state rotary stiffness. Figure 4.3 shows the values of the core size, r_c, and fluid chamber size, t_{fc}, for the pareto-optimal set, as a function of the field-induced braking torque.

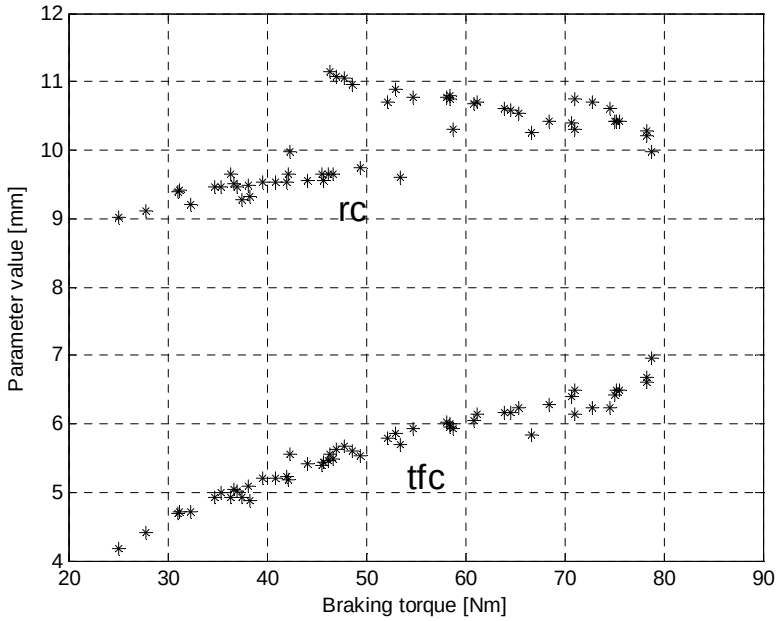

Figure 4.3. Values for the core size, r_c, and the fluid chamber size, t_{fc}, as a function of the field-induced braking torque, from the pareto-optimal set.

Figure 4.3 shows that with an increasing fluid chamber size, the braking torque increases. The larger the area of the blades shearing the fluid, the larger the field-induced braking torque. The core radius does not exhibit this simple linear relationship. It is coupled with the number windings in the coil. The highest braking torque is exhibited with a core radius of approximately 10 mm, with all other parameters free to take any feasible value. A magnetic FE analysis has shown the cobalt iron core to be saturated, at low values of the core size, at a maximum current amplitude of 1.5 A. This means that gains in braking torque can be expected by increasing the core size, at low values. At larger core sizes, the braking torque is shown to decrease, with an increasing core size. This is believed to be due the decreasing number of coil windings due to the coil wire length constraint. The increase in fluid chamber size has a negative effect on the off-state rotary stiffness. The negative effect can, however, be countered with a larger gap between the blades.

Figure 4.4 shows the number of blades in the fluid chamber, n, as a function of the field-induced braking torque for the pareto-optimal set. All other parameters are free to take any feasible value.

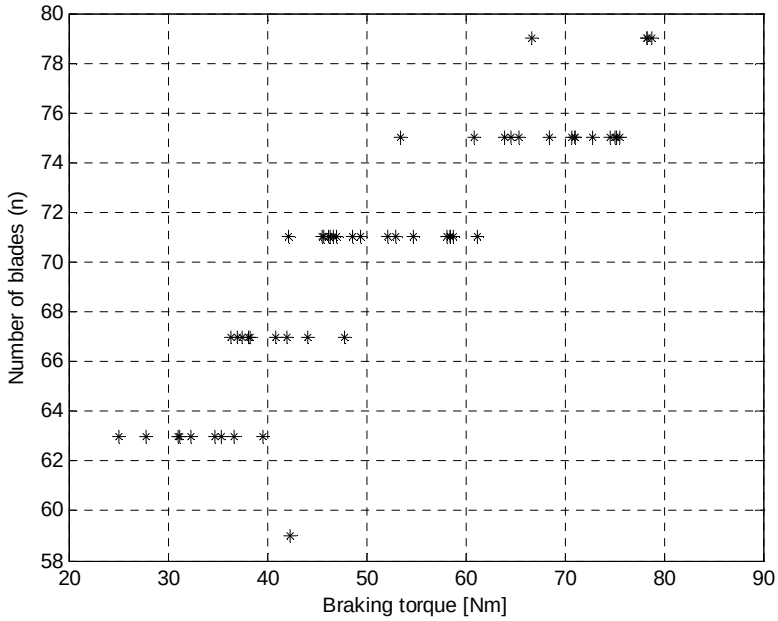

Figure 4.4. Values for the number of blades, n, as a function of the field-induced braking torque, from the pareto-optimal set.

The trend is that an increased number of blades results in a higher braking torque. The number of blades is increased in a set of fours due to manufacturing reasons. Again, the increase in off-state rotary stiffness due to the augmented number of blades can be reversed with an increase in gap size, as Figure 4.5 shows. Figure 4.5 shows the values of the gap size, *d*, for all solutions in the pareto-optimal set, as a function of the off-state rotary stiffness.

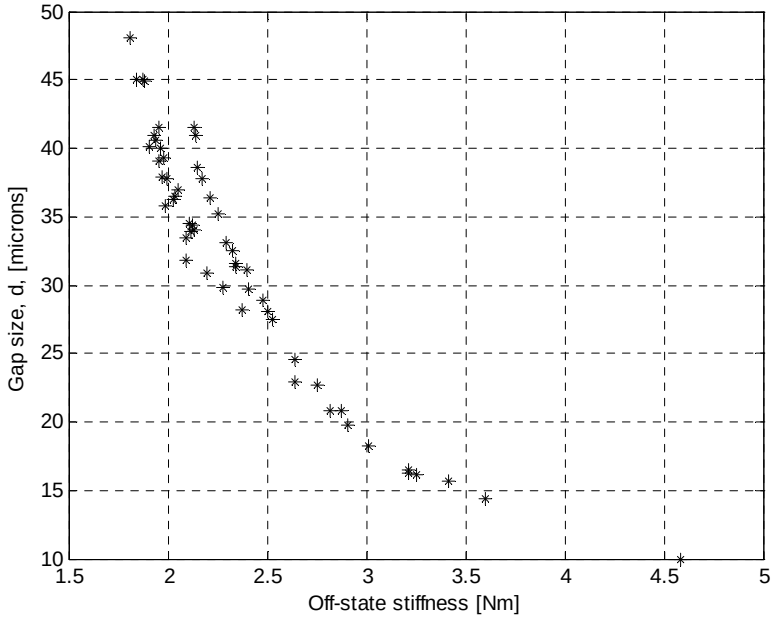

Figure 4.5. Values for the gap size, *d*, as a function of the off-state rotary stiffness, from the pareto-optimal set.

It can clearly be seen how the off-state rotary stiffness decreases with an increasing gap size. For an off-state rotary stiffness of 2.4 Nm, an optimal value for the gap size, *d*, is approximately 30-35 μm. This is a considerably larger gap when compared to a gap size of 20 μm in a reference design of the brake. The analysis implies that a greater number of blades and a greater gap size is better suited for the current application.

4.5 Summary

The design of the MR rotary brake in the prosthetic knee can be approached in various ways. The study shows how design optimization techniques can aid the design of the brake. The design is a trade-off between many objectives and the multi-objective approach aims to select the appropriate balance between the selected design objectives. Maximizing the field-induced braking torque has strong negative effect on the off-state rotary stiffness. A design with a maximum braking torque is clearly the worst solution with respect to the off-state rotary stiffness. It is, therefore, a design decision to select the highest tolerable off-state rotary stiffness and to use the valuable simulation data to determine the design parameters for the optimal design.

The analysis implies an optimal core size of 10.7 mm, an optimal gap between blades of 30-35 μm, and an optimal number of blades to be equal to 71. This allows the off-state rotary stiffness to remain at a maximum tolerable value of 2.4 Nm. Given this, a design can be obtained with a field-induced braking torque of 60 Nm. This is a considerably higher braking torque to that of 40-45 Nm for the reference design. The simulation data can be used to obtain further optimal parameter values, for a higher or a lower off-state rotary stiffness. This can aid the designer in making informed design decisions on further developments of the MR rotary actuator in the prosthetic knee.

5 MR fluid design

Motivated by the use of MR technology in an actuator for a prosthetic knee (Deffenbaugh et al., 2004; Jonsdottir et al., 2009; Ossur Inc., 2011), this study investigates MR fluids with a potential application in small devices. In the aforementioned prosthetic knee actuator, the MR fluid is contained between a number of thin steel blades that move relative to one another. As the knee rotates into flexion or extension, the blades shear the particle chains to create resistance; the result is a varied fluid shear force within the knee. The MR fluid gap in the knee actuator is micron-sized and hence, in order for the fluid to be active in the gap, it can not be loaded with particles bigger than a few microns. Due to this size limitation, the research looks towards small micron-sized particles and nano-sized particles as a feasible option for the MR fluid compositions to be used in the actuator. Low solid loadings are preferred due to problems injecting fluids with high solid loading into the small actuator.

5.1 Background

A common goal in the design of MR fluids is to have a high yield-stress, good dispersion stability, and keep a reasonably low off-state viscosity (Goncalves, Koo and Ahmadian, 2006; Wang and Gordaninejad, 2008). The same holds true for MR fluids designed for prosthetic devices. The performance characteristics of the knee joint relate directly to the MR fluid. The viscosity of the carrier liquid affects the sedimentation stability of the MR fluid and hence the durability of the knee. The capability of the knee joint to rotate fast, in the absence of a magnetic field, is affected by the off-state viscosity of the MR fluid. Furthermore, the field-induced shear yield stress of the MR fluid determines the ability of the knee to provide a rigid support.

Perhaps the most widely employed technique for increasing the yield stress in MR fluids is increasing the volume fraction of iron powder. However, it is well documented that increasing the particle loading will increase the field-independent plastic viscosity of the fluid (Goncalves et al., 2006). The current work aims to increase the strength of an MR fluid without increasing to a large extent the concentration of solid particles and also to explore means to reduce the off-state viscosity. Previous studies do not provide the quantitative data needed to make an informed decision about a potential MR fluid for the prosthetic device. The fluid design endeavor is aiming to tailor an MR fluid for the proposed application, given a set of fluid design constraints relating to the size of the actuator. Prominent MR fluid compositions are selected for the MR prosthetic knee.

In general, magnetorheological (MR) fluid compositions can vary widely. However, the majority of existing MR fluids are composed of micron-sized iron particles suspended

in a carrier fluid (Carlson, 2005). Common carrier fluids are silicone-based, hydrocarbon-based and water-based (Jolly et al., 1999). An example of MR fluid structure can be seen in Figure 5.1.

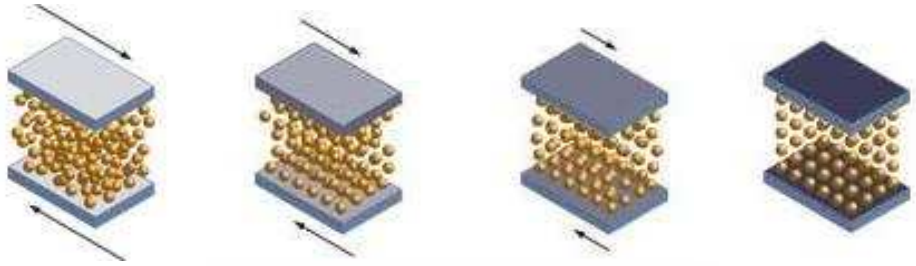

Figure 5.1. MR fluid off-state and on-state structure.

The effect of particle size and particle size distribution on the on-state and the off-state rheological behavior of MR fluids have been studied by several research groups (Lemaire et al., 1995; Genc and Phule, 2002; Bombard et al., 2005). Lemaire et al. (1995) have investigated the field-induced shear stresses at low solid concentrations and low magnetic field strengths. They show that the on-state yield stress will increase with particle size, for small particles (approximately 1 μm), but to is independent of particle size for large particles (approximately 50 μm). A yield stress that is independent of particle size relies on the magnetic energy to be large compared to the thermal energy. Genc and Phule (2002) experimentally investigated the effect of particle size (2 μm and 7-9 μm) on the on-state rheological characteristics of MR fluids. They reported the coarse particles to have higher shear yield stresses compared to the fluids using the fine particles. They suggested this to be due to the finer particles having a smaller magnetic saturation value.
The on- and off-state rheological behavior of bimodal MR fluids has been studied experimentally by Trendler and Böse (2005). They reported the off-state viscosity to decrease with an increasing ratio between coarse particles (6.7 μm) and the fine particles (1.8 μm). They also reported a bimodal MR fluid (33 % coarse particles / 67% fine particles) to have higher field-induced shear stresses when compared to the corresponding unimodal fluids. Foister (1997) and Weiss et al. (2000) have also used bimodal size distributions to increase the yield-stress while simultaneously reducing the off-state viscosity of MR fluids.

Ternary mixtures have been studied by Ierardi and Bombard (2009), aiming to maximize the shear yield stress and minimize the off-state viscosity. The minimum off-state viscosity was found to be a mixture of the coarse (9 μm) and fine (1.7 μm) powder, leaving out the medium powder (6 μm), with 32% coarse powder and 68% fine powder. The maximum shear yield stress was found to be a composition made solely of the coarse powder (no blend).

In addition to experimental evaluations, the on-state shear yield stress in bimodal MR fluids has been simulated, at the particle level, by Kittipoomwong et al. (2002; 2005) and Ekwebelam and See (2009). They reported bimodal MR fluids to have a higher field-induced yield stress when compared to unimodal MR fluids. Kittipoomwong et al (2005) also reported that the enhancement of the on-state shear yield stress in bimodal MR fluids is due to the tendency of the smaller particles to induce the larger particles to form more chainlike aggregates.

The rheological properties of conventional MR fluids have been researched extensively; see, for example, Wang and Gordaninejad (2008). It is well established that the shear yield stress can be increased by simply increasing the volume fraction of iron particles (Carlson, 2005; Foister, 1997; Genc and Phule, 2002; Ginder and Davis, 1994; Rabinow, 1951). A clear drawback, however, is that an increase in particle loading, increases the field-independent plastic viscosity of the fluid (Barnes, Hutton and Walters, 1989). It has been demonstrated that the yield stress is related to particle sizes and particle size distributions. For example, bigger particles exhibit higher yield stresses than smaller particles because they have a higher magnetic saturation value (Genc and Phule, 2002; Ginder and Davis, 1994). Furthermore, bidisperse suspensions have demonstrated higher yield stresses than unimodal fluids (Foister, 1997; Kittipoomwang, Klingenberg and Ulicny, 2005; Trendler and Böse, 2005).

All of the studies mentioned above, deal with micron-sized particles. When the size of the particles becomes smaller, Brownian motion may reduce the strength of the MR fluids, although it can aid in stabilizing against sedimentation. Several researchers have studied the effect on rheological behavior of adding nano-sized particles to MR fluids. Lemaire et al. (1995) studied the influence of particle size on the rheological behavior and found that if the ratio of magnetic interaction energy to thermal energy is much larger than unity, the yield stress increases with particle size. Kormann et al. (1996) made stable fluids with nano particles in polar liquids, but reported a low yield stress. Rosenfeld et al. (2002) and Poddar et al. (2004) prepared fluids with nano-sized iron powders, micron-sized powder and hybrid fluids, that is, a mixture of micron-sized and nano-sized particles. Both groups found that the micron-scale fluid exhibited the highest yield stress. However, Chaudhuri et al. (2005) and Wereley et al. (2006) found that replacing micro particles with nano particles, in small concentrations, tended to increase the field dependent yield stress. Furthermore, the nano particles reduced the sedimentation rate (Wereley et al., 2006). Similar results were seen by Park, Song and Choi (2009). Burguera et al. (2008) found that yield stress decreased with increasing concentration of nano particles, although stability was improved. Fang et al. (2009) have studied the effect of carbon nanotubes on sedimentation stability and yield stress. Finally, Lopez-Lopez et al. (2009) analyzed the dependence on rheological behavior of cobalt powder for particle diameters in the range 50 nm to 1 μm and found that particle size did not have much influence on the MR response for particles larger than 100 nm.

Intrigued by the studies mentioned above, the focus of this project is on developing MR fluids suitable for a particular application in a prosthetic device. An MR fluid composition is sought that gives a suitable balance between the shear yield stress and off-state viscosity. As previous studies on MR fluids, containing nano-sized particles, have focused on improved yield strength and sedimentation stability, this work provides a comprehensive experimental investigation of the field-induced shear yield stress versus the off-state viscosity for a number of different fluid mixtures.

5.2 An MR fluid figure of merit function

In the prosthetic knee, the on-state and the off-state braking torques are of equal importance. It is desirable for the knee joint to be as rigid as possible, under the influence of a magnetic field, and to be as flexible as possible, in the absence of a magnetic field. The on-state and the off-state torque are described by Equation (5.1) and (5.2), respectively (Gudmundsson et al., 2010),

$$T_{on} = \frac{2}{3} \cdot \pi \cdot \tau_y(B) \cdot n \cdot (r_o^3 - r_i^3) + \frac{1}{2} \cdot \frac{\pi \cdot \mu_{p-y} \cdot \omega \cdot n}{d} (r_o^4 - r_i^4) \quad (5.1)$$

$$T_{off} = \frac{1}{2} \frac{\pi \cdot \mu_{off} \cdot \omega \cdot n}{d} (r_o^4 - r_i^4) \quad (5.2)$$

where T_{on} is the on-state torque and T_{off} is off-state torque. The off-state viscosity of the MR fluid is denoted by μ_{off} and the field-induced shear yield stress as $\tau(B)$ where B is the magnetic flux density in the fluid. The post-yield viscosity of the MR fluid is denoted by μ_{p-y}. The geometry of the rotary brake is defined by the design parameters r_i, r_o, d and n (Gudmundsson et al., 2010), shown in Figure 3.7, where r_i and r_o are the inner and outer radii of the rotating blades, d is the gap size and n is the number of blades in the fluid chamber.

A figure of merit function for the prosthetic device is the ratio between the field-induced torque and the off-state torque, shown in Equation (5.3),

$$F = \frac{\frac{2}{3} \cdot \pi \cdot \tau \cdot n \cdot (r_o^3 - r_i^3)}{\frac{1}{2} \cdot \frac{\pi \cdot \mu_{off} \cdot \omega \cdot n}{d} (r_o^4 - r_i^4)} = C \cdot \frac{\tau}{\mu_{off}} \cdot d \cdot \frac{(r_o^3 - r_i^3)}{(r_o^4 - r_i^4)} \quad (5.3)$$

where F is the figure of merit and defines the torque range of the device. To simplify the equation, the shear yield stress and the post-yield viscosity have been combined to a single shear stress value, denoted by τ, at a shear-rate of 500 s^{-1}, which is the working shear-rate in the knee. From this simple analysis, it can be seen that this particular figure of merit F, for the MR prosthetic device, can be improved by increasing the ratio between the field-induced yield stress and the off-state viscosity. Similar figures of merit are shared by other MR applications (Jolly et al., 1999). The effect of the gap size, d, the radii of the blades, r_o and r_i, will be explored in the actuator design sections, showing optimal values for these parameters for the defined design objectives. The investigation will pursue the on-state to of-state ratio of the MR fluids in Chapter Six by experimentally evaluating selected MR fluid compositions for the MR prosthetic knee.

5.3 Base fluid

The base liquid for all samples is a relatively heavy and fairly high viscosity perfluorinated polyether (PFPE) oil (Hsu et al., 2006; Gudmundsson et al., 2009). This base fluid has attractive thermal properties and enhances sedimentation stability. The base fluid is composed of two PFPE oils. It is 95% NYE UNIFLOR^{TM} 8510 (Nye Lubricants, 2011) and 5% Krytox^{TM} 157-FSL (Dupont, 2011), the latter being a dispersion agent and will keep the particles dispersed in the liquid. A PFPE liquid is a chain of carbon, oxygen and fluorine atoms where the molecular structure can be either linear or pendent. The carrier liquid employed has a relative density of approximately 1.9 compared to that of water. It has a viscosity of approximately 0.3 Pa·s which promotes sedimentation stability for the MR suspensions. Among other applications for PFPE oils are lubricants in hard disk drive systems (Choi et al., 2005) and generally in various lubricant applications. In addition to

sedimentation stability, PFPE oils have been selected in the current application due attractive thermal properties. A relatively low vapor pressure is an important quality and makes PFPE oils better suited for the current application rather than the more common hydrocarbon oils. Its volatility is very low which is believed to decrease the tendency for pressure build-ups in the fluid chamber. And with the help of a flexible diaphragm (Asgeirsson et al., 2010), the pressure build-ups can be prevented in the sealed fluid chamber of the knee. Pressure increase was a problem in the device and was believed to cause leakage in the fluid chamber, a problem which has now been solved.

The density of UNIFLOR^{TM} 8510 is 1870 kg/m^3 and that of Krytox^{TM} 157-FSL is 1960 kg/ m^3. A base fluid viscosity of 0.3 Pa·s is relatively high when compared to more common MR fluid base fluids. This has a considerable negative effect on the off-state viscosity of the resulting MR fluid composition (Gudmundsson et al., 2009). But as mentioned before, the PFPE base fluid has other qualities that are important for the proposed application.

5.4 Iron particles

The gap between rotating steel blades in the MR prosthetic knee is approximately 20 μm. The study does therefore employ carbonyl iron powder with mean particle diameter ranging from 1 μm to approximately 8 μm, shown in Table 5.1 and two grades of nano-sized powder.

Table 5.1. Micron-sized carbonyl iron powders used in the MR fluids (BASF, 2011).

Particles	Mean particle diameter [D_{50} μm]	Iron content [%]	Mechanically hard or soft
HQ	1.0	> 97.0	Hard
HS	2.1	> 97.0	Hard
OM	4.6	> 97.0	Hard
CC	6.0	> 99.5	Soft
CM	8.3	> 99.5	Soft

Nanoparticles are also explored has a potential solid medium due to the small gap in the actuator. The nanoparticles are 25 nm in diameter with an iron content of 99.5% (Nanostructured & Amorphous Materials Inc., 2011) and 100-250 nm in diameter with an iron content of 98.0% (Nanostructured & Amorphous Materials Inc., 2011). The 25 nm particles where handled in an argon glove box while preparing the MR suspensions.

5.4.1 Morphology and magnetization characteristics

The morphology of the HS iron powder, shown in Figure 5.2, was investigated with a scanning electron microscope (SEM Gemini 1530 FEG).

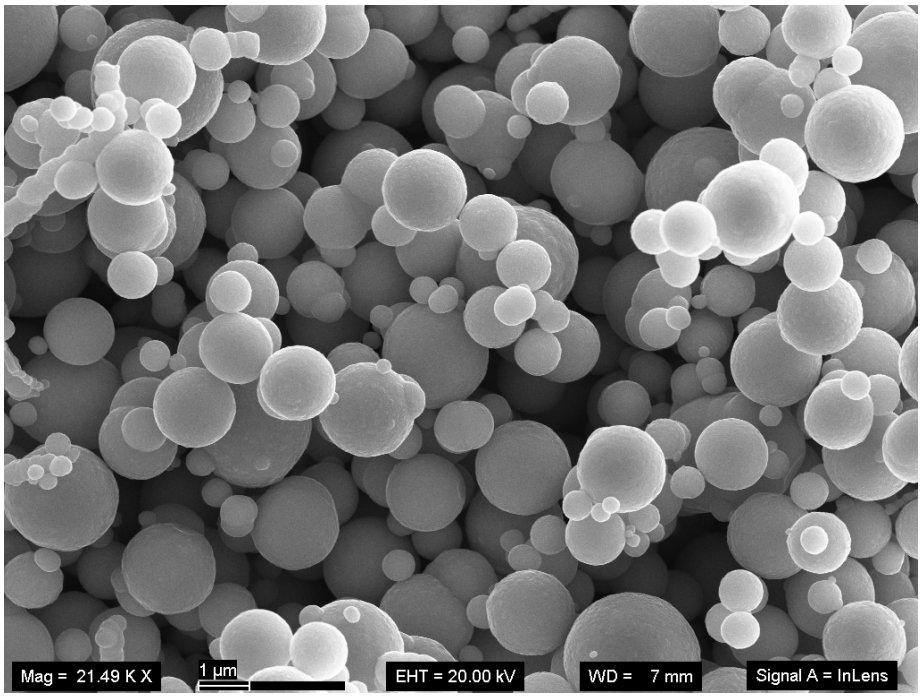

Figure 5.2. Morphology of the HS carbonyl iron powder.

The figure shows the HS particles to be regularly shaped spheres with a mean diameter of approximately 2 µm. Notably, the powder also contains submicron-sized particles. The mean particle diameter is 2.1 µm, as specified by the manufacturer (BASF, 2011) and the iron content is above 97%. The low iron content is believed to make the particles brittle and affect the durability of the MR fluid, employing this particular carbonyl iron powder.

The magnetization characteristics of the HS iron powder were measured with a superconducting quantum interference device (SQUID Quantum Design MPMS-5S). Figure 5.3 shows a magnetization curve for the HS carbonyl iron powder.

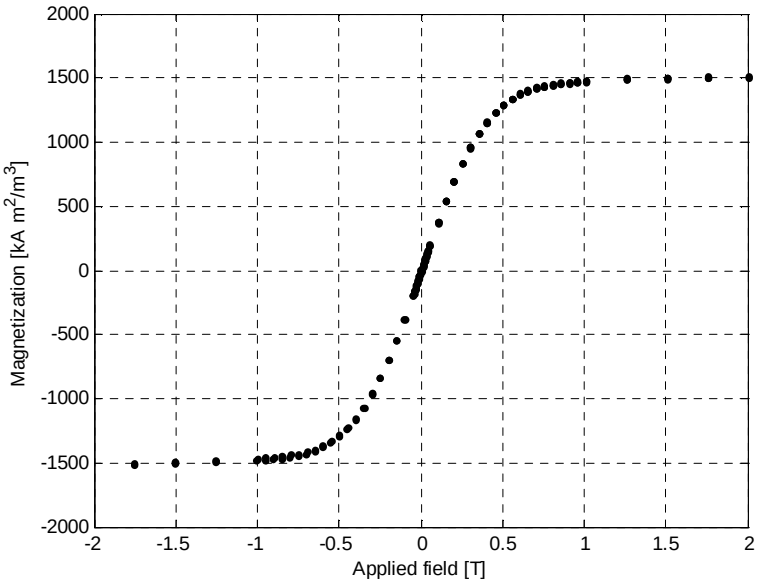

Figure 5.3. Magnetization characteristics of the HS carbonyl iron powder.

The sample size was 0.0678 g of new HS carbonyl iron powder before mixing the powder and fluids. Measurements were performed at a temperature of 20°C. The figure shows the powder to have a saturation value of approximately 1500 kAm^2/m^3 at a magnetic flux density of approximately 1 T.

5.4.2 Solid loading

Solid loading is the amount of solid materials (particles) in the fluid. Experience with the MR prosthetic knee actuator has shown problems to arise when injecting MR fluids with high solid loading into the device (Bisbee et al., 2007). This is due to a small micron-sized gap between the densely packed steel blades in the actuator. The focus of the study is therefore on MR fluids with lower solid concentration than many commercially available MR fluids (BASF, 2011; Lord, 2011; Jolly et al., 1999). As a rule of thumb, a solid concentration of 0.28 by volume, or approximately 60% by mass, has been shown to be injectable into the knee (Bisbee et al., 2007). Table 5.2 lists the solid concentrations considered in the study, where unimodal refers to a particle size distribution with a single peak while bimodal refers to a distribution with two peaks.

Table 5.2. Potential solid loadings for the prosthetic knee.

Solid loading	MR Fluids
0.25	Unimodal
0.28	Unimodal / Bimodal micron-sized / Bimodal nano-sized
0.287	Unimodal / Bimodal nano-sized
0.32	Unimodal
0.35	Unimodal

Another reason for the low solid loading is to keep the off-state viscosity at a reasonably low value. It is important for the knee to rotate freely in load free motion and this gives preference to low particle loadings.

5.5 MR fluid compositions

Using the base fluid, iron powder and the solid loadings described in the previous sections, twenty two different MR fluid compositions were prepared for a potential application in the MR prosthetic knee.

Five unimodal MR fluid samples were prepared, each representing a carbonyl iron powder with a particle diameter ranging from 1 μm to approximately 8 μm, all using a solid loading of 0.28 by volume.

Five unimodal MR fluid samples were prepared, each representing a particular solid loading ranging from 0.25 to 0.35 by volume. All these fluids employ a single grade of carbonyl iron powder, the HS powder with a particle mean diameter of approximately 2 μm.

Three bimodal micron-sized MR fluid samples were prepared using a fine powder with a mean particle diameter of approximately 1 μm (HQ powder) and a coarse powder with a mean particle diameter of approximately 8 μm (CM powder).

Ten bimodal MR fluid samples with micron-sized and nano-sized particles were prepared. All ten employ a micron-sized powder with a mean diameter of 2.1 (HS powder). Five use nanoparticles with an average diameter of 25 nm and five use nanoparticles with a diameter range of 100 nm to 250 nm. The details of the selected MR fluid samples are given in Table 5.3.

Table 5.3. MR Fluid compositions evaluated for potential application in an MR prosthetic knee.

Samples	Type	Particles	Solid loading [% v/v]
11	Unimodal	HS	0.25
12/22	Unimodal	HS	0.28
13	Unimodal	HS	0.287
14	Unimodal	HS	0.32
15	Unimodal	HS	0.35
21	Unimodal	HQ	0.28
12/22	Unimodal	HS	0.28
23	Unimodal	OM	0.28
24	Unimodal	CC	0.28
25	Unimodal	CM	0.28
31	Bimodal / micron	75%-HQ / 25%-CM	0.28
32	Bimodal / micron	50%-HQ / 50%-CM	0.28
33	Bimodal / micron	25%-HQ / 75%-CM	0.28
41	Bimodal / 25 nano	58.75%-HS / 1.25%-nano	0.28
42	Bimodal / 25 nano	57.5%-HS / 2.5%-nano	0.28
43	Bimodal / 25 nano	56.25%-HS / 3.75%-nano	0.28
44	Bimodal / 25 nano	55.0%-HS / 5.0%-nano	0.28
45	Bimodal / 25 nano	57.5%-HS / 4.17%-nano	0.287
51	Bimodal / 100 nano	58.75%-HS / 1.25%-nano	0.28
52	Bimodal / 100 nano	57.5%-HS / 2.5%-nano	0.28
53	Bimodal / 100 nano	56.25%-HS / 3.75%-nano	0.28
54	Bimodal / 100 nano	55.0%-HS / 5.0%-nano	0.28
55	Bimodal / 100 nano	57.5%-HS / 4.17%-nano	0.287

All compositions have a solid loading of 0.28 by volume, apart from the unimodal compositions using the HS particles to investigate the effect of solid loading. Also, two of the nanoparticle based samples are allowed to exceed a solid loading of 0.28. These two were prepared to investigate the difference between increasing the total solid concentration, by simply adding micron-sized particles or by increasing the concentration of nano-sized particles.

The accuracy of the scale, employed in the mixing of the fluids, was one-hundred of a gram. The particles were weighed prior to adding the corresponding amount of fluid to the solution. The MR fluid samples were mechanically stirred for 15 minutes at the time of preparation and then stirred again for 60 minutes at the time of measurement. All fluid

samples were subjected to 3 minutes of ultrasonic bath. The samples containing 25 nm where then subjected to an additional 5 minutes of ultrasonic bath to avoid agglomeration.

The MR fluid compositions, listed in Table 5.3, will in the following chapter be experimentally evaluated for a potential application in the MR prosthetic knee.

6 Experimental evaluation of MR fluids

The aim of the experimental evaluation is to select an MR fluid composition for the proposed applications with a maximum ratio between the on-state shear-yield stress and the off-state viscosity.

6.1 Background

All measurements were performed with an Anton-Paar Physica MCR 100 rheometer, shown in Fig 4.1, with a parallel plate measuring system. Plates with a diameter of 20 mm were used, with a gap of 1 mm. Both, on-state and off-state behavior were measured, for shear-rates ranging from 10^{-3} s^{-1} to 10^{3} s^{-1} for the on-state characteristics, and for shear-rates ranging from 10^{-3} s^{-1} to 200 s^{-1} for the off-state characteristics. The upper shear-rate limit is lower in off-state measurements than in the on-state study since the parallel plate geometry of the rheometer did now allow for higher shear-rates with the magnetic field off. On-state measurements were performed with values of the magnetic flux density ranging from 0.1 T to 0.55 T. All on-state and off-state rheological measurements are performed at a temperature of 20°C.

Figure 6.1. An Anton-Paar Physica MCR 100 rheometer used in the experimental evaluation of the MR fluids.

Figure 6.2 shows an example of an MR fluid sample in the rheometer. The sample is the unimodal MR fluid using the HS iron powder and a solid loading of 0.28 by volume.

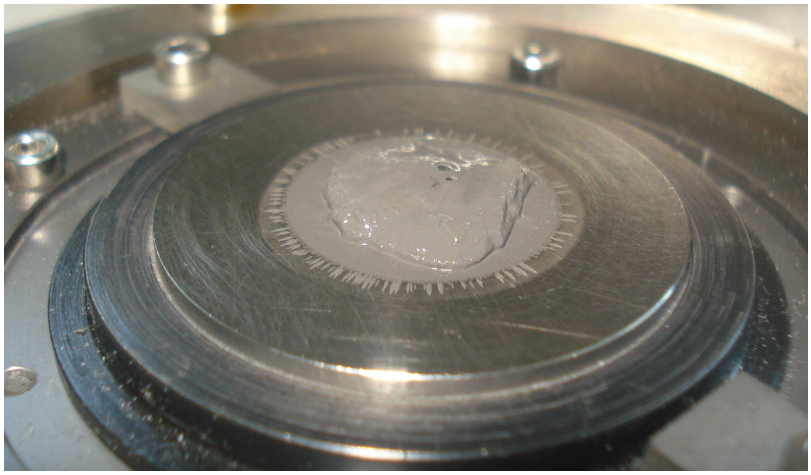

Figure 6.2. An MR fluid with the HS iron powder and a solid loading of 0.28 by volume.

The linear Bingham model is fitted to the measured on-state flow curves, using a least-squares error fit. The fit is based on shear-stress values for shear-rates between 200 s^{-1} and 1000 s^{-1}. This is the linear region of the flow curves and it is representative for the high shear-rates in the proposed application (Gudmundsson et al., 2009). The on-state and off-state rheological characteristics of the selected MR fluids will now be investigated.

6.2 Unimodal MR fluids with a varying particle size

Five unimodal fluids were prepared to investigate the effect of particle size. All fluids, samples 11-15, have a solid concentration of 0.28, by volume, and each fluid employs a particular grade of micron-sized carbonyl iron powder, listed in Table 5.1.

6.2.1 Rheological characteristics

Figure 6.3 shows on-state flow curves for the unimodal MR fluids, samples 11-15, at a magnetic flux density of 0.55 T.

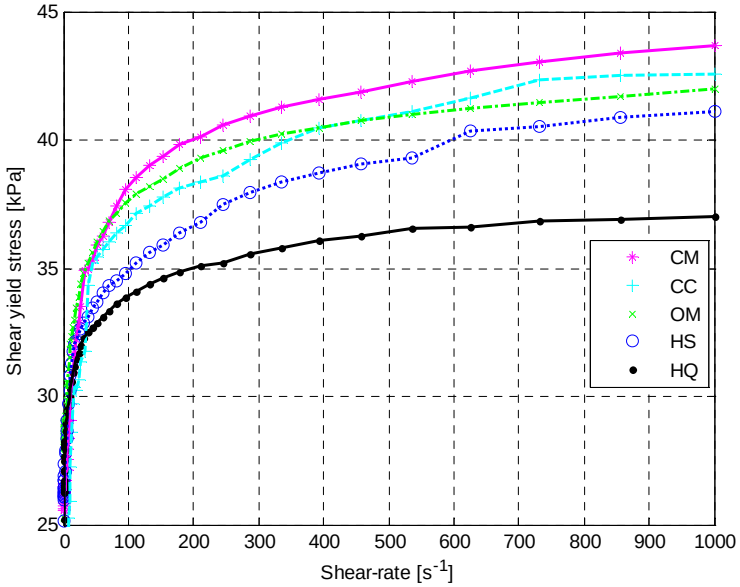

Figure 6.3. On-state flow curves for unimodal MR fluids, samples 11-15, each representing a particular iron powder. Measurements are performed at a magnetic flux density of 0.55 T.

Distinctively, the smallest particles exhibit the lowest shear stresses and the largest particles exhibit the highest shear stresses. The figure indicates an increase in the field-induced shear stress when going from fine powder to coarse powder. Measurements are now performed for six different values of the magnetic field. Figure 6.4 shows the shear yield stress, exhibited by the five samples, as a function of the applied magnetic field.

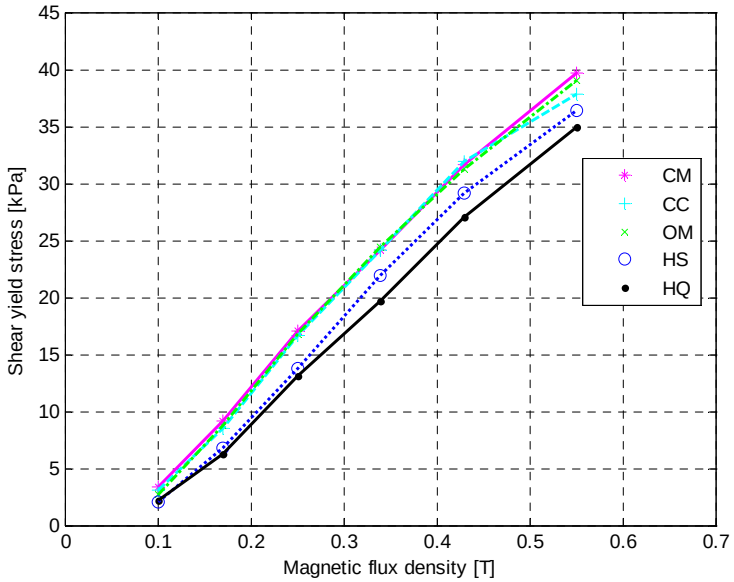

Figure 6.4. The field-induced shear yield stress, as a function of the magnetic flux density, for unimodal MR fluids, each representing a particular iron powder.

The figure shows that the field-induced shear yield stress increases with an increasing particle size. The fine powder exhibits the lowest shear yield stress while the coarse powder exhibits the highest shear yield stress. The difference is approximately 15%, at magnetic flux density of 0.55 T. Leaving the smallest particles out of the comparison, the difference in shear yield stress between the coarse powder and the HS powder, is approximately 10%, at a magnetic flux density of 0.55 T. The other powders exhibit a lesser difference in shear yield stress.

The general behavior, showing the larger particles to produce a higher field-induced shear yield stress, is in agreement with previous studies by Lemaire et al. (1995) and Bombard et al. (2002); the study by Bombard being partially based on the same carbonyl iron powder.

The results show an advantage in using larger particles when looking at the on-state rheological behavior. This is providing that the application allows for larger particles, the gap size limits the particle size for the proposed application. For usage in the MR prosthetic knee, a particle size upper limit exists due a small gap between the rotating blades in the brake. The gap is approximately 20 μm which still allows the powder in this study to be used.

The effect of particle size on off-state viscosity of MR fluids will now be investigated. Figure 6.5 shows the off state viscosity of the five MR fluids, each representing a particular iron powder.

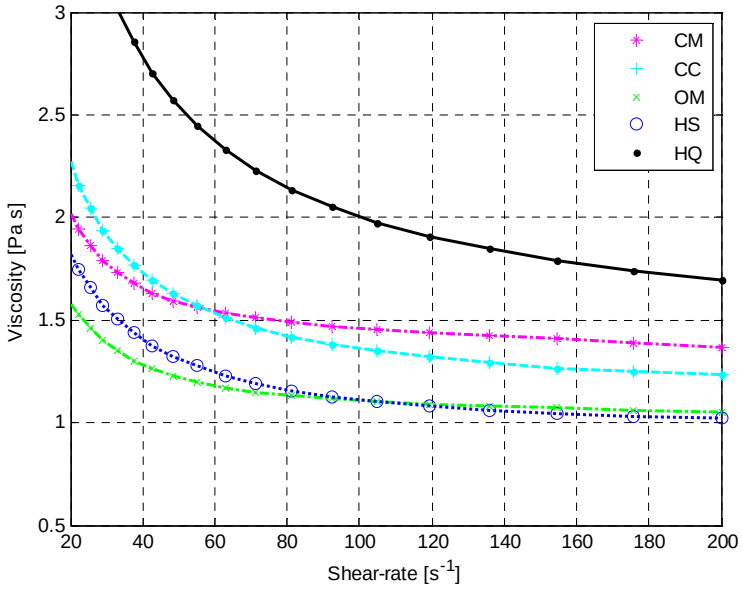

Figure 6.5. The off-state viscosity, as a function of shear-rates, for unimodal MR fluids, each representing a particular iron powder.

The well known shear-thinning characteristic of MR fluids can readily be observed. All fluid samples exhibit a high viscosity at low shear-rates while, at high-shear-rates, the viscosity approaches a constant minimum value. The high working shear-rates in the proposed application relieves the functionality of knee from the high viscosities at low shear-rates.

Figure 6.5 shows the fine powder to have the highest viscosity, with a high-shear rate value of 1.7 Pa·s. The lowest viscosity is exhibited by the powders HS and OM, both having a comparable viscosity curve. The two have a high shear-rate viscosity of approximately 1.0 Pa·s. The coarse powder (CM), which has been shown to have the largest field-induced shear yield stress, has high shear-rate viscosity of 1.4 Pa·s which is about 40% higher than the lowest observed.

The combined on-state and off-state rheological characteristics of MR fluids are of importance in the proposed application. Figure 6.6 shows the combined characteristics of the unimodal MR fluids representing a particular grade of iron powder. The yield stress is measured at a magnetic flux density of 0.55 T and the off-state viscosity is measured at a shear-rate of 200 s^{-1}.

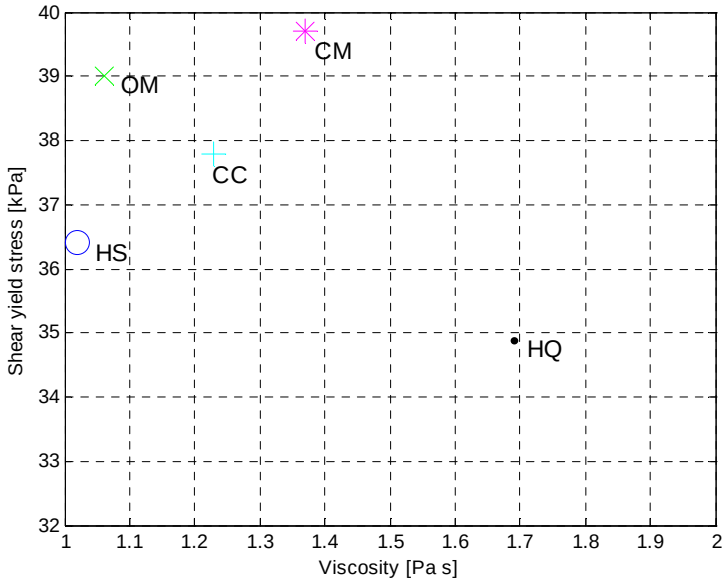

Figure 6.6 The on-state shear yield stress as function of the off-state viscosity, for the unimodal fluids each representing a particular iron powder. The yield stress is measured at a magnetic flux density of 0.55 T and the off-state viscosity is measured at a shear-rate of 200 s^{-1}.

This type of figure is a valuable tool for designers of MR fluids and MR fluids devices as it shows the trade-offs between these two competing properties. The figure shows how the unimodal fluid employing OM powder is low in off-state viscosity and high in shear yield stress. It has an off-state viscosity close to the minimum observed and on-state performance close to the maximum observed. The unimodal fluid employing the coarse powder (CM) exhibits the highest shear yield stress.

6.3 Unimodal MR fluids with a varying solid loading

Five unimodal fluids were prepared to investigate the effect of solid loading. All fluids, samples 21-25, use a single grade of micron-sized carbonyl iron powder, the HS powder, with a particle mean diameter of approximately 2 μm.

6.3.1 Rheological characteristics

The on-state flow curves for an MR fluid, sample 22, using a solid loading of 0.28 and the HS iron powder, are shown in Figure 6.7.

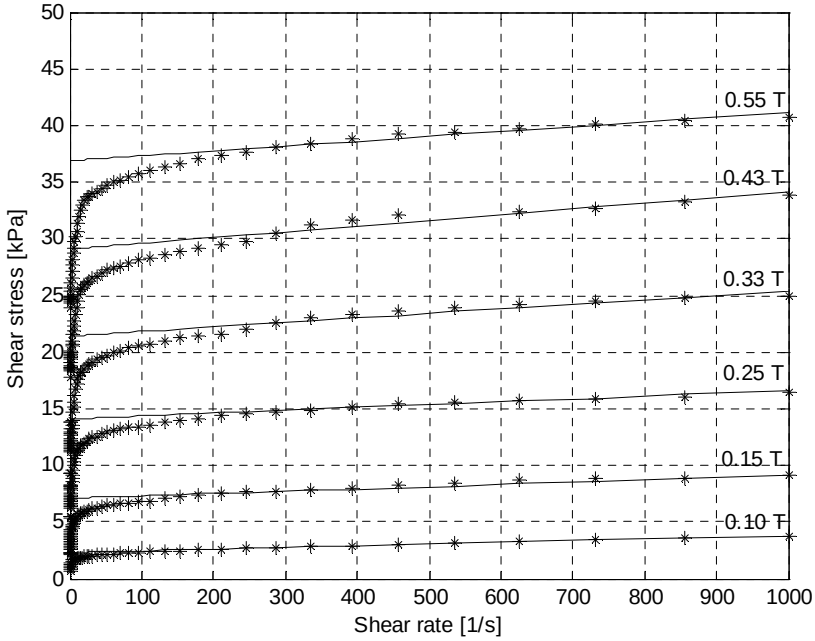

Figure 6.7**.** On-state measurements for a unimodal MR fluid having a solid concentration of 0.28 and the HS carbonyl iron powder. The Bingham model is fitted to the flow curves.

The effect of particle loading on the rheological properties of the fluid is of interest. Hence, in addition to the fluid shown in figure 6.7, four more unimodal MR fluids were prepared and measured. All these fluids use the HS carbonyl iron powder. The volume fractions of particles are: 0.25, 0.28, 0.287, 0.32, and 0.35. The shear-yield stresses for all five MR fluids, samples 21-25, are shown in Figure 6.8a, as a function of the magnetic flux density, and in Figure 6.8b, as a function of solid loading.

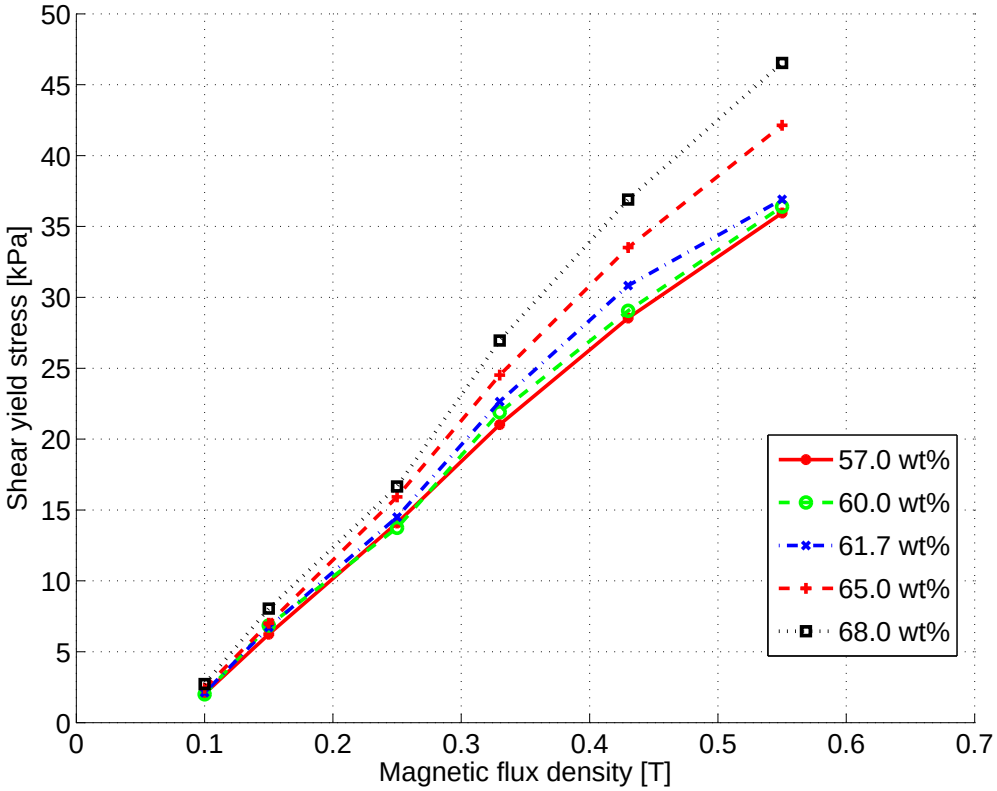

Figure 6.8a: The shear yield stress of the unimodal MR fluid, samples 21-25, as a function of the magnetic flux density.

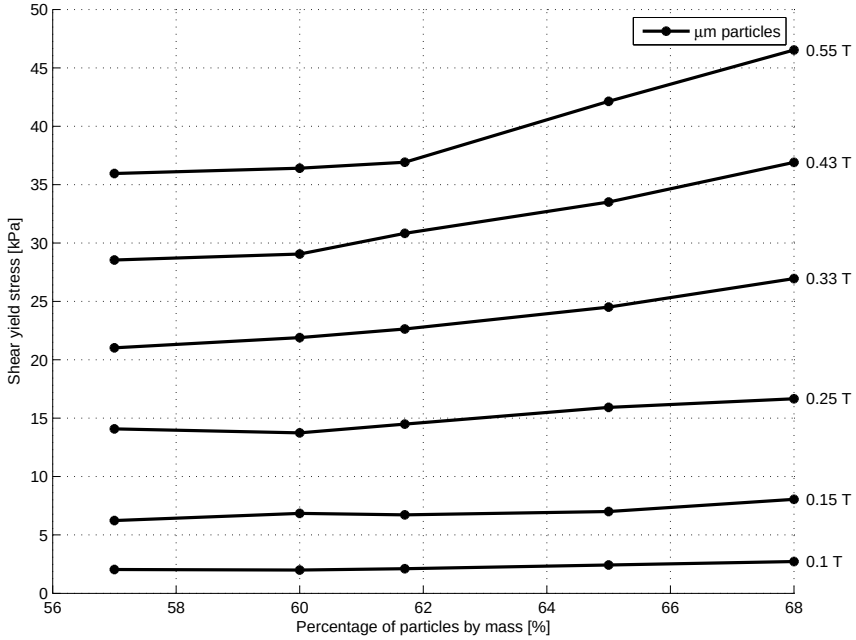

Figure 6.8b: The shear yield stress of the unimodal MR fluids, samples 21-25, as a function of the solid concentration.

The slope of a calculated average curve from Figure 6.8a is 2.05, when plotted in a log scale against the magnetic field intensity instead of the flux density. This compares to results obtained by Fang et al. (2009). In this study, the range of the field intensity is from 25 kA/m to approximately 200 kA/m which has been reported to have a slope of 2.

Clearly, as expected, Figure 6.8a shows an increase in shear yield stress with increased particle loading. However, as Figure 6.8b demonstrates, the change is inconsequential for low values of applied field (0.1 T) but significant for higher field values. For example, at a magnetic flux density of 0.55 T, an increase in volume fraction from 0.28 to 0.35 results in approximately 30% increase in shear yield stress. This would give a 30% increase in on-state output torque for the MR prosthetic actuator, which is significant. Furthermore, it is noteworthy that the sample with the highest solid loading demonstrates a more nonlinear behavior than the other samples. This is in agreement with other studies that have shown an increased nonlinear behavior for fluids with high particle loadings (Foister, 1997). Although there is a clear benefit in shear yield stress by using a higher particle loading, the penalty in off-state viscosity needs to be determined as well.

In the absence of a magnetic field, the unimodal MR fluids, samples 21-25, exhibit a strong shear thinning behavior, shown in Figure 6.9, resulting in a high viscosity at low shear-rates.

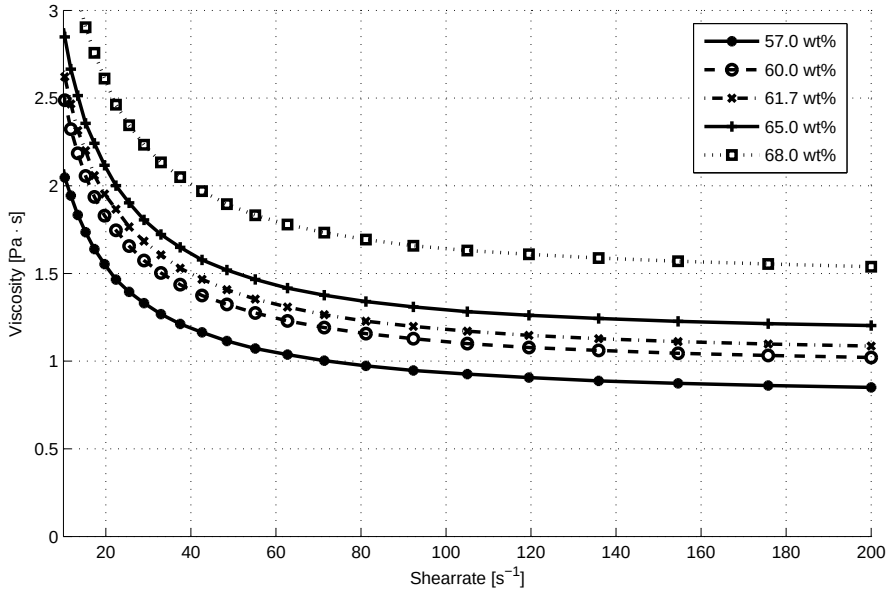

Figure 6.9. The off-state viscosity as a function of the shear rate for the unimodal MR fluids.

At high shear-rates the fluids approach lower viscosity limits. The figure shows a strong a dependence of the off-state viscosity on the concentration of micron-sized particles. The difference between the lowest particle loading and the highest is more than 50%, at high shear-rates. As stated previously, the PFPE carrier fluid has a viscosity of 0.3 Pa·s and is Newtonian in behavior with shear-rate independent viscosity.

6.4 Bimodal MR fluids with micron-sized particles

Three bimodal fluids were prepared with varying portions of coarse (the CM powder) and fine powder (the HQ powder). This gives a particle size ratio of approximately 8. These are denoted as samples 31-33. Table 6.1 shows the compositions of these MR fluids.

Table 6.1. Bimodal micron-sized MR fluids with a total solid concentration of 0.28 by volume.

Fine powder	Coarse powder	Percentage of coarse powder [%]	Fine powder mass [gr]	Coarse powder mass [gr]	Base fluid mass [gr]	MR fluid volume [ml]
HQ	CM	25.00	61.24	20.41	50.00	37.05
HQ	CM	50.00	40.82	40.82	50.00	37.05
HQ	CM	75.00	20.41	61.24	50.00	37.05

Bimodal micron-sized particle distributions will now be investigated aiming to maximize the ratio between the field-induced shear-stress and the off-state viscosity.

6.4.1 Rheological characteristics

Three bimodal MR fluids, shown in Table 6.1, are now investigated. Figure 6.10 shows the on-state flow curves for the MR fluids, at a magnetic flux density of 0.55 T.

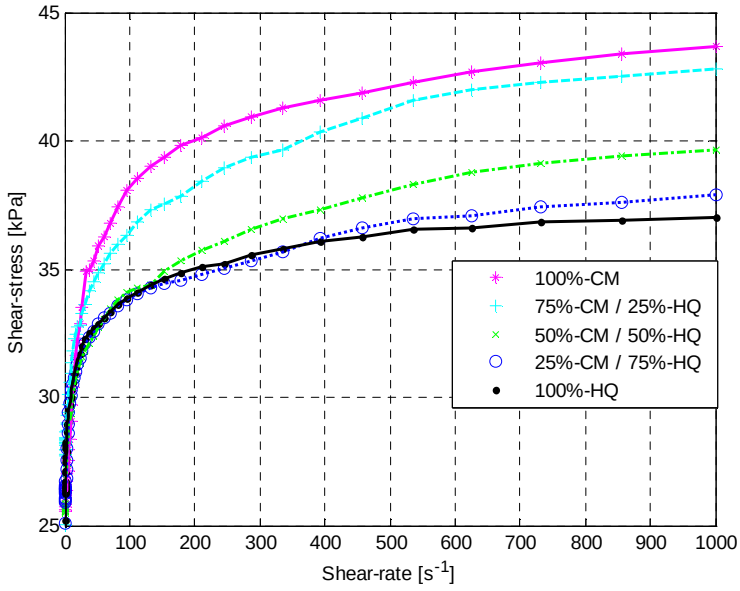

Figure 6.10. Flow curves for bimodal MR fluids and their corresponding unimodal MR fluids. Measurements are performed at a magnetic flux density of 0.55 T.

The fluid with 75% coarse powder and 25% fine powder exhibits on-state shear stresses that are comparable to that of the fluid containing solely coarse powder. In all

cases, the bimodal fluids exhibit higher shear stresses when compared to the unimodal fluid containing solely the fine powder.

Figure 6.11 shows the shear yield stress, as a function of the applied magnetic field, for the bimodal micron-sized MR fluids along with their corresponding unimodal MR fluids.

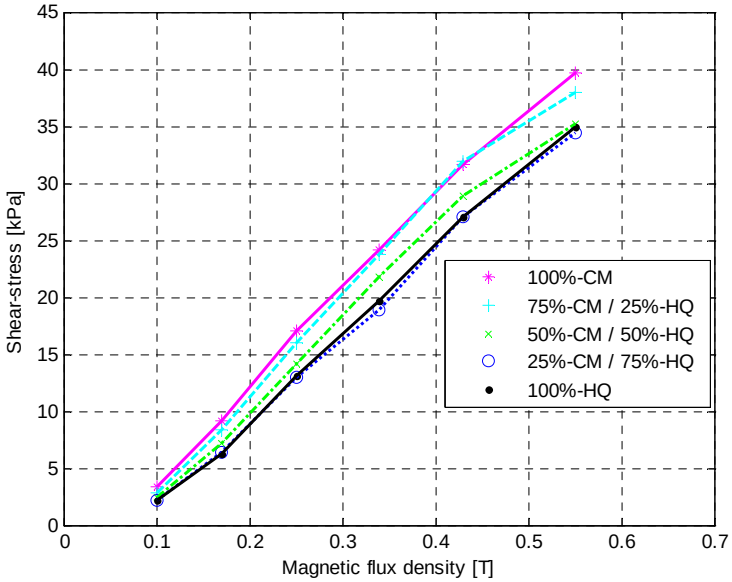

Figure 6.11. The field-induced shear yield stress, as a function of the magnetic flux density, for bimodal MR fluids and their corresponding unimodal fluids.

The figure shows the shear yield stress to increase with an increasing percentage of the coarse powder. The fluid using 50% coarse powder and 50% fine powder, exhibits a behavior closer to the unimodal fluid containing solely fine powder; the same being true for the fluid using 75% fine powder. The fluid containing solely coarse powder exhibits the highest shear yield stress. Interestingly, the bimodal fluid containing 75% coarse powder and 25% fine powder, exhibits nearly the same high shear yield stress, the difference being very small at the lower levels of the applied magnetic field. This concludes the on-state investigation and the off-state rheological characteristics of the same MR fluids will now be explored.

Figure 6.12 shows the off-state viscosity of the fluids along with their corresponding unimodal fluids.

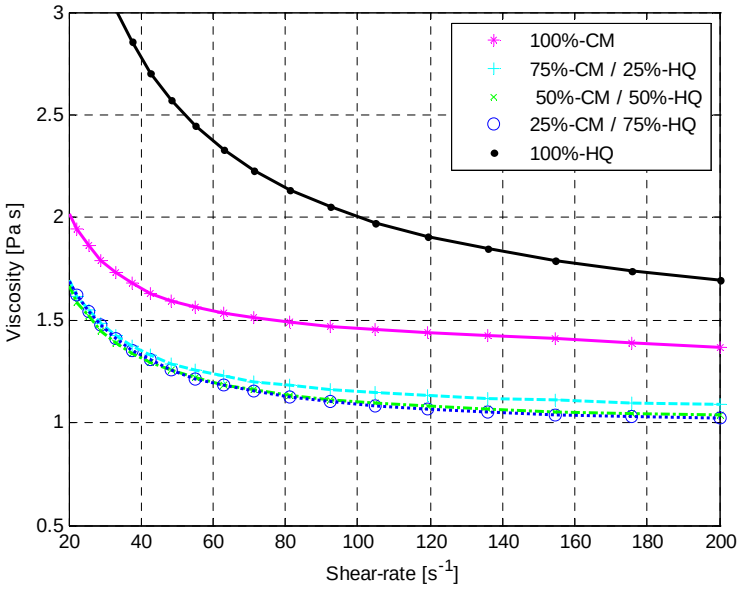

Figure 6.12. The off-state viscosity, as a function of shear-rates, for bimodal MR fluids and their corresponding unimodal fluids.

The MR fluids containing solely fine powder or solely coarse powder, show distinctively higher off-state viscosities when compared to bimodal MR fluids employing the same powder. The bimodal fluids have a high shear-rate viscosity value ranging from 1.0 Pa·s to 1.1 Pa·s while the unimodal fluids have an off-state viscosity of 1.4 Pa·s and 1.7 Pa·s. The difference is significant and, interestingly, the MR fluid containing 75% coarse powder and 25% fine powder has also been shown to have a field-induced shear yield stress that is close to the maximum observed in this study. The low-off state viscosity of the bimodal MR fluids makes them attractive for the proposed application.

Figure 6.13 shows the combined on-state and off-state characteristics of the bimodal micron-sized MR fluids along with their corresponding unimodal fluids.

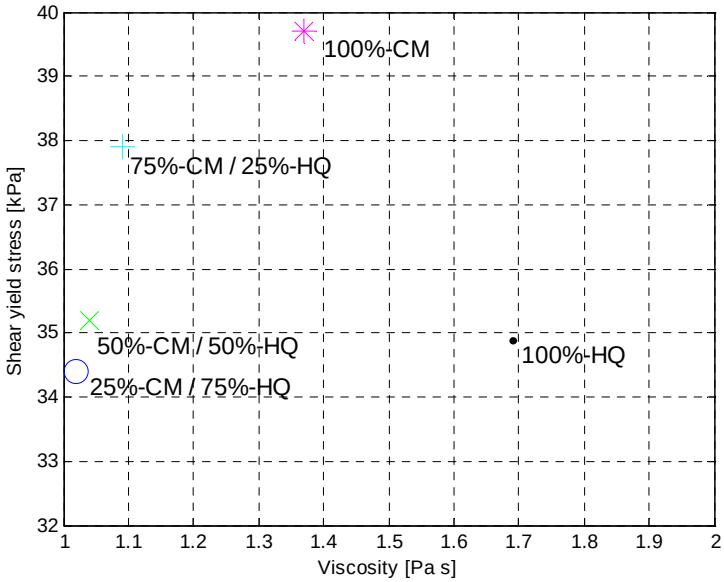

Figure 6.13. The shear yield stress as a function of the off-state viscosity, for the bimodal fluids and their corresponding unimodal fluids. The yield stress is measured at a magnetic flux density of 0.55 T and the off-state viscosity is measured at a shear-rate of 200 s^{-1}.

The bimodal MR fluids exhibit a lower off-state viscosity, in all cases, when compared to their corresponding unimodal fluids. The MR fluid with 75% coarse powder and 25% fine powder is, also, notably high in on-state yield stress.

6.5 Bimodal MR fluids with nanoparticles

Rheological measurements are carried out for a number of bimodal samples, comprising a combination of micron- and nano-sized particles. The influence on the rheological properties of adding nano particles to the fluids is investigated. In particular, the rheological behavior for different sizes of nano particles is determined. The MR fluid samples are characterized with respect to both field-induced and off-state properties.

6.5.1 Rheological characteristics

As a reference fluid, the unimodal MR fluid with a solid loading of 0.28 by volume or 0.60 by mass is used. . This MR fluid (sample 22) is used in the study to compare the unimodal fluid with the bimodal nanoparticle fluid mixtures. Figure 6.14 shows flow curves for the unimodal MR fluid, sample 22, and two bimodal nanoparticle MR fluids, samples 44 and 54, at a magnetic flux density of 0.55 T, each using a particular grade of nanoparticle powder.

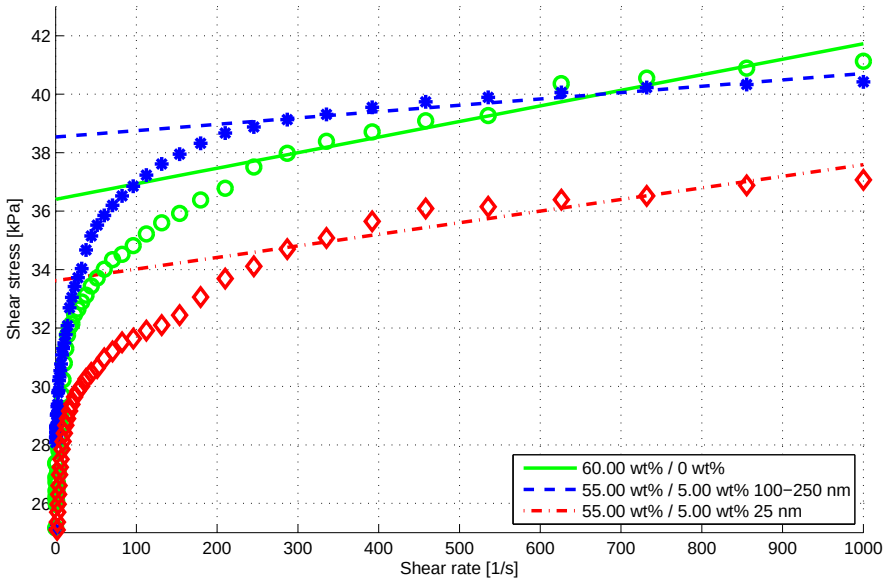

Figure 6.14. Flow curves for a unimodal fluid with a solid concentration of 60% by mass and two bimodal fluids with nano-sized particle concentration of 5% and a micron-sized particle concentration of 55% by mass. Measurements were conducted at a magnetic flux density of 0.55 T.

The figure shows sample 54, with a nanoparticle size of 100-250 nm, to exhibit a higher shear yield stress than the sample 44, with a nanoparticle size of 25 nm. Furthermore, sample 54 has a higher yield stress than the unimodal reference fluid using the same solid loading. However, for a shear rate value of 500 s^{-1}, which is close to the operating shear rate for the MR fluid actuator, these two have similar shear stress values. It is interesting to note that the post-yield viscosity of the MR fluids containing nano-sized particles is lower than that of the corresponding unimodal fluid.

To illustrate the effect of the concentration of nano-sized particles on the shear-yield stress, Figure 6.15 shows the shear yield-stress as a function of concentration for the two different nano particle grades, for values of magnetic flux density varying from 0.1 T to 0.55 T.

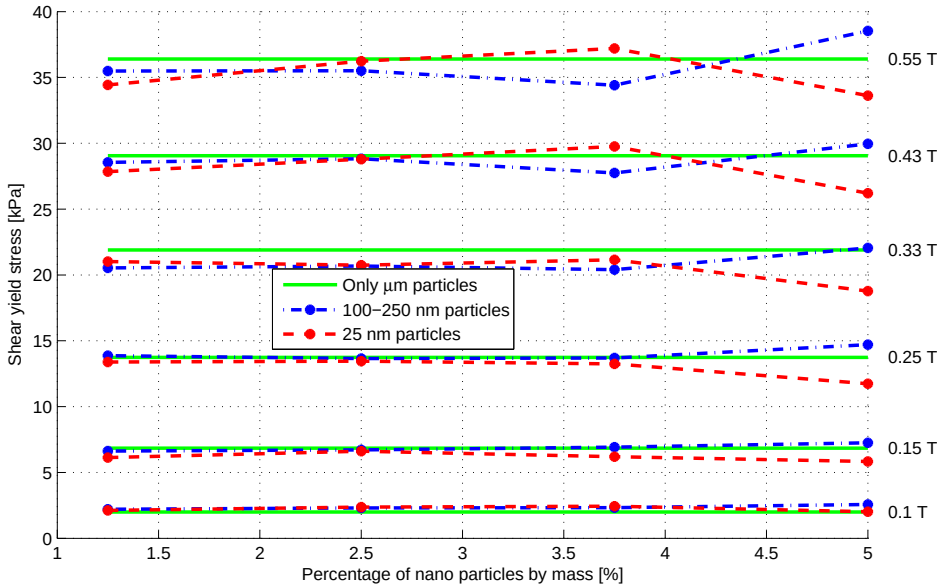

Figure 6.15. Shear-yield stress of MR fluid compositions with 25 nm and 100-250 nm particles at various concentrations, compared to the shear-yield stress of the corresponding unimodal fluid. The total solid concentration is 0.28 in all cases.

The figure shows that the field-induced shear-yield stress of the nano-sized MR fluid compositions are comparable to that of the corresponding unimodal MR fluid. This holds true until a nano-sized particle concentration of 5% is reached. The bimodal sample 44, containing a 55% of micron-sized particles and 5% of nano-sized particles, exhibits a drop in shear-yield stress. This drop is not observed when using the 100-250 nm iron powder. The measurements suggest that the field-induced shear-yield stress of the PFPE-based MR fluid can not be increased with nano-sized particles with an average diameter of 25 nm, given that the total solid concentration is not allowed to exceed that of the unimodal fluid. However, a moderate increase in shear-yield stress is observed when the 100-250 nm particles are employed at a solid concentration of 5%.

Illustrating this further, Figure 6.16 shows the shear-yield stress as a function of the magnetic flux density for the reference unimodal sample and samples 44 and 54. The figure shows that the sample 54 exhibits a higher yield stress than the 44 sample, for all values of magnetic flux density. Sample 45 exhibits a moderately higher shear yield stress than the corresponding unimodal MR fluid.

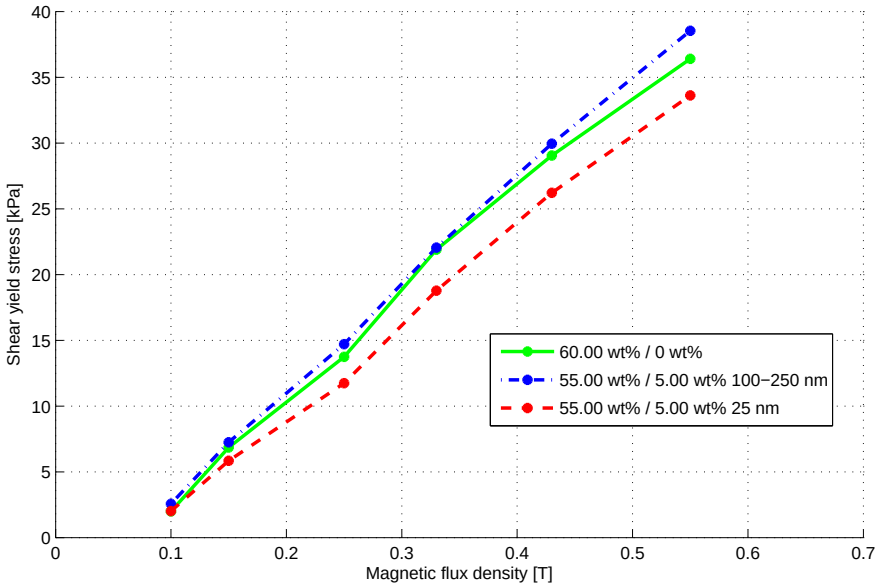

Figure 6.16. The shear yield stress as a function of the magnetic flux density for MR fluid compositions, containing 55% micron-sized particles and 5% nano-sized particles, and the corresponding unimodal MR fluid.

The slope of Figure 6.16 in a log plot is approximately 2 which is in a agreement with the study by Fang et al. (2009). In order to compare unimodal and bimodal samples, at total solid concentration higher than 60%, Table 6.2 shows the shear yield-stress of samples with a total solid concentration of 61.67% at a magnetic flux density of 0.55T.

Table 6.2. The shear-yield stress of samples with a total solid concentration of 61.67% at a magnetic flux density of 0.55T.

Sample	Total solid concentration [% mass]	Micron–sized particles [% mass]	Nano-particles [% mass]	Nano-particle size [nm]	Shear yield stress [kPa]
13 (unimodal)	61.67	61.67	0		36.9
45	61.67	57.50	4.17	25	37.9
55	61.67	57.50	4.17	100-250	37.4

The table shows similar behavior for the samples with a total solid concentration 61.67 as that of the samples with a total solid concentration of 60%. Again, the shear yield-stress can be slightly increased with nano-sized particles. This holds true for both nanoparticle grades. A nanoparticle concentration of 4.17% does not exhibit a drop in this case when compared to the corresponding unimodal sample. The 25 nm particle composition shows a comparable shear yield-stress to that of the 100-250 nm particle composition.

An important characteristic of MR fluid is the post-yield viscosity. In the current application, it affects how sensitive the on-state response of the actuator is to the rotary speed or the shear-rate in the fluid. A higher post-yield viscosity will result in a response

that is more sensitive to the shear-rate. This is not preferable in the proposed application in a prosthetic knee.

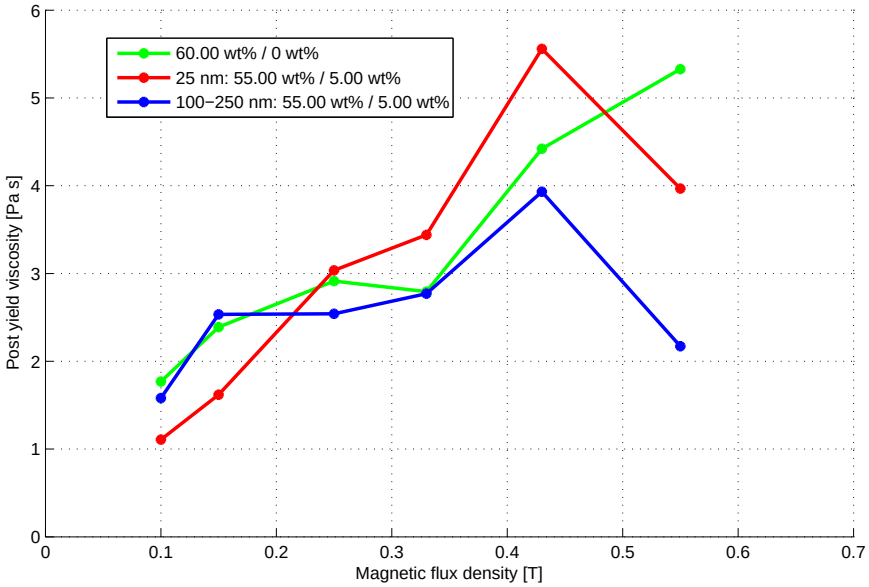

Figure 6.17. The post-yield viscosity as a function of the magnetic flux density for MR fluid compositions containing 55% micron-sized particles and 5% nano-sized particles and the corresponding unimodal MR fluid.

Figure 6.17 shows the post-yield viscosity for three selected fluid samples as a function of the magnetic flux density. The fluid samples are: a unimodal sample, with a solid concentration of 60%, and two bimodal samples, one for each nanoparticle grade, with a total solid concentration of 60%. The nano particle concentration is 5% in both cases. As expected, the post-yield viscosity increases with an increasing magnetic field. However, it is noteworthy that the post-yield viscosity of the bimodal samples starts to drop as the magnetic field reaches a high value of 0.55T.

Summarizing the on-state behavior, the field-induced shear-yield stress has been shown to increase moderately when using 100-250 nm particles. A peak in shear-yield stress was found at a nano particle concentration of 5%. This was the highest nano particle concentration tested. Using the same nano particle concentration but employing smaller particles, with an average diameter of 25 nm, has been shown to decrease the field-induced shear-yield stress. Using 25 nm particles, a peak in shear-yield stress was observed with a nano particle concentration of 3.75%. This peak, however, is not higher than the shear-yield stress in a corresponding unimodal fluid. A drop in shear-yield stress is observed when allowing the nano concentration of 25 nm particles to exceed that of 3.75%.

The effect of nano particles on the off-state viscosity of the bimodal nanoparticle MR fluid is now investigated. Figure 6.18 shows viscosity curves for all nanoparticle compositions and the corresponding unimodal fluid, all with a total solid concentration of 0.60 by mass or 0.28 by volume.

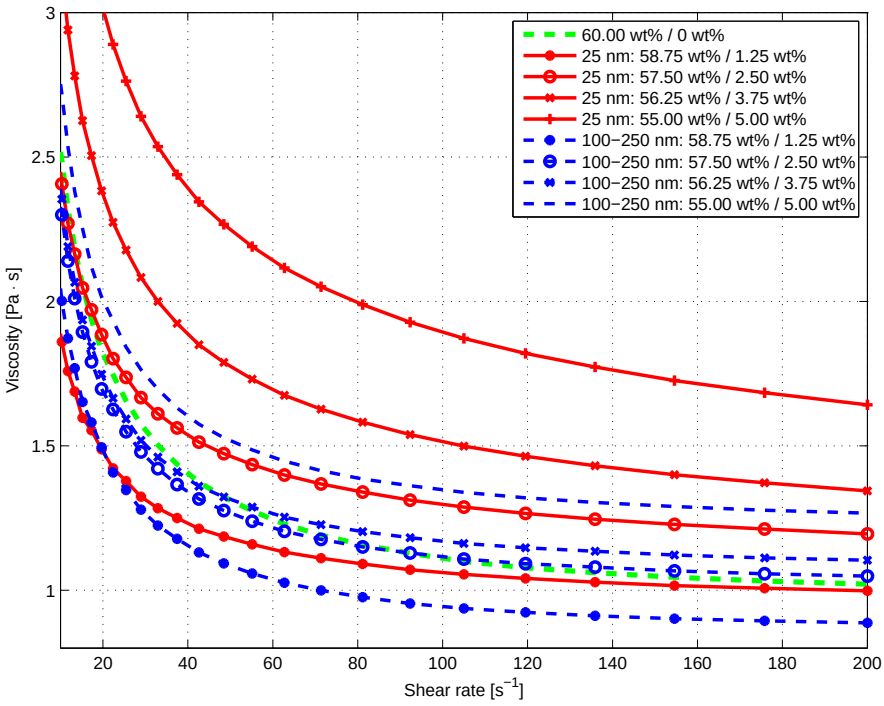

Figure 6.18. The off-state viscosity as a function of the shear rate for a unimodal fluid and bimodal fluid samples with a total solid concentration of 60%.

The figure shows the off-state viscosity to increase by a large extent when micron-sized particles are replaced by nano-sized particles. For example, a 25 nm fluid with 5% particle concentration exhibits approximately 60% higher viscosity, at high shear rates, than its corresponding unimodal fluid. Such a high increase in off-state viscosity is not acceptable for the proposed application. Similarly, the viscosity curves for nano particle compositions, containing 100-250 nm particles, show an increase in off-state viscosity but not to the same extent as the 25 nm particles. For example, a MR fluid composition, using 100-250 nm particles, with 55% micron-sized particles and 5% nano-sized particles, exhibits an approximately 25% higher viscosity, at high shear rates, when compared to its corresponding unimodal fluid.

Figure 6.19 shows the shear-yield stress as a function of the off-state viscosity for nano MR fluid compositions with a total solid concentration of 60% and for all unimodal compositions.

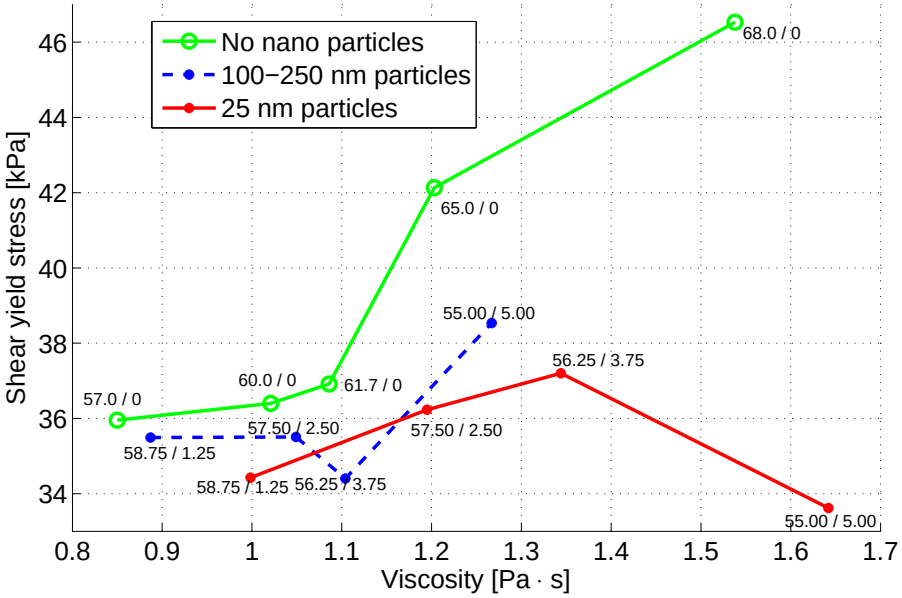

Figure 6.19. Shear yield-stress as a function of off-state viscosity for the bimodal nanoparticle fluid compositions.

The figure clearly demonstrates the 25 nm particles to have a stronger effect on the off-state viscosity than the 250 nm particles. Furthermore, recall that the smaller nano particles exhibit a lower shear yield stress which leaves the 100-250 nm particles in favor for the proposed application. However, a comparison between the nano and the unimodal compositions shows the unimodal fluids to be superior with respect to the two characteristics, the field-induced shear-yield stress and the off-state viscosity.

The study shows that although nano-sized particles have a favorable effect on sedimentation stability, the increase in off-state viscosity is too high for such particles to be beneficial in applications such as the prosthetic knee actuator. It is concluded that micron-sized particles are more effective in increasing the shear yield stress while keeping the off-state viscosity within set limits for this application.

6.5.2 Comparison to previous nanoparticle MR fluid studies

Since, most studies differ with regards to the sizes of micron- and nano- particles, the type of carrier fluid, the micron to nano particle ratios, and the particle loading, it is difficult to make a direct quantitative comparison between studies. We only attempt to highlight some issues as follows. Chaudhuri et al. (2005) studied fluid samples with 45% mass concentration and detected an increase in shear yield stress when replacing 5% (by mass) of 10 µm particles with 30-40 nm particles. However, increasing the amount of nano-sized particles to 7.5% had an adverse effect, dropping the dynamic yield stress to below the level of the unimodal fluid.

In another study, by Wereley et al. (2006), a larger range of micron- to nano-sized particles ratios was investigated. The concentration of nano-sized particles was varied from 1.5% to 24% by mass (denoted 2.5% - 15% in their study) in ten steps, while keeping the total particle loading at 60%, by mass. The micron- and nano-sized particles had average diameters of 30 µm and 30 nm, respectively. Their results also demonstrated an increase in

yield stress, with increasing nano particle fraction at first, but then a decrease after a certain optimal value of nano-sized particle concentration was reached. The optimal value was about 9.0% by mass.

Contrary to the results by Chaudhuri et al. (2005) and Wereley et al. (2006), a more recent study by Burguera et al. (2008) reports a decrease in yield stress for fluids with nano particles when compared to an all micron fluid. They measured one fluid with only micron particles, and two fluids with micron to nano ratios, 90%:10% and 85%:15%, respectively. The study was carried out for fluids with total particle loadings of 50% and 60%. Converted to mass percentages, this gives fluids with 5% and 7.5% nano particles, by mass, for the 50% fluid, and 6% and 9% nano particles, by mass, for the 60% fluid. Interestingly, their micron and nano particle sizes are comparable with the ones in this paper; 2.6 µm and 40 nm in diameter, respectively.

6.6 Figure of merit

The ratio between the on-state shear-yield stress and the off-state viscosity defines the torque range of the MR prosthetic knee. This ratio is used as figure of merit for the potential MR fluid compositions. Summarizing, Table 6.3 shows the ratio between the on-state and the off-state characteristics of the MR fluids in this study.

Table 6.3. An MR fluid figure of merit for the prosthetic knee. The ratio between the on-state yield stress and off-state viscosity. The yield stress is measured at magnetic flux density of 0.55 T and the off-state viscosity is measured at a shear-rate of 200 s^{-1}.

Nr.	MR fluid type	Solid load. by vol.	Iron powder	On-state shear yield stress [kPa]	Off-state viscosity [Pa·s]	On- to off-state ratio [s^{-1}]
11	Unimodal	0.25	HS	36.0	0.85	42.4
12/22	Unimodal	0.28	HS	36.4	1.02	35.7
13	Unimodal	0.287	HS	37.0	1.10	33.6
14	Unimodal	0.32	HS	42.0	1.20	35.0
15	Unimodal	0.35	HS	46.5	1.55	30.0
21	Unimodal	0.28	HQ	34.9	1.69	20.7
12/22	Unimodal	0.28	HS	36.4	1.02	35.7
23	Unimodal	0.28	OM	39.0	1.06	36.8
24	Unimodal	0.28	CC	37.8	1.23	30.7
25	Unimodal	0.28	CM	39.7	1.37	29.0
31	Bimodal	0.28	25% CM, 75% HQ	34.4	1.02	33.7
32	Bimodal	0.28	50% CM, 50% HQ	35.2	1.04	33.8
33	Bimodal	0.28	75% CM, 25% HQ	37.9	1.09	34.8
41	Bimo.-nano	0.28	1.25%/ 60% 25 nm	34.4	1.00	34.4
42	Bimo.-nano	0.28	2.50%/ 60% 25 nm	36.3	1.19	30.5
43	Bimo.-nano	0.28	3.75%/ 60% 25 nm	37.2	1.34	27.8
44	Bimo.-nano	0.28	5.00%/ 60% 25 nm	33.5	1.85	18.1
45	Bimo.-nano	0.287	4.17%/ 61.67% 25 nm	37.9	1.63	23.3
51	Bimo.-nano	0.28	1.25%/ 60% 100 nm	35.4	0.89	39.8
52	Bimo.-nano	0.28	2.50%/ 60% 100 nm	35.5	1.05	32.3
53	Bimo.-nano	0.28	3.75%/ 60% 100 nm	34.2	1.10	31.1
54	Bimo.-nano	0.28	5.00%/ 60% 100 nm	38.7	1.27	30.5
55	Bimo.-nano	0.287	4.17%/61.67% 100 nm	37.4	1.28	29.2

Interestingly, the MR fluid with the highest turn-up ratio is the unimodal fluid with a low solid concentration of 0.25, by volume, and using the HS iron powder. This suggests that MR fluids with low solid concentration are appropriate for the proposed application. Although low in on-state shear-yield stress, the reduction in off-state viscosity dominates the figure of merit function. Among the evaluated fluids, this fluid will results in a maximum torque range in the actuator.

Next in line in the turn-up ratio is sample 51, a bimodal nanoparticle MR fluid with a total solid concentration of 0.28 by volume (60% by mass) and thereof 1.25% nanoparticles by mass. This fluid is using nanoparticles with a size range o 100-250 nm. After analyzing the measurement data thoroughly, it is concluded that the off-state measurement of this fluid is faulty, with a suspiciously low off-state viscosity. This is most likely due the fluid sample in the rheometer being too small and not spanning the 20 mm diameter of the parallel plates.

The unimodal MR fluids (samples 22 and 23) employing the HS and OM iron powder exhibit a high turn up ratio. These are also prominent fluids to be used in the prosthetic knee actuator. With a slightly lesser turn-up ratio is the bimodal micron-sized MR fluid (sample 33) with 75% coarse particles and 25% fine particles. This is using a particle size ratio of approximately 8. The bimodal fluids have been found to have attractive off-state characteristics for the proposed application. The bimodal MR fluid (sample 33) and the unimodal fluids (samples 11, 22 and 23) are prominent fluids to be used in the prosthetic actuator.

6.7 Summary

The investigation has quantified the effect of solid loading for the proposed application. As expected, with an increasing solid loading, the on-state shear-yield stress and the off-state viscosity tend to increase. A fluid with a solid loading of 0.25 by volume has been shown to have the highest ratio between the on-state shear-yield stress and the off-state viscosity for all the fluids in this study.

The effect of particle size on the on-state performance of the MR fluids has shown the shear yield stress to increase when going from fine powder to coarse powder. The increase is significant when comparing the fluid employing the coarse powder to the fluid employing the fine powder. The effect of particle size on the off-state viscosity is shown not to be directly proportional to the particle size. The fluid employing the smallest particles exhibits the highest off state-viscosity to a large extent while the fluid employing HS powder exhibits the lowest off-state viscosity. The measurements show an increase in off-state viscosity when replacing the HS powder with larger particles.

The investigation of bimodal micron-sized MR fluids shows the on-state shear yield stress to increase with an increasing percentage of coarse powder. The MR fluid with 75% coarse powder and 25% fine powder exhibits a comparable on-state yield stress to that of the corresponding MR fluid using solely the coarse powder. The bimodal MR fluids exhibit a lower off-state viscosity when compared to their corresponding unimodal fluids. The difference is significant. An MR fluid using 75% coarse powder and 25% fine powder exhibits a 25% lower off-state viscosity than a corresponding MR fluid containing solely coarse powder. It exhibits a 50% lower off-state viscosity when compared to the MR fluid containing solely fine powder. This is an attractive advantage of bimodal size distributions for the proposed application.

The addition of a small concentration of nanoparticles is found to moderately increase the field-induced shear yield-stress. However, for a larger concentration of nanoparticles, the yield stress begins to decrease. Nanoparticles exhibit an undesirable effect on the off-state viscosity. MR fluid compositions, using nano-sized particles with a diameter range of 100 nm to 250 nm, exhibit a higher field-induced shear yield-stress when compared to their corresponding 25 nm compositions. However, the yield stresses of the bimodal 100-250 nano samples are comparable to the corresponding unimodal MR fluid. Only, a fluid with a 5% particle concentration, exhibits a moderately higher shear-yield stress when compared to the corresponding unimodal composition. The contrary holds true for the 5% fluid composition, using nano-sized particle with diameter of 25 nm. It exhibits a lower shear yield-stress than the corresponding unimodal fluid. The effect of nano-sized particles on the off-state viscosity is significant even though the total solid concentration is held to a constant value. The 25 nm particles increase the off-state viscosity to a larger

extent when compared to compositions of the same solid concentration using 100-250 nm particles. The 100-250 nm particle compositions exhibit both higher shear yield stress and lower off-state viscosity when compared to their corresponding 25 nm particle compositions.

The results reveal valuable information for the designers of MR fluids and designers of prosthetic actuators. Three MR fluid compositions have been selected as candidates for an MR fluid to be used in the prosthetic knee:

- Unimodal MR fluid with a solid loading of 0.25 by volume with the HS iron powder (sample 11)
- Unimodal MR fluid with a solid loading of 0.28 by volume with the OM iron powder (sample 23)
- Bimodal MR fluid with a total solid loading of 0.28 by volume using 75% coarse powder and 25% fine powder (sample 33).

These MR fluids have been found to have a high turn-up ratio, given the constraints of the proposed application regarding the base fluid, the solid loading and the particle size. They are selected as prominent MR fluids for the proposed application in the prosthetic knee actuator.

7 MR fluid models

This chapter describes existing MR fluid models and compares them to the experimental data described in the previous chapter.

7.1 Background

Many MR fluid modeling approaches have been described by numerous authors (Bossis et al., 1991; Ginder et al., 1994; Jolly et al.; 1996). Most of these models are based on evaluating the magnetic interparticle forces between particles within a particle chain in the fluid. For example, Klingenberg and Zukoski (1990) and Bossis and Lemaire (1991), used a dipolar sphere model and calculated the restoring force which tends to align two spheres on the axis of the field. Ginder and Davis (1994) and Ginder et al. (1996) modeled the fluid as a collection of infinite chains of spherical magnetizable particles and used the Maxwell stress tensor to determine the shear stress needed to shear the chains. Furthermore, Jolly et al. (1996) developed a quasi-static one-dimensional model. More recently, Si et al. (2008) proposed a micromechanical model for MR fluids, based on theory of magnetics and statistical analysis.

In addition to the particle interaction models, continuum type models have been developed, in order to determine the yield stress. For example, Rosensweig (1995) developed a continuum model of a composite based on a laminar layer structure with magnetic elements aligned in the field direction. Later, Tang and Conrad (2000) extended these models and developed two- and three-dimensional laminar structure models.

The models investigated here are a simple magnetic dipole model, a model from Ginder and co-workers (1994; 1996) and an empirical model described by Carlson (2005).

7.2 A simple magnetic dipole model

A preliminary attempt in modeling the on-state rheological behavior of the MR fluids is made. The approach described is based on the established model of magnetic dipole-dipole interaction energy. From there, a computational model is developed to quantitatively predict the shear-yield stress for MR fluid suspension. The interaction energy is a function of the magnetic properties of the particles. However, instead of using magnetic saturation values for the particles, as many studies do, a magnetization curve for a MR suspension is obtained experimentally and used in the computational model. Hence, the model takes into account the effects of the intensity of the applied magnetic field, along with the particle

size and particle fraction. The results from the computational model are compared to experimental flow curves for an MR fluid sample.

Looking at two equally sized isolated particles of radius a, each particle carries a magnetic moment, shown in Equation (7.1),

$$\left|\vec{m}_1\right| = M_1 \cdot 4/3 \cdot \pi \cdot a^3 \tag{7.1}$$

where M_1 is the magnetization of the particle. The magnetization characteristics, M, of one particular iron powder has been experimentally evaluated as a function of the applied field and is shown in Figure 5.3. These measurements will be used to quantify the theoretical analysis.

The interparticle magnetic potential energy between two isolated dipoles, in contact, is shown in Equation (7.2) (Jolly et al., 1995).

$$U(\vec{r}, \vec{m}_1, \vec{m}_2) = \frac{\mu_0}{4\pi} \frac{\vec{m}_1 \cdot \vec{m}_2 - 3(\hat{r} \cdot \vec{m}_1)(\hat{r} \cdot \vec{m}_2)}{\left|\vec{r}\right|^3} \tag{7.2}$$

where r is the distance vector between the particles, m_1 and m_2, the magnetic moment of particles 1 and 2, respectively. The dipolar interaction force is the derivative of the potential energy with respect to distance. The distance can be a measure of tension to obtain the normal force or a measure of shear to obtain the shearing force. The derivative of Equation (7.2) with respect to distance, in the tension direction, is shown in Equation (7.3) and, furthermore, with respect to distance, in the shearing direction, in Equation (7.4).

$$F_n = \frac{3\mu_0}{2\pi d^4}(m_1 m_2) \tag{7.3}$$

$$F_s = \frac{\mu_0}{4\pi(d^2 + x^2)^{5/2}}(m_1 m_2) \cdot (5x\frac{d^2}{d^2 + x^2} - 3x) \tag{7.4}$$

where d is the distance between the dipoles or the diameter of the particles and x is the shearing distance.

To estimate the yield stress of a particular MR suspension, an imaginary unit cube is used with a defined solid concentration and a uniform particle size. Particles are assumed to be perfect spheres. Thus, Equation (7.5) gives the number of particles in an imaginary unit cube as a function of solid concentration, φ, and particle diameter, d:

$$n_V = \frac{\phi \cdot 1}{4/3 \cdot \pi \cdot (d/2)^3} \tag{7.5}$$

Assuming long linear chains of particles in with particles, within a chain in contact, the number of particles in a line along the cube is 1/d and thus the number particles in a unit area normal to the chains is shown in Equation (7.6).

$$n_A = \frac{n_V}{1/d} \tag{7.6}$$

An estimate of the shear-yield stress in a simple shear deformation is obtained by looking at the outer-most unit area, normal to the chains. The total shearing force to shear the outer-most layer is the force by which an estimate of the shear-yield stress can be obtained. The shear force has a maximum which can be found by looking at the derivative of Eq. (7.4) which equals the yield stress. This equals a shear yield stress of 13 kPa, at the saturation level. This value is obtained for a particle diameter of 2 μm, a solid loading of 0.28 by volume, at saturation magnetization given by Figure 5.3, and by shearing the outer-most layer. This gives a shear yield stress of the correct order of magnitude but small when compared to measured shear-yield stress. Research has suggested that yielding behavior is contributed only from a few of the outer-most layers (Tang et al., 1996) but the exact number is unknown. Accounting for more than one layer would increase the predicted shear yield stress.

Using this simple model to analyze the shear-yield stress gives a preliminary insight into the behavior of MR fluids. Accounting for particle aggregates will improve predictions of the model. It remains the subject of further research to model more thoroughly the effect of particle size and solid concentration on the field-induced shear-yield stress of MR fluids.

7.3 Existing models

Several analytical and empirical models have been introduced in the literature that connects the shear-yield stress of MR fluids to the volume fraction of particles. Carlson (2005) gives an empirical model that predicts the shear-yield stress as:

$$\tau_{MR} = C \cdot 271700 \cdot \varphi^{1.5239} tanh(6.33x10^{-6} H) \tag{7.7}$$

where ϕ is the volume fraction of iron powder, τ_{MR} is the field-induced shear-stress (in Pa), H is the magnetic field strength (in A/m) and C is a constant that depends on the carrier liquid. Applying this empirical model to the unimodal PFPE-based MR fluids in this study, gives a constant of approximately C = 1.4 - 1.5, for all volume fractions. This is based on shear-yield stress values calculated from shear-rates, varying from 200 s^{-1} to 1000 s^{-1}. The value of our carrier liquid constant is considerably higher than the constants proposed for other carrier liquid types by Carlson (2005). In his study, the proposed values for the constant are 1.16 for water, 1.0 for hydrocarbon and 0.95 for silicone carrier liquid. Keep in mind, that his model does not consider the effect of particle size on the yield-stress. The fluids in this study have micron-sized particles with diameters ranging from 1 μm to 8 μm.

Another model for the shear-yield stress in MR fluids suggests the following relationship (Ginder and Davis, 1996):

$$\tau_{ys}^{sat} = (\frac{4}{5^{5/2}}) \cdot \xi(3) \cdot \phi \cdot \mu_0 \cdot M_s^2 \tag{7.8}$$

where $\xi(3) = 1.202$, ϕ is the volume fraction of particles, μ_0 is the permeability of free space, and M_s is the saturation magnetization. Calculating the shear yield stress, at saturation level, for the PFPE-based MR fluid, using the Ginder-Davis model, gives a shear

yield stress of approximately 40 kPa, for a solid volume fraction of 0.28 (mass fraction of 60%), which is in good agreement with the experimental results in this study.

7.4 Empirical tuning

The models by Ginder et al. (1994; 1996) and Carlson et al. (2005) will now be empirically tuned to comply with the experimental data obtained in the previous chapter.

The magnetization characteristics of one PFPE based MR fluid sample were obtained with a SQUID magnetometer. The magnetic moment was measured as a function of the applied field, at a temperature of 20°C. The sample has a solid concentration of 0.28, by volume, using a carbonyl iron powder, from BASF, with an average particle diameter of approximately 2 μm. Particles have an iron content of 97%. Figure 7.1 shows the magnetization hysteresis loop for the MR suspension or the magnetic moment per unit volume. The magnetization is calculated using the sample's specific weight of 3.55 g/cm3 and a sample size of 0.1014 g.

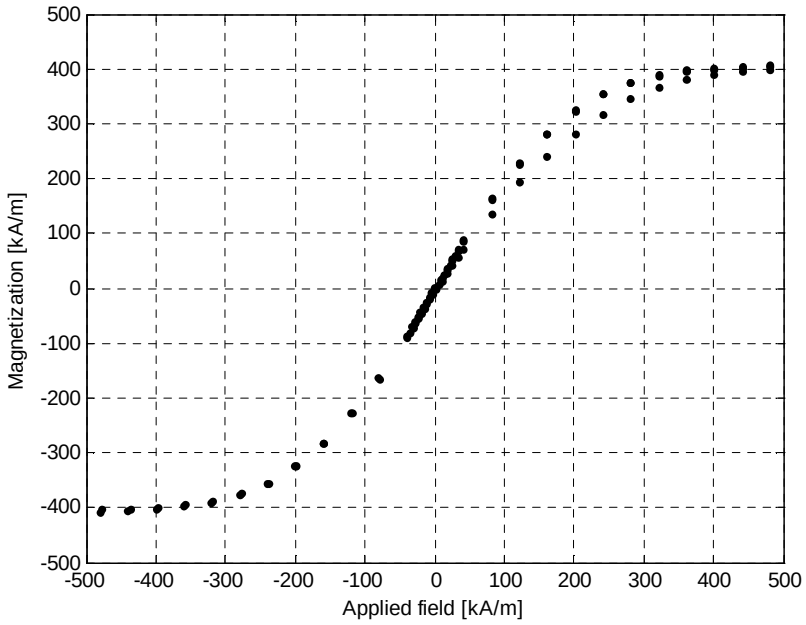

Figure 7.1. The magnetization hysteresis loop of a perfluorinated polyether (PFPE) based MR fluid sample with a solid loading of 0.28, by volume, and an average particle diameter of approximately 2 μm. Particles have an iron content of 97%. Measurements are performed at a temperature of 20°C.

The magnetic flux density, B, is related to the applied field, H, and the magnetization, M, by $B = \mu_0 (H + M)$. Thus, the B-H curve for a MR fluid suspension is shown in Figure 7.2.

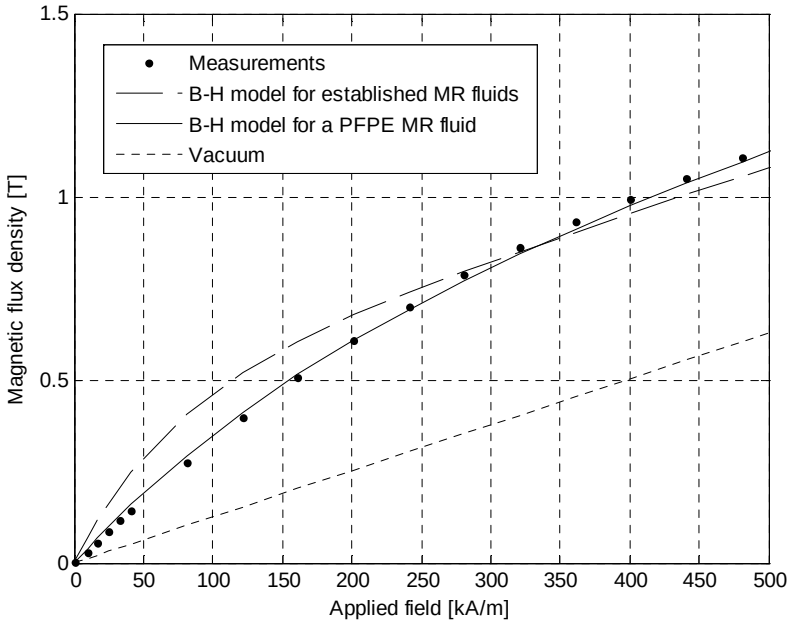

Figure 7.2. The B-H relation for a perfluorinated polyether (PFPE) based MR fluid with a solid concentration of 0.28, by volume, and an average particle diameter of 2 μm. Particles have an iron content of 97%. A B-H model for established MR fluids is also shown and a fine tune of that model for a FPEE based MR fluid composition.

The figure shows how a B-H model for established MR fluids, presented by Carlson (2005), can easily be adopted to accurately describe the magnetization characteristics of the PFPE base MR fluid. The model is shown in Eq. (7.9).

$$B = C_1 \cdot \phi^{1.133}(1-\exp(-C_2 \cdot \mu_0 \cdot H)) + \mu_0 \cdot H \tag{7.9}$$

Carlson presents this model with the parameter values C_1 = 1.91 T and C_2 = 10.97 T^{-1}. Fine tuning this model for the PFPE based MR fluid, using a least-square error fit, gives parameters values of C_1 = 2.24 T and C_2 = 4.39 T^{-1}. The induction at high applied fields can be set by the parameter C_1 and the parameter C_2 can be used to set the position the saturation point at 500 kA/m, for example. This results in an accurate relation between the induction and the applied field for PFPE based MR fluid with a solid loading of 0.28. Thus, Eq. (7.10), based on a model presented by Carlson et al. (2005), is an expression for the magnetization of the PFPE based MR fluid, M, as a function of solid loading and the applied field.

$$M = \frac{2.24}{\mu_0} \cdot \phi^{1.133}(1-\exp(-4.39 \cdot \mu_0 \cdot H)) \tag{7.10}$$

Following the magnetic analysis, a rheological analysis is now performed. The rheological characteristics of four PFPE based MR fluids samples, each with a different solid loading, were measured. Measurements are performed at shear-rates from 10^{-3} s^{-1} to 10^{3} s^{-1} for a magnetic field strength ranging from 20 kA/m to 200 kA/m. Figure 7.3 shows

the shear-yield stress for the samples as a function of the applied magnetic field and solid loading.

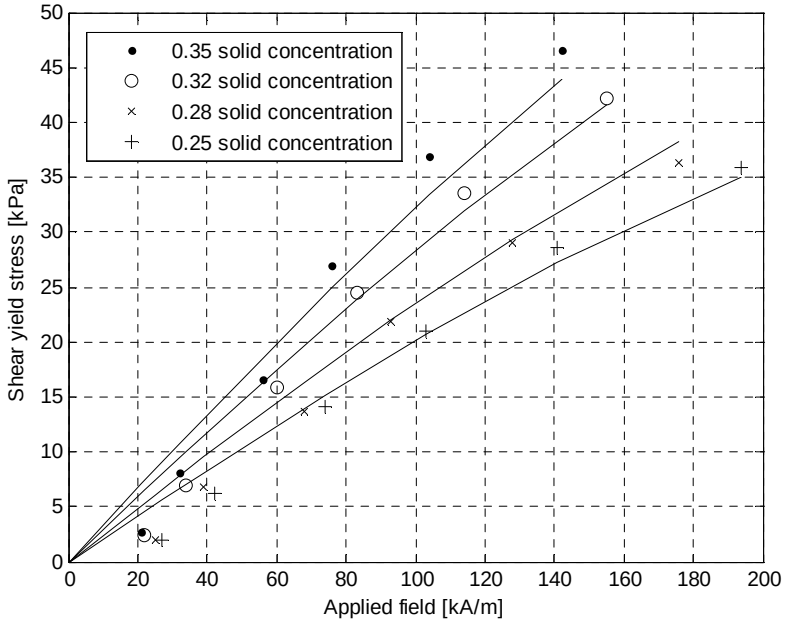

Figure 7.3. The shear-yield stress of perfluorinated polyether (PFPE) based MR fluid samples with a solid loading ranging from 0.25 to 0.35, by volume, and an average particle diameter of 2 μm. An empirically fitted model, based on Carlson (2005), is also shown for each particle loading. Measurements are performed at a temperature of 20°C.

The figure shows also an empirically fitted model, based on Carlson (2005), shown in Equation (7.11).

$$\tau_y = C \cdot 271700 \cdot \phi^{C_3} tanh(C_4 \cdot 10^{-6} \cdot H) \tag{7.11}$$

Carlson (2005) suggests the C constant to be base fluid dependent having a value of C = 0.95, 1.0 and 1.16, depending on the base fluid. For established MR fluids, the parameters C_3 and C_4 have been found to have a value of C_3 = 1.5239 and C_4 = 6.33. This study suggests values of C = 1.5, C_3 = 1.40 and C_4 =3.60 for the PFPE based MR fluids, where the squared error is used to quantify the difference between the model and the measurements.

Ginder et al. (1994; 1996) suggest a shear yield stress model, below the saturation level. The model suggests a linear dependency on solid loading and a subquadratic field dependency, shown in Equation (7.12),

$$\tau_{ys} = C_5 \cdot \varphi \cdot \mu_0 \cdot H^{C_6} M_s^{2-C_6} \tag{7.12}$$

where M_s is the saturation magnetization for the MR fluid. The value of M_s was measured for a MR fluid composition with solid concentration of 0.28. For other solid concentrations, Equation (7.10) is used to determine the saturation magnetization.

Figure 7.4 shows the measured shear-yield stress, again, with the model from Ginder *et al.* (1994; 1996) fitted with a least squared error fit.

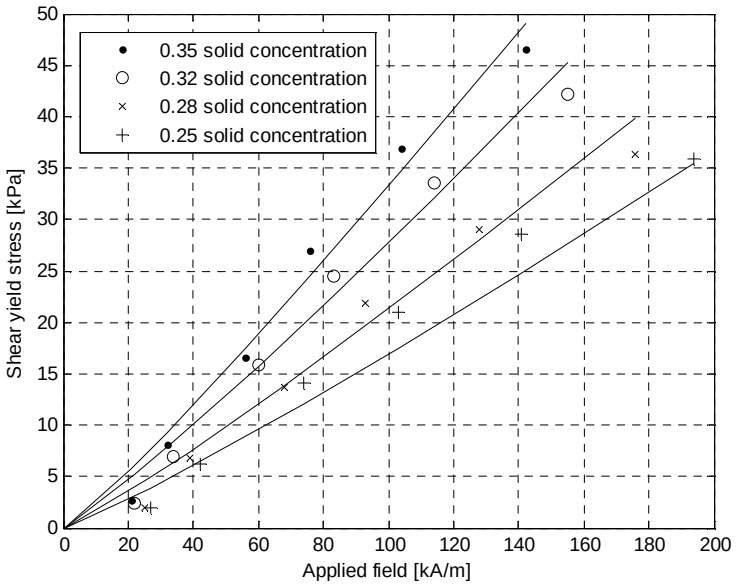

Figure 7.4. The shear-yield stress of perfluorinated polyether (PFPE) based MR fluids with a solid loading ranging from 0.25 to 0.35, by volume, and an average particle diameter of 2 microns. An empirically fitted model, based on Ginder et al. (1994; 1996), is also shown. Measurements are performed at a temperature of 20°C.

The resulting model for the PFPE based MR fluids has a parameter value of $C_5 = 1.7$ and $C_6 = 1.1$ which compares to parameter values of $C_5 = 2.4$ and $C_6 = 0.5$ in the model from Ginder and co-workers (1994; 1996).

The analysis has shown how a fine tune of established models for MR fluids can be used to represent the characteristics of PFPE based MR fluids. This completes the MR fluid analysis.

8 Conclusions and future work

A combined MR fluid design approach and an MR device design approach has been presented, motivated by improving the quality of life of amputees using an MR prosthetic knee.

The MR device approach has shown that the on-state braking torque of the device can be increased from 40-45 Nm to 60 Nm without increasing the off-state rotary torque from that of the reference design. A key design parameter to achieve this is the gap size between the rotating steel blades in the fluid chamber. A gap size of 24 μm and a blade number of 67 has been implemented in newly available prosthetic knee product, with good results. However, the analysis suggests that these values should be increased further to improve the qualities of the prosthetic knee.

The MR fluid design approach has shown a fluid with a solid concentration of 0.25 by volume, using the HS iron powder, to have the highest figure of merit value for the proposed application. This was the lowest solid concentration tested in this research. Increasing the iron particle size from 1 μm to approximately 8 μm has shown the on-state shear-yield stress and the off-state viscosity to increase. The OM iron powder has been shown to have the highest figure of merit value for a constant solid concentration of 0.28. Bimodal MR fluids with micron-sized particles have been shown to have a lower off-state viscosity than their corresponding unimodal fluids. Bimodal MR fluids with nano-sized particles have been shown to increase the shear-yield stress moderately but undesirably increase the off-state viscosity.

The results of this study provides a valuable guidance for developers of MR fluids and designers of prosthetic devices who face challenges in designing a field-induced high strength fluid while at the same time minimizing off-state viscosity. Interesting areas that deserve further research are:

1. Surprisingly, the MR fluid with the lowest solid concentration has the highest ratio between the on-state shear-yield stress and the off-state viscosity. This suggests that even lower solid concentrations might be appropriate for the MR prosthetic actuator. Further mapping of effect of solid concentration on the proposed merit function is needed.
2. Bimodal MR fluids with a mixture of micron-sized iron powder are believed to have potential for the proposed application. Further investigation is needed to determine the effect of the mixing portions, between the coarse and the fine powder, on the proposed merit function. Also, the effect of size ratio between the coarse and fine powder needs a further investigation.

3. Further modeling of the experimental MR fluid data is needed. The goal is to be able to predict characteristics of future MR fluid compositions without needing to use expensive experimental evaluations.
4. A combined device-fluid optimization is an interesting research area. Assuming successful MR fluid models, the fluid models can be incorporated into the device model. This would make a combined optimization possible that includes, in addition to geometrical parameters, selected fluid parameters like solid concentration or particle size, for example.
5. The durability of the MR fluid in the prosthetic knee is of concern and a problem after long periods of usage. This issue deserves further research.
6. Using field dependent solid materials in prosthetics, for adaptive structures, is believed to have interesting potentials. Magnetorheological elastomers, with an application in prosthetics, deserve the attention of further research.

The results of this study give a valuable insight into further developments of the MR prosthetic knee joint with regards to strength and comfortability. The approach has been shown to furthering the success of the MR prosthetic knee joint.

References

Ahmadkhanlou, F., Zite, J. and Washington, G. 2007. “A magnetorheological fluid-based controllable active knee brace,” *Smart Structures and Materials Proc. SPIE* 6171 148-56.

Anton Paar, 2011. http://www.anton-paar.com/001/en/60/47

Asgeirsson, S.A, Bisbee III, C.R. and Hsu, H.H. 2010. “Systems and methods of controlling pressure within a prosthetic knee,” *US Patent Specification* 7,691,154.

Aydar, G., Evrensel, C. A., Gordaninejad, F. and Fuchs, A. 2007. “A Low Force Magneto-rheological (MR) Fluid Damper: Design, Fabrication and Characterization,” *Journal of Intelligent Material Systems and Structures*, 18(12):1155-1160.

Barnes, H.A., Hutton, J.F. and Walters, K. 1989. *An Introduction to Rheology*, New York: Elsevier Science Publishers.

BASF AG, 2011. BASF Corporation. North America Regional Headquarters, 100 Campus Drive, Florham Park, NJ 07932.

Biedermann, L. 2002. “Leg Prosthesis With An Artificial Knee Joint Provided With An Adjustment Device,” *US Patent Specification* 6,423,098.

Bisbee III, C.R. and Hsu, H.H. 2007. “Systems and methods of loading fluid in a prosthetic knee,” *US Patent Specification* 7,198,071.

Bombard, A.J.F., Alcantara, M.R., Knobel, M. and Volpe, P.L.O. 2005. “Experimental study of MR suspensions of carbonyl iron powders with different particle sizes,” *Int. J. of Modern Physics B* 19: 1332-1338.

Bombard, A.J.F., Knobel, M., Alcantara, M.R. and Joekes, I. 2002. “Evaluation of Magnetorheological Suspensions Based on Carbonyl Iron Powders,” *J. Intell. Mater. Syst. Struct.* 13: 471-478.

Bossis, G. and Lemaire, E. 1991. “Yield stresses in magnetic suspensions,” *J. of Rheol*. 35: 1345-1354.

Burguera, E.F., Love, B.J., Sahul, R., Ngatu, G. and Wereley, N.M. 2008. “A Physical Basis for Stability in Bimodal Dispersions Including Micrometer-sized Particles and Nanoparticles using Both Linear and Non-linear Models to Describe Yield,” *Journal of Intelligent Material Systems and Structures*, 19(11):1361-1367.

Carlson, J.D., Matthis, W. and Toscano, J.R. 2001. “Smart prosthetics based on magnetorheological fluids,” *Smart Structures and Materials Proc.SPIE* 4332 308-16

Carlson, J.D. 2002. “What Makes a Good MR Fluid?,” *J. Intell. Mater. Syst. Struct.* 13 431-435

Carlson, J.D. 2005. “MR Fluids and Devices in the Real World,” *Int. J. of Modern Physics B* 19: 1463-1470.

Carlson, J.D., Catanzarite, D.M. and St. Clair, K.A. 1996. “Commercial Magneto-rheological Fluid Devices,” *International Journal of Modern Physics B*, 10(23):2857-2865.

Chaudhuri, A., Wang, G., Wereley, N.M., Tasovksi, V. and Radhakrishnan, R. 2005. “Substitution of Micron by Nanometer Scale Powders in Magnetorheological Fluids,” *International Journal of Modern Physics B: Condensed Matter Physics*, 19(7-9):1374-1380.

Chen, J. and Loao, W.H. 2006. “A leg exoskeleton utilizing a magnetorheological actuator,” *Proc. of the 2006 IEEE Int. conf. of Robotic and Biomimetics* 824-29

Choi, H.J., Lim, S.T., Izumisawa, S. and Jhon, M.S. 2005. “Viscoelasticity and solution viscosity of perfluoropolyether lubricants,” *Tribology International*, 38(6-7):682-686.

Coello, C.A.C., Lamont, G.B. and Van Veldhuizen, D.A. 2007. “Evolutionary Algorithms for Solving Multi-Objective Problems,” *Springer, 2nd Edition.*

Deffenbaugh, B.W., Herr, H.M., Pratt, G.A. and Wittig, M.B. 2004. “Electronically controlled prosthetic knee,” *US Patent Specification* 6,764,520.

Dong, S.F., Lu, K.Q., Sun, J.Q. and Rudolph, K. 2006. “Adaptive Force Regulation of Muscle Strengthening Rehabilitation Device With Magnetorheological Fluids,” *IEEE Trans Neural Syst Rehabil Eng.* 14 55-63

DuPont, 2011. http://www2.dupont.com/Lubricants/en_US/products/krytox/krytox.html

Dyke, S.J., Spencer, B.F., Sain, M.K. and Carlson, J.D. 1998. “An experimental study of MR dampers for seismic protection,” *Smart Mater. Struct.* 7 693-703

Ekwebelam, C. and See, H. 2009. “Microstructural investigations of the yielding behaviour of bidisperse magnetorheological fluids,” *Rheol Acta* 48: 19-32.

Fang, F.F., Choi, H.J. and Jhon, M.S. 2009. “Magnetorheology of soft magnetic carbonyl iron suspension with single-walled carbon nanotube additive and its yield stress scaling function,” *Colloids and Surfaces A: Physicochemical and Engineering Aspects*, 351(1-3):46-51.

Foister, R.T. 1997. “Magnetorheological Fluids,” *US Patent Specification* 5,667,715.

Gangopadhyay, S., Hadjipanayis, G.C. Dale, B., Klabunde, K.J., Papaefthymiou, V. and Kostikas, A. 1992. “Magnetic properties of ultrafine iron particles,” *Physical Review B*, 45(17):9778-87.

Gavin, H., Hoagg, J. and Dobossy, M. 2001. “Optimal design of MR dampers,” *Proc. US. Japan Workshop on Smart Struct. For Improved Seismic Perf. In Urban Regions*, 225-36

Genc, S. and Phule, P.P. 2002. “Rheological Properties of Magnetorheological Fluids,” *Smart Materials and Structures*, 11(1): 140-146.

Ginder, J.M. and Davis, L.C. 1994. “Shear Stresses in Magnetorheological Fluids: Role of Magnetic Saturation,” *Applied Physics Letters*, 65(26): 3410-3412.

Ginder, J.M., Davis, L.C. and Elie, L.D. 1996. “Rheology of Magnetorheological Fluids: Models and Measurements,” *Int. J. Mod. Phys.*, 10(23-24): 3293-3303.

Golden, M. A., Ulicny, J. C., Snavely, K. S. and Smith, A. L., 2005, “Magnetorheological fluids,” *US Patent Specification 6,932,917 B2*.

Goncalves, F.D., Koo, J.H. and Ahmadian, M. 2006. “A review of the state of the art in magnetorheological fluid technologies - Part I: MR fluid and MR fluid models,” *The Shock and Vibration Digest* 38: 203-219.

Gudmundsson, K.H., Jonsdottir, F. and Thorsteinsson, F. 2010. “A geometrical optimization of a magneto-rheological rotary brake in a prosthetic knee,” *Smart Materials and Structures* 19(035023).

Gudmundsson, K.H., Jonsdottir, F., and Olafsson, S. 2008. “Multi-objective Optimization of a Magneto-Rheological Prosthetic Knee Actuator,” *Proceedings of the 19th International Conference on Adaptive Structures and Technologies,* Ascona, Switzerland.

Gudmundsson, K.H., Jonsdottir, F., and Olafsson, S. 2008. “The Viscosity of Magneto-Rheological Fluids in a Prosthetic Knee Actuator,” *Proceedings of the 11th International Conference on New Actuators*, Bremen, Germany.

Gudmundsson, K.H., Jonsdottir, F., and Thorsteinsson, F. 2009 “A Multi-Objective Design Optimization of a Smart Magneto-Rheological Prosthetic Knee,” *Proceedings of the ASME 2009 Conference on Smart Materials, Adaptive Structures and Intelligent Systems*, Oxnard, California.

Gudmundsson, K.H., Jonsdottir, F., Palsson, H. and Karlsson, S.G. 2007. “Optimization of a Magneto-rheological Rotary Brake,” *Proceedings of the 3th ECCOMAS Thematic Conference on Smart Structures and Materials*, Gdansk, Poland.

Gudmundsson, K.H., Jonsdottir, F., Thorsteinsson, F. and Gutfleisch, O. 2009. “A Perfluorinated Polyether-based Magneto-rheological Fluid in a Prosthetic Knee,” *Proceedings of the 4th ECCOMAS Thematic Conference on Smart Structures and Materials*, Porto, Portugal.

Gudmundsson, K.H., Jonsdottir, F., Thorsteinsson, F. and Gutfleisch, O. 2010. “Modeling Perfluorinated Polyether Based MR Fluids,” *Proceedings of the 12th International Conference on Electrorheological (ER) Fluids and Magnetorheological (MR) Suspensions*, Philadelphia, Pennsylvania.

Gudmundsson, K.H., Jonsdottir, F., Thorsteinsson, F. and Gutfleisch, O. 2010. “An Experimental Investigation into the Off-state Viscosity of MR Fluids,” *Proceedings of the 12th International Conference on Electrorheological (ER) Fluids and Magnetorheological (MR) Suspensions*, Philadelphia, Pennsylvania.

Gudmundsson, K.H., Jonsdottir, F., Thorsteinsson, F. and Gutfleisch, O. 2011. “An Experimental Investigation of Unimodal and Bimodal Magnetorheological Fluids with an Application in Prosthetic Devices,” *Journal of Intelligent Material Systems and Structures*, **22**(6), 539-49.

Herr, H. and Wilkenfeld, A. 2003. “User-adaptive control of a magnetorheological prosthetic knee,” *Industrial Robot - an International Journal* 30 42-55

Heyes, D. M. and Sigurgeirsson, H., The Newtonian viscosity of concentrated stabilized dispersions: Comparisons with the hard sphere fluid, *Journal of Rheology*, 48:223-248, 2004.

Hsu, H.H., Bisbee III, C.R., Palmer, L., Lukasiewicz R.J., Lindsay, M.W. and Prince, S.W. 2006. “Magnetorheological fluid compositions and prosthetic knees utilizing same,” *US Patent Specification* 7,101,487.

Huang J, Zhang J Q, Yang Y 2002 Analysis and design of a cylindrical MR fluid brake *J. of Mat. Proc. Tech.* 129 559-62

Ierardi, R.F. and Bombard, A.J.F. 2009. “Off-state viscosity and yield stress optimization of magneto-rheological fluids: a mixture design of experiments approach,” *J. of Phys.: Conference Series* 149: 012037.

Jolly, M.R., Bender, J.W. and Carlson, J.D. 1999. “Properties and applications of commercial magnetorheological fluids,” *J. Intell. Mater. Syst. Struct*. 10: 5-13.

Jolly, M.R., Carlson, J.D. and Munoz, B.C. 1996. “A model of the behaviour of magnetorheological materials,” *Smart. Materials and Structures*, 5: 607-614.

Jonsdottir, F., Gudmundsson, K.H. and Thorsteinsson, F. 2009 “Bidisperse Perfluorinated Polyether (PFPE)-Based Magneto-Rheological Fluids in a Prosthetic Knee,” *Proceedings of the ASME 2009 Conference on Smart Materials, Adaptive Structures and Intelligent Systems*, Oxnard, California.

Jonsdottir, F., Gudmundsson, K.H., Dijkman, T.B., Thorsteinsson, F. and Gutfleisch, O. 2010. “Rheology of Perfluorinated Polyether-based MR Fluids with Nanoparticles,” *Journal of Intelligent Material Systems and Structures*, 21(11), 1051-60.

Jonsdottir, F., Gudmundsson, K.H., Hreinsson, E., Thorsteinsson, F. and Gutfleisch, O. 2010. “A Simple Shear Analysis of MR Fluids,” *Proceedings of the 12th International Conference on Electrorheological (ER) Fluids and Magnetorheological (MR) Suspensions*, Philadelphia, Pennsylvania.

Jonsdottir, F., Gudmundsson, K.H., Thorsteinsson, F. and Gutfleisch, O. 2009 “A Magneto-rheological Suspension for a Prosthetic Knee Joint,” *Proceedings of the Nordic Rheology Society*, Reykjavík, Iceland.

Jonsdottir, F., Thorarinsson, E.T., Palsson, H. and Gudmundsson, K.H. 2009. “Influence of Parameter Variations on the Braking Torque of a Magnetorheological Prosthetic Knee,” *Journal of Intelligent Material Systems and Structures*, 20(6), 659-67.

Karakoc, K., Park, E.J, and Suleman, A. 2008. “Design considerations for an automotive magnetorheological brake,” *Mechatronics* 18 434-47.

Kavlicoglu, B.M., Gordaninejad, F., Evrensel, C.A., Cobanoglu, N., Liu, Y., Fuchs, A. and Korol, G. 2002. “A High-Torque Magneto-rheological Fluid Clutch,” *Proceedings of SPIE Conference on Smart Materials and Structures*, San Diego.

Kavlicoglu, B.M., Gordaninejad, F., Evrensel, C.A., Fuchs, A., and Korol, G. 2006. “A semi-active, high-torque, magnetorheological fluid limited slip differential clutch,” *Journal of Vibration and Acoustics-Transactions of the ASME*, 128(5): 604-10.

Kavlicoglu, N.C., Kavlicoglu, B.M., Liu, Y.M., Evrensel, C.A., Fuchs, A., Korol, G. and Gordaninejad, F. 2007. “Response Time and Performance of a High-torque Magneto-rheological Fluid Limited Slip Differential Clutch,” *Smart Materials & Structures*, 16(1):149-59.

Kittipoomwong, D., Klingenberg, D.J. and Ulicny, J.C. 2002. “Simulation of bidisperse magnetorheological fluids,” *Int. J. of Modern Physics B* 16:2732-2738.

Kittipoomwong, D., Klingenberg, D.J. and Ulicny, J.C. 2005. “Dynamic yield stress enhancement in bidisperse magnetorhelogical fluids,” *J. of Rheol.* 49:1521-1538.

Klingenberg, D.J. and Zukoski IV, C.F. 1990. “Studies on the steady-shear behavior of electrorheological suspensions,” *Langmuir*, 6(1): 15-24.

Kormann, C., Laun, H. and Ritcher, H. 1996. “MR Fluids with Nanosized Magnetic Particles,” *Int. J. Mod. Phys. B*, 10: 3167–72.

Lemaire, E., Meunier, A. , Bossis, G., Liu, J., Felt, D., Bahtovoi P. and Matoussevitch, N. 1995. “Influence of the Particle Size on the Rheology of Magnetorheological Fluids,” *Journal of Rheology*, 39:1011-1020.

Li, W.D. and Du, H. 2003. “Design and experimental evaluation of a magnetorheological brake,” *The Int. J. of Adv. Manuf. Techn. Technology* 21 508-15

Lindler, J.E., Choi, Y.T. and Wereley, N.M. 2003. “Double adjustable shock absorbers utilizing electrorheological and magnetorheological fluids,” *Int. J. of Vehicle Design* 33 189-206

Liu, Y.Q., Matsuhisa, H., Utsuno, H. and Park, J.G. 2006. “Vibration Control by a Variable Damping and Stiffness System with Magnetorheological Dampers,” *JSME International Journal Series C-Mechanical Systems Machine Elements and Manufacturing*, 49(2):411-417.

Lopez-Lopez, M. T., Kuzhir P, Meunier, A. and Bossis, G. 2009. “Synthesis and Magnetorheology of Suspensions of Cobalt Particles with Tunable Particle Size,” *J. of Phys.: Conf. Series*, 149:012073.

Lord Corporation, 2011. http://www.lord.com/mr/

Nam, Y.J., Moon, Y.J., Park, M. K. 2008. “Performance improvement of a rotary MR fluid actuator based on electromagnetic design,” *J. Intell. Mater. Syst. Struct.* 19 695-705

Nanostructured & Amorphous Materials Inc., 2011. http://www.nanoamor.com

Nguyen, Q-H., Choi, S-B. and Wereley, N.M. 2008. "Optimal design of magnetorheological valves via a finite element method considering control energy and a time constant," *Smart Mater. Struct.* 17 025024

Nguyen, Q-H., Han, Y-M., Choi, S-B. and Wereley, N.M. 2007. "Geometry optimization of MR valves constrained in a specific volume using the finite element method," *Smart Mater. Struct.* 16 2242-52

Nye Synthetic Lubricants, 2011. http://www.nyelubricants.com/pdf/8510_copy1.pdf

Martys, N. S., Study of a dissipative particle dynamics based approach for modeling suspensions, *Journal of Rheology*, 49:401-424, 2005.

Ossur Inc., 2011. http://www.ossur.com/prosthetics.

Park, B.J, Song, K.H. and Choi, H.J. 2009 "Magnetic Carbonyl Iron Nanoparticle Based Magnetorheological Suspension and its Characteristics," *Materials Letters,* 63(15):1350-1352.

Philips, R.W. 1969. "Engineering applications of fluids with a variable yield stress," *Ph.D. Thesis, University of California, Berkeley*.

Philips, R.W., 1969, "Engineering applications of fluids with a variable yield stress," *Ph.D. Thesis, University of California, Berkeley*.

Poddar, P., Wilson, J.L., Srikanth. H., Yoo, J.-H., Wereley, N.M., Kotha, S., Barghouty, L. and Radhakrishnan, R. 2004. "Nanocomposite Magneto-Rheological Fluids with Uniformly Dispersed Fe Nanoparticles," *Journal of Nanoscience and Nanotechnology*, 4(1-2):192-196.

Rabinow, J., 1951, "Magnetic Fluid Torque and Force Transmitting Device," *US Patent 2,575, 360*.

Rosenfeld, N., Wereley, N.M., Radhakrishnan, R. and Sudarshan, T.S. 2002. "Behavior of Magnetorheological Fluids Utilizing Nanopowder Iron," *International Journal of Modern Physics B*, 16(17-18): 2392-2398.

Rosensweig, R.E. 1995. "On magnetorheology and electrorheology as states of unsymmetric stress," *J. of Rheol.*, 39: 179-192.

Sassi, S., Cherif, K., Mezghani, L., Thomas, M. and Kotrane, A. 2005. "An innovative damper for automotive suspension: from design to experimental characterization," *Smart Mater. Struct* 14 811-22

Si, H., Peng, X. and Li, X. 2008 "A Micromechanical Model for Magnetorheological Fluids," *J. Intell. Mater. Syst. Struct.* 19(1): 19-23.

Tang, X., Zhang, X., Tao, R. and Rong Yiming. 2000. "Structure-enhanced yield stress of magnetorheological fluids," *Journal of Applied Physics*, 87

Tang, X. and Conrad, H. 2000 "An analytical model for magnetorheological fluids," *J. of Phys. D: Appl. Phys.* 33(23): 3026-3032.

Tang, X., Chen, Y. and Conrad, H. 1996 "Structure and Interaction Force in a Model Magnetorheological System," *J. Intell. Mater. Syst. Struct.* **7**(5): 517-521.

Thorarinsson, E. Th. 2006. "Analysis of magnetorheological prosthetic knee," *M.Sc. Thesis, University of Iceland*

Thurm, S. and Odenbach, S., 2003, Particle Size Distribution as Key Parameter for the Flow Behavior of Ferrofluids, *Physics Of Fluids*, Vol. 15, 1658–1664

Trendler, A.M. and Böse, H. 2005. "Influence of Particle Size on the Rheological Properties of Magnetorheological Suspension," *International Journal of Modern Physics B*, 19(07-09): 1416-1422.

URL: http:// http://www2.dupont.com/Lubricants/en_US/.

URL: http://www.ansys.com
URL: http://www.anton-paar.com
URL: http://www.basf.com.
URL: http://www.nyelubricants.com.
URL: http://www.ossur.com/prosthetics
Vacuumshmelze, 2011. www.vacuumshmelze.de.
Wang, X. and Gordaninejad, F. 2008. "Magnetorheological Materials and their Applications," *Intelligent Materials*, edited by Shahinpoor, M. and Schneider H. J., Cambridge, UK: Royal Society of Chemistry, pp. 339-385.
Weiss, K.D., Carlson, J.D. and Nixon, D.A. 2000. "Method and Magnetorheological Fluid Formulations for Increasing the Output of a Magnetorheological Fluid," *US Patent Specification* 6,027,664.
Wereley, N.M, Chaudhuri, A., Yoo, J.H., John, S., Kotha, S., Suggs, A., Radhakrishnan, R., Love, B.J. and Sudarshan, T.S. 2006. "Bidisperse Magnetorehological Fluids using Fe Particles at Nanometer and Micron Scale," *Journal of Intelligent Material Systems and Structures*, 17(5): 393-401.
Wereley, N.M., Cho, J.U., Choi Y.T. and Choi, S.B. 2008. "Magnetorheological dampers in shear mode," *Smart Mater. Struct.* 17(1): 015022.
Yang, G., Spencer, B.F., Carlson, J.D. and Sain, M.K. 2002. "Large-scale MR fluid dampers: modeling and dynamic performance considerations," *Eng. Struct.* 24 309-23
Yang, L., Duan, F. and Eriksson, A. 2008. "Analysis of the optimal design strategy of a magnetorheological smart structure," *Smart Mater. Struct.* 17 015047
Ye, M. and Wang, X. 2007. "Parameter estimation of the Bouc-Wen hysteresis model using particle swarm optimization," *Smart Mater. Struct.* 16 2341-9
Zhang, H.H., Liao, C.R., Chen, W.M. and Huang, S.L. 2006. "A Magnetic Design Method of MR Fluid Dampers and FEM Analysis on Magnetic Saturation," *J. Intell. Mater. Syst. Struct.* 17 813-18
Zhou, W., Chew, C.M. and Hong, G.S. 2007. "Development of a compact double-disk magneto-rheological fluid brake," *Robotica* 25 493-500
Zite, J.L., Ahmadkhanlou, F., Neelakantan, V.A., Washington, G.N. and Gregory, N.. 2006. "A Magnetorheological Fluid Based Orthopedic Active Knee Brace," *Smart Materials & Structures*, 6171:148-156

Appendix A: Publications

The following journal and conference papers where published during the project.

Journal papers:

1. Jonsdottir F, Thorarinsson E T, Palsson H and Gudmundsson K H 2009 Influence of Parameter Variations on the Braking Torque of a Magnetorheological Prosthetic Knee *Journal of Intelligent Material Systems and Structures* **20**(6) 659-67

2. Gudmundsson, K.H., Jonsdottir, F. and Thorsteinsson, F. 2010 "A geometrical optimization of a magneto-rheological rotary brake in a prosthetic knee," *Smart Materials and Structures* **19**(035023).

3. Jonsdottir, F., Gudmundsson, K.H., Dijkman, T.B., Thorsteinsson, F. and Gutfleisch, O. 2010. "Rheology of Perfluorinated Polyether-based MR Fluids with Nanoparticles," *Journal of Intelligent Material Systems and Structures*, **21**(11), 1051-60.

4. Gudmundsson, K.H., Jonsdottir, F., Thorsteinsson, F. and Gutfleisch, O. 2011. "An Experimental Investigation of Unimodal and Bimodal Magnetorheological Fluids with an Application in Prosthetic Devices," *Journal of Intelligent Material Systems and Structures*, **22**(6), 539-49.

Conference papers:

1. Gudmundsson, K.H., Jonsdottir, F., Palsson, H. and Karlsson, S.G. 2007. "Optimization of a Magneto-rheological Rotary Brake," *Proceedings of the 3th ECCOMAS Thematic Conference on Smart Structures and Materials*, Gdansk, Poland.

2. Gudmundsson, K.H., Jonsdottir, F., and Olafsson, S. 2008 "The Viscosity of Magneto-Rheological Fluids in a Prosthetic Knee Actuator," *Proceedings of the 11th International Conference on New Actuators*, Bremen, Germany.

3. Gudmundsson, K.H., Jonsdottir, F., and Olafsson, S. 2008 "Multi-objective Optimization of a Magneto-Rheological Prosthetic Knee Actuator," *Proceedings of the 19th International Conference on Adaptive Structures and Technologies*, Ascona, Switzerland.

4. Gudmundsson, K.H., Jonsdottir, F., Thorsteinsson, F. and Gutfleisch, O. 2009. "A Perfluorinated Polyether-based Magneto-rheological Fluid in a Prosthetic Knee,"

Proceedings of the 4th ECCOMAS Thematic Conference on Smart Structures and Materials, Porto, Portugal.

5. Gudmundsson, K.H., Jonsdottir, F., and Thorsteinsson, F. 2009 "A Multi-Objective Design Optimization of a Smart Magneto-Rheological Prosthetic Knee," *Proceedings of the ASME 2009 Conference on Smart Materials, Adaptive Structures and Intelligent Systems*, Oxnard, California.

6. Jonsdottir, F., Gudmundsson, K.H., Thorsteinsson, F. and Gutfleisch, O. 2009 "A Magneto-rheological Suspension for a Prosthetic Knee Joint," *Proceedings of the Nordic Rheology Society*, Reykjavík, Iceland.

7. Jonsdottir, F., Gudmundsson, K.H. and Thorsteinsson, F. 2009 "Bidisperse Perfluorinated Polyether (PFPE)-Based Magneto-Rheological Fluids in a Prosthetic Knee," *Proceedings of the ASME 2009 Conference on Smart Materials, Adaptive Structures and Intelligent Systems*, Oxnard, California.

8. Gudmundsson, K.H., Jonsdottir, F., Thorsteinsson, F. and Gutfleisch, O. 2010. "Modeling Perfluorinated Polyether Based MR Fluids," *Proceedings of the 12th International Conference on Electrorheological (ER) Fluids and Magnetorheological (MR) Suspensions*, Philadelphia, Pennsylvania.

9. Gudmundsson, K.H., Jonsdottir, F., Thorsteinsson, F. and Gutfleisch, O. 2010. "An Experimental Investigation into the Off-state Viscosity of MR Fluids," *Proceedings of the 12th International Conference on Electrorheological (ER) Fluids and Magnetorheological (MR) Suspensions*, Philadelphia, Pennsylvania.

10. Jonsdottir, F., Gudmundsson, K.H., Hreinsson, E., Thorsteinsson, F. and Gutfleisch, O. 2010. "A Simple Shear Analysis of MR Fluids," *Proceedings of the 12th International Conference on Electrorheological (ER) Fluids and Magnetorheological (MR) Suspensions*, Philadelphia, Pennsylvania.